Transformation of Sugar-Derived Compounds over Supported Metal Catalysts

(担持金属触媒による糖化合物の変換)

Yayati Naresh Palai

Hokkaido University

北海道大学

2022

Table of Contents

Chapter 1

General Introduction

1.1 Background

Present day scientific research has increasing interest in clean energy and renewable chemicals to embrace sustainability and carbon neutrality, while still meeting the demands of ever-growing population. Based on current human understanding, wind,[1] solar,[2] hydro power[3] can be a source of clean energy, while CH_4,[4–6] CO_2[7,8] and biomass[9–11] can be resource for green chemicals and renewable fuels. Among the mentioned resources biomass is an abundantly available waste. Hence it is important to focus on the use of biomass as renewable feedstock for chemical and fuel synthesis. The human society has grown with the emergence and establishment of fossil fuel since the beginning of industrial era. Therefore, the first major challenge of biomass chemistry is establishing a set of chemicals which can be used in the same way as fossil fuels.

Most plants cultivated by humans contain edible or inedible components. While the use of edible portion, such as corn or rice, for chemical synthesis comes with ethical implications of food scarcity, the use of inedible portion is suitable for biorefinery application. Inedible components such as wheat stalk, corncob, bagasse are agricultural waste and that are abundantly obtained without the need of separate real estate for their production.

1.2 Composition of plant-based crop waste

Terrestrial plant biomass is mainly composed of lignocellulose, having 30–50 % cellulose, 25–30 % hemicellulose, 15–20 % lignin and a small fraction of proteins, amino acids, and other minor components. Several methods are used for fractionation of cellulose, hemicellulose, and lignin and their chemistry is studied in commercially available purified samples. Further advances in reducing the cost and energy consumption of fractionation are required for their implementation.

Based on the composition, cellulose is the most abundant biopolymer in lignocellulose. The basic building block of cellulose are polymeric chains consisting of β-D-glucose linked through a β-1,4-glycosidic bonds (Figure 1.1). Intra chain hydrogen bonding and interchain hydrogen bonding links adjacent chains to make sheets, which stack together to become a layered three-dimensional structure. The three-dimensional network of hydrogen bonding polymeric chains makes cellulose a crystalline material.

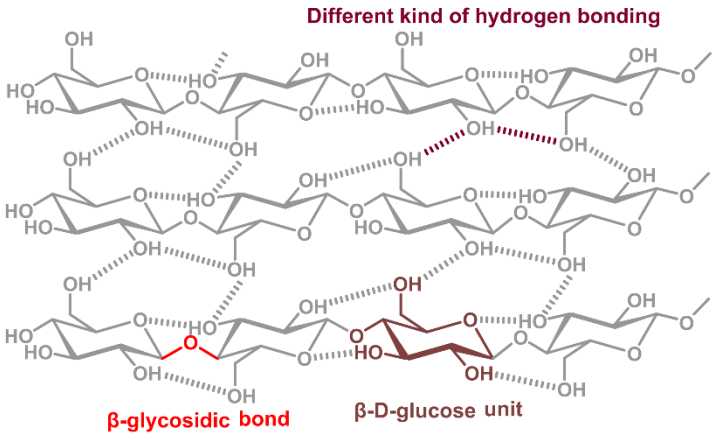

Figure 1.1. Cellulose structure.

Hemicellulose on the other hand is a branched heteropolymer. It can either have a backbone of xylose called xylan or alternating units of hexoses like mannose, glucose, and galactose. Hemicelluloses also has side chains with different sugar units and linkages

(Figure 1.2). Unlike cellulose, hemicellulose consists of only 50 – 3000 sugar units, and the branched structure makes it amorphous and relatively easy to process compared to cellulose.

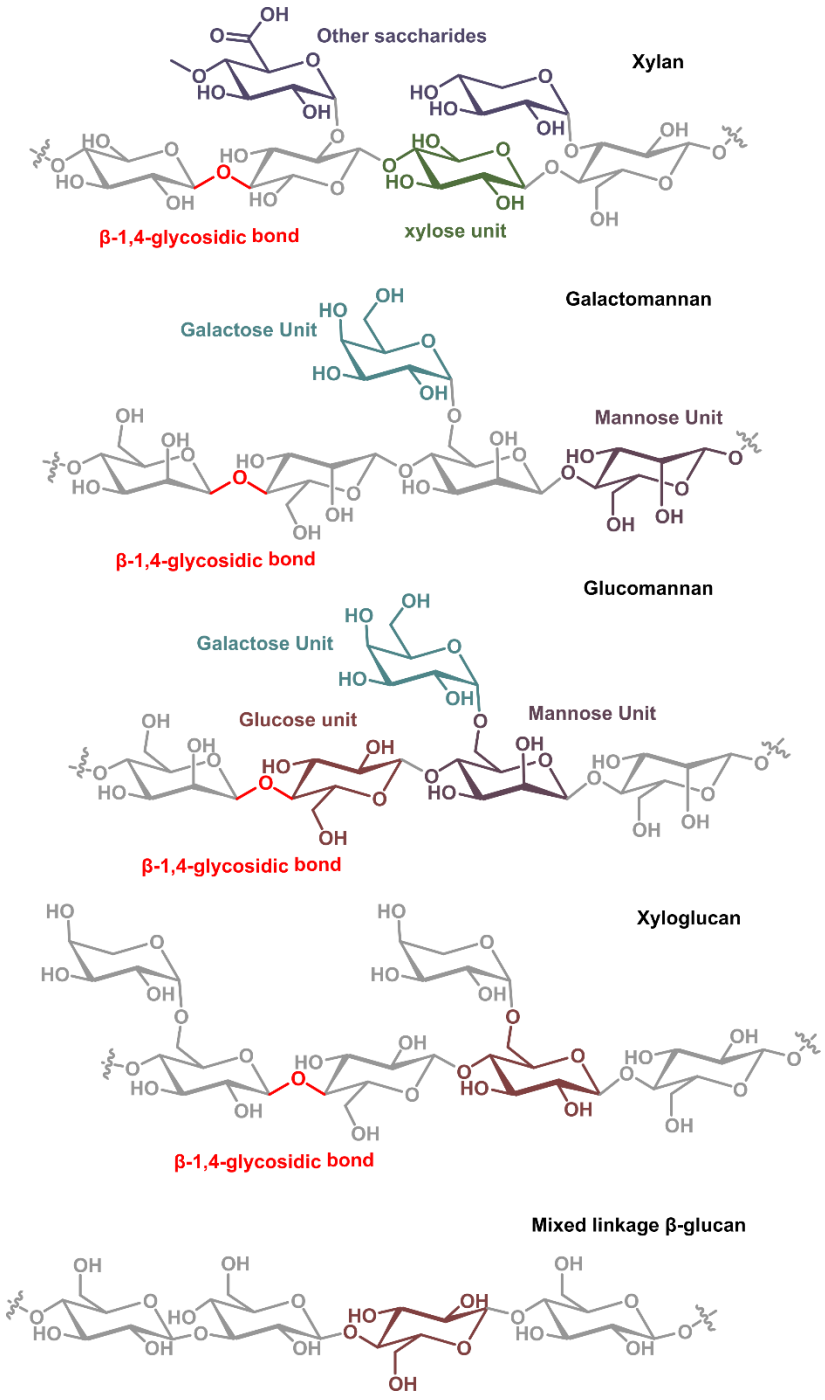

Figure 1.2. Structure of various types of hemicellulose.

Lignin is a crosslinked aromatic polymer of three monomers derived from phenylpropane structure, namely coniferyl alcohol, synapyl alcohol and paracoumaryl alcohol (Figure 1.3).

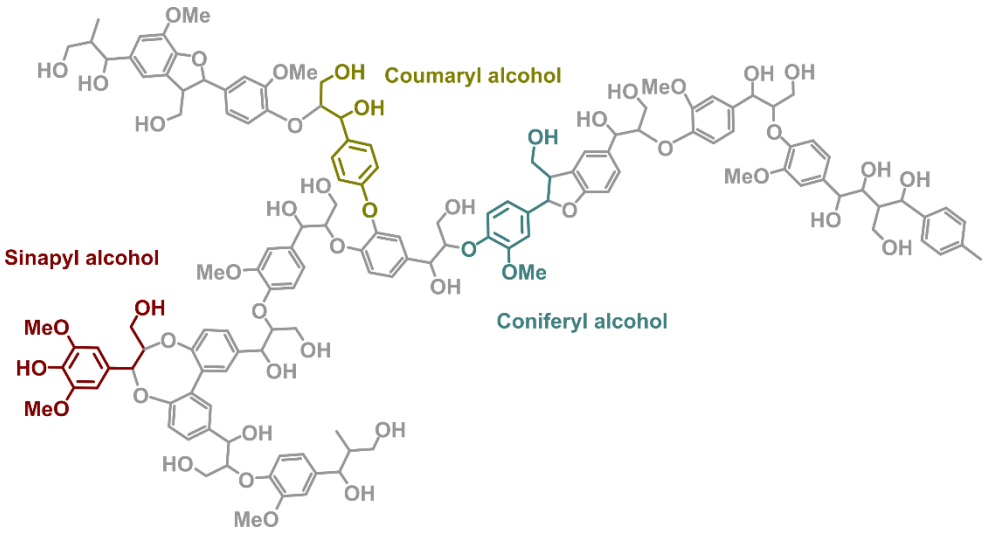

Figure 1.3. Structure of lignin

Given the poly aromatic nature of lignin, it is less reactive compared to cellulose and hemicellulose. Hence, cellulose and hemicellulose chemistry are much more explored compared to lignin. In this thesis chemicals that can be obtained from cellulose and hemicellulose derived compounds are studied.

1.3 Platform chemicals from cellulose and hemicellulose

Chemicals derived from fossil fuels range have a wide range of carbon number from two carbon ethylene to dodecane consisting of 12 carbon atoms.[12] With the long history of fossil fuel extraction and cracking, Industrial production and fractionation of chemicals by carbon number is now straightforward.

However, chemical synthesis of sugars is still developing and only a narrow range of compounds can be produced. Figure 1.4 shows a list of useful chemicals that can be obtained from cellulose and hemicellulose. Cellulose can be hydrolyzed to glucose which

serves as a precursor to other six carbon chemicals.[13–17] Glucose can be isomerized either in presence of acids or bases to fructose or mannose.[18–20] These sugars can be dehydrated to form furanic compounds like 5-hydroxymethylfurfural[21] and furfural[22] or levulinic acid,[23] which are all precursors to other bulk or fine chemicals. Alternatively, sugars can be hydrogenated to sugar alcohols such as sorbitol and mannitol.[24,25] These alcohols can be further dehydrated to form isosorbide[26] and isomannide,[27] which are used in the synthesis of polycarbonates. Hydrodeoxygenation of sugar alcohols can produce either terminal alcohols which are fuel additives[28] or alkanes which can be directly used as fuel.[29] Oxidative transformation of glucose produces gluconic acid,[30] glucaric acid[31] etc. having niche applications.

Like hexoses, xylose can be dehydrated to furfural,[32] hydrogenated to xylitol,[33] and oxidized to xylonic acid.[34] Furfural can be transformed to a variety of C5 chemicals like cyclopentanone,[35] methyl furan,[36] furfuryl alcohol,[37] tetrahydrofurfuryl alcohol,[38] methyl tetrahydrofuran,[39] 1,4 or 1,2-pentane diols etc.[38] Xylitol also serves as a food additive[38] and a precursor to pentane and 1,2-pentane diols.[38]

Unlike hexoses and pentoses, tetroses are not abundant in biomass. Consequently, C4 carbon chemicals are not directly produced from biomass. Erythritol can be produced via retro aldol condensation of either C6 sugars or sugar alcohols.[40,41] The selectivity control of the process is still a challenge. Erythritol is then converted to 1,4-butanediol, butanol, and even n-butane by hydrodeoxygenation. Alternate method of C4 chemical synthesis is the C-C bond cleavage of furfural in an oxidative or reductive reaction.[42,43] However, these reaction are not easily controlled and product selectivity is low.

C3 range of products can be obtained either directly from sugars or from sugar alcohols via retro aldol condensation in tandem with other type of elementary reaction

steps. For instance, lactic acid can be formed from glucose or fructose over base catalyzed retro aldol reactions, which can be further reacted to acrylic acid and pyruvic acid.[44] Glycerol obtained as a byproduct of biodiesel synthesis is also an abundant source of bioderived C3 Chemicals. Retro aldol reaction of sugar alcohols produces ethylene glycol a bulk C2 chemical.[44] Similar C-C cleavage reaction can produce acetic acid, ethanol, and oxalic acid. In addition, bio-ethanol produced by fermentation is also a source of C2 chemicals.

Therefore, the synthesis of C6 and C5 compounds is straightforward from sugars without the need for C-C bond cleavage. Abundant alternative sources such as glycerol and bioethanol are available for synthesis of C3 and C2 compounds. The largest gap in replacing fossil derived chemical lies in production of C4 chemicals such as butadiene, butanediol, tetrahydrofuran, and succinic acid etc. Formation of these chemicals require several reaction steps along with C-C cleavage to reduce carbon number.

This thesis discusses catalyst design for reaction that leads to conversion of abundantly available glucose and xylose to C4 compounds such as succinic acid and γ-butyrolactone. Chapter 2 investigates isomerization of glucose to fructose, which is an aldose to ketose conversion. This reaction is crucial for synthesis of furanic precursors such as 5-hydroxymethyl furfural and furfural. Chapter 3 deals with oxidation of furfural, derived from pentose or hexoses to succinic acid a C4 value added chemical and precursor. Chapter 4 utilizes succinic acid as a C4 precursor to produce γ-butyrolactone, which a green solvent as well as substrate for synthesis of pyrrolidone derivatives. The following sections will discuss the current state of art for these reactions along with gap in knowledge and technological shortcomings.

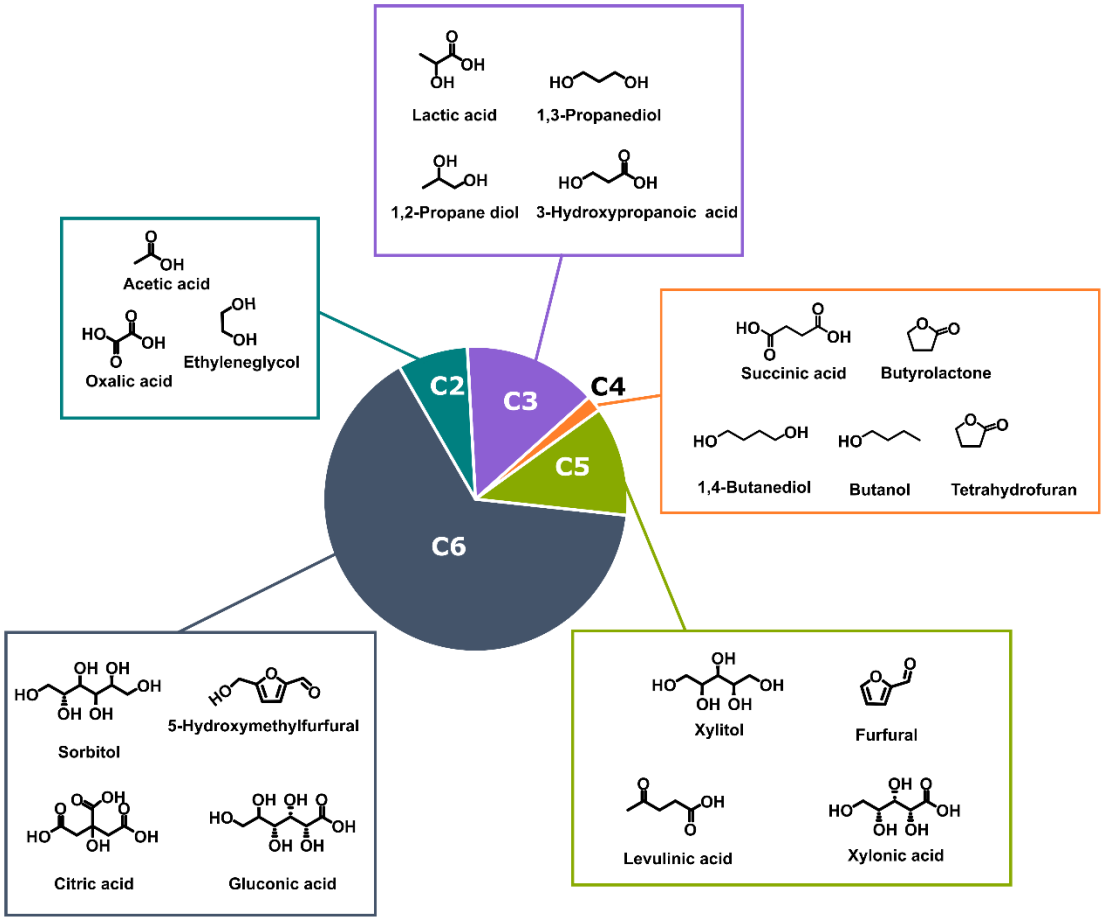

Figure 1.4. Relative industrial production of biobased chemicals classified based on the number of carbon atoms. The total production all biobased chemicals shown in this scheme is 4260 kilotonnes per anum (kta). This figure highlights the difficulty in synthesis of crucial C4 chemicals because of the lack of a suitable platform chemical as feedstock. Data for this figure was obtained from a report by International Energy Agency.[45]

1.4 Glucose isomerization to fructose

Glucose is the monomer of cellulose polymer and is obtained as the primary product upon hydrolysis. Although, glucose can be directly converted to chemicals like

sorbitol[24,25] and ethylene glycol,[44] its isomerization to fructose is the first step for formation of furanic compounds such as 5-hydroxymethyl furfural (HMF) and furfural. Fructose is also much more reactive than glucose owing to its furanose structure. Consequently, glucose isomerization to fructose holds a key role in shaping the future of biomass derived chemicals.

1.4.1 Reaction mechanism

Glucose and fructose have a 6-membered ring pyranose form and a 5-membered furanose form, respectively along with open chain form in solution. The isomerization step, occurring in open chain form, involves the change in position of the carbonyl group from C1 position in glucose to C2 position in fructose (Scheme 1.1).

The change can be brought about in two different reaction mechanisms. The first mechanism involves an internal Meerwein-Ponndorf-Valery (MPV) reduction between the aldehyde group at C1 position and the alcohol group in the C2 position (Scheme 1.1a). This mechanism requires presence of Lewis acids, which facilitate a 1,2-hydride shift. In the second mechanism, termed as Lobry de Bruyn–Alberda van Ekenstein (LdB–AvE) mechanism, formation of a tautomeric ene-diol is facilitated by a base with abstraction of α-hydrogen atom (Scheme 1.1b). Fructose formation happens when there is an exchange of hydrogen atom between the diol groups along with recovery of one proton from the base.

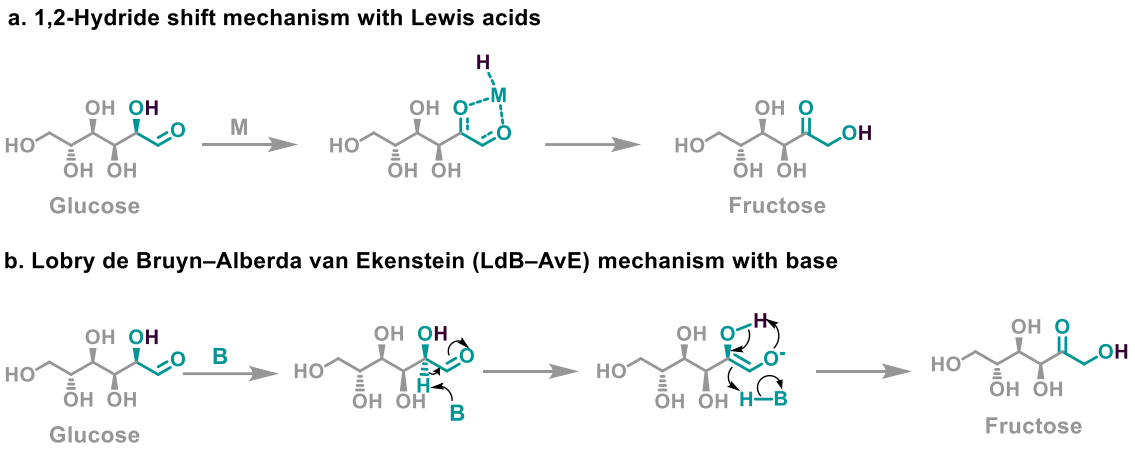

Scheme 1.1. Two different mechanism of glucose isomerization.

1.4.2 Catalyst design approaches in the literature

Catalysts used for glucose isomerization promote one of the above two mechanism. The earliest known catalysts for this process are naturally occurring enzymes. Many kinds of bacteria contain xylose isomerase which despite its name also catalyzes the isomerization of glucose to fructose. Xylose isomerase[46] was in shadows for a while after its discovery until the synthesis of immobilized xylose isomerase[47], which is the industrial catalyst for this process. However, the enzymatic process is quite condition specific and not suitable for integration with other downstream processes in a biorefinery. As a result, catalysts were designed to emulate the working principles of xylose isomerase. Initially, it was believed that the base sites in the cystine ligands were the active sites. Subsequently, advanced characterization techniques revealed role of cations, which led to the discovery of Lewis acid catalysts.

The development of the base catalysts started before the discovery of the the immobilized enzyme. Thinking of base catalysts one would expect to use inorganic bases like alkali or alkaline metal hydroxides, carbonates or phosphates etc. as homogeneous catalysts.[48] While moderate yields up to 29 % of fructose has been obtained with such

bases, they also catalyze the retro aldol reaction of sugar owing to their strong Brønsted basicity (Table 1.1).[48] There has been few attempts to add borates or aluminates during reaction to make a complex and prevent the ketose from undergoing retro aldol reaction.[49,50] Weaker Lewis bases such as amines and amino acids[51] have also shown moderate success as homogeneous catalysts for glucose isomerization.

Heterogeneous base catalysts are recyclable and environment friendly in comparison to their homogeneous counterparts. Basic anion exchange resins have shown good activity, however they are sensitive to reaction condition used.[53] Immobilized organic amines or organo-ammonium salts are a class of heterogenized homogeneous catalyst, which yields up to 41 % fructose.[62–64] Polymeric organic amines also show similar activity.[66] Metal oxides like ZrO_2 and TiO_2 show moderate activity, as they possess weak base sites. Doped metal oxides, for example MgO doped ZrO_2, improve the intrinsic activity of metal oxides, but the product yields are far from the equilibrium that can be achieved by the enzymes.[54,55] Alkali or alkaline earth metal silicates show similar moderate activity as the metal oxides.[56] Commercial hydrotalcites as well as other modified hydrotalcites have proven to be active catalysts in alcohol media, with fructose yields of up to 63 %.[57–61] Zr carbonates and hydroxides can be regarded as solid bases as they are insoluble in water.[65] They possess moderate activity for glucose isomerization reaction.

Compared to base catalyzed glucose isomerization reaction, literature about acid catalyzed glucose isomerization was quite scares until recently. Brønsted acids do not catalyze this reaction instead they tend to cause dehydration reaction to produce levoglucosan. Metal chlorides acting as homogeneous Lewis acid catalysts showed some activity for glucose isomerization but they were not effective to achieve high fructose

selectivity.

Table 1.1. Classification of catalysts used for glucose isomerization reaction showing glucose conversion and fructose yield achieved.

Catalyst classification	Catalyst(s)	Conv.(Yield) %
Enzyme	Immobilized xylose isomerase [47] (commercial catalyst)	48 (48)
Homogeneous base	Alkaline carbonate, hydroxide, phosphate, and sulfate [48]	32–100 (23–29)
	Metal borates and aluminates + Strong Brønsted bases [49,50]	(90)
	Al_2O_3 in pyridine solution [52]	46–59 (36–43)
	Different kind of amines [51]	43–62 (17–31)
	Amino acids (Arginine) [51]	41 (31)
Heterogeneous base	Basic anion exchange resins [53]	65–90 (44–72)
	Metal oxides and doped metal oxides [54,55]	25–80 (5 – 21)
	Alkaline metallosilicates [56]	27–56 (20-39)
	Hydrotalcites [57–61]	10–65 (10–63)
	Immobilized organic amine [62–64]	3–55 (1-41)
	Zirconium carbonate, hydroxide [65]	28–47 (12 – 34)
	Hydrotalcite, Amberlyst A21 and A26 [65]	26–53 (19-24)
	Polymeric organic amines [66]	53 (41)
Homogeneous acid	Metal salts [67]	30–70 (25–35)
Heterogeneous Lewis acid	Metal (IV) phosphates [68]	40 (1 – 90)
	Metal (IV) in zeolite framework [68–73]	56 (33)
	H-form of beta, Y, and USY zeolites [74]	11–72 (0 – 55)

Conventional Lewis acids does not isomerize glucose in aqueous solution, as they lose Lewis acidity as soon as they come in contact with water. Initial heterogeneous Lewis

acid catalysts to be used for the process were phosphates of metals like tin and zirconium.[68] The discovery of a catalyst with Sn in the framework of pure silica Beta zeolite was a turning point for Lewis acid catalyzed isomerization of glucose.[18] It was reported that due to microporous nature of the zeolites, the framework Sn sites, or the small extra framework clusters were confined in hydrophobic environment and hence, the Lewis acidity remained. After the first report, the interest in Lewis acid catalyzed isomerization of glucose increased dramatically owing to high selectivity obtained and the possibility of catalyzing simultaneous downstream reactions.[75,76]

Sn containing zeolites are durable, recyclable and easily recoverable (organic deposits and other substances can be easily removed by a simple calcination). The most advantageous property of the catalyst is its wide range of working conditions, which is favorable for integration with downstream processing. However, original method for synthesis of Sn-Beta catalysts required long synthesis time.[77] This was overcome by development of solid-state post synthesis procedures.[78] In this method, dealumination of the commercial beta zeolite is performed to create vacancies which are filled by adding tetravalent metal precursors and annealing. However, in Sn-Beta zeolites Sn sites are present as framework atom. All of Sn sites are not available for reaction. Therefore, future studies should focus on creation of these sites on surface of catalyst.

1.5 Furfural Oxidation to succinic acid

Furfural is a five-carbon furanic compound with an aldehyde group. It can be obtained by isomerization and dehydration of xylose[22,79–81] and from fructose through elimination of a carbon atom.[32,82–84] Therefore it is feasible to synthesize furfural from both cellulose and hemicellulose fractions of biomass. In addition, furfural has high reactivity and is therefore suitable as a precursor for synthesis of C4 chemicals.

Conversion of furfural to succinic acid (SA) is promising method to produce bio-succinic acid (Scheme 1.2). Succinic acid has the potential to replace the use of petrochemical based C4 chemicals. It can be directly used as a C4 building block[85], for synthesis of polyesters[86–88], polyurethane[89], cosmetics[90,91] and pharmaceuticals[92–95], and as precursors to other fine chemicals like 1,4-BDO[96,97], vinyl pyrrolidone[98], and succinamide[99]. Until now bacterial fermentation of C6 sugars with the help of bovine rumen bacteria is the most successful method for synthesis of bio-succinic acid.[100] Although bacterial fermentation provides succinic acid in good selectivity, its industrial application has not been successful due to high operation cost.[101] Consequently, catalytic pathways for succinic acid synthesis are desired.

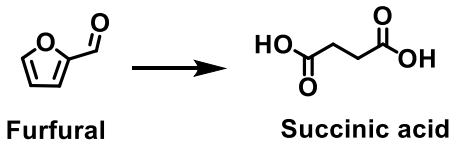

Scheme 1.2. Succinic acid synthesis reaction scheme from biomass derived furfural.

1.5.1 Reaction pathway and nature of elementary reactions involved

Scheme 1.3 shows a probable reaction pathway of furfural oxidation to succinic acid. The first elementary step of the reaction is Baeyer-Villiger oxidation of furfural to form a furan-2-yl formate, which is hydrolyzed to furan-2-ol and formic acid. The furan-2-ol is converted to 2(3H)-furanone, which then can undergo hydrolytic ring opening and oxidation to succinic acid.

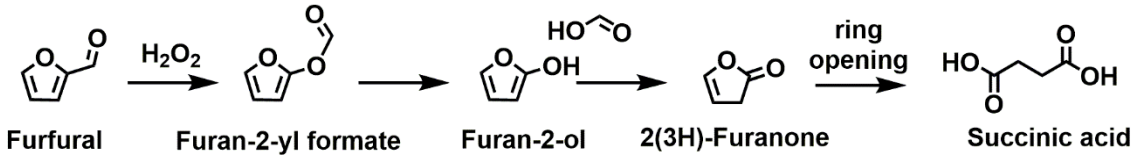

Scheme 1.3. A probable reaction pathway for furfural oxidation to succinic acid.

1.5.2 Catalyst design approach in literature

Table 1.2 shows list of publications, that use H_2O_2 for catalytic oxidation of furfural to succinic acid. Choudhary et al. first reported use of heterogeneous catalyst for the process.[42,102] They studied the role of sulfonates with Brønsted acid sites in vicinity of aromatic group for furfural oxidation to succinic acid.[42,102] Amberlyst-15 was best performing catalyst among several Brønsted acid catalysts. The authors hypothesized that aromatic rings in catalyst framework have a π-π interaction with furfural and stabilize the ring from opening in oxidizing conditions, hence leading to higher succinic acid selectivity of 72 % at full conversion. Following these finding a similar report was published by Zhu and co-workers,[103] where sulfonated graphene oxide was use to yield 88 % succinic acid at full furfural conversion.

Table 1.2 . Furfural to succinic acid production in literature

Nature of catalyst	Catalyst	Conv. / yield (%)
Sulfonic acid group in vicinity of aromatic group	Amberlyst 15[42,102]	72
	Sulphonated graphene oxide[103]	88

These catalysts have a carbon framework and cannot be reactivated by calcination, which is a prerequisite for furfural chemistry owing to catalyst deactivation due to organic deposition. Hence, future research in this topic should focus on designing reusable catalysts.

1.6 Succinic acid hydrogenation to GBL

Bio-succinic acid can serve as an entry point for the synthesis of other C4 chemicals. γ-Butyrolactone (GBL) is a promising solvent that can be obtained from succinic acid.

GBL is proposed as a safe electrolyte in Li^+ ion batteries and capacitors, because of its high flash point (98 °C) and particularly high ability to solubilize Li^+ ions.[104] Due to its polarity, it can be used as polar aprotic solvent instead of hazardous chlorinated solvents.[105–107] Low melting point (-43.5 °C) and high boiling point (204 °C) makes it a green solvent in photosensitive resins synthesis.[108,109] In addition, GBL is used for production of 2-pyrrolidone (2P), N-methyl-2-pyrrolidone (NMP), N-vinyl-2-pyrrolidone (NVP) in a commercial scale.[110] It is recently reported that ring opening polymerization of GBL forms a polymer, which can be easily recycled by simple heat treatment in the range of 200 °C to 300 °C.[111,112] The above discussed properties make GBL a commercially important C4 chemical.

GBL is industrially produced via Reppe process (Scheme 1.4), by oxidative dehydrogenation of fossil fuel based 1,4-butane diol over copper catalyst.[113] The reaction is suggested to proceed through formation of an oxyaldehyde by dehydrogenation of one of the terminal alcohol groups. The oxyaldehyde then undergoes intramolecular acetalization, followed by dehydrogenation to form the lactone. Alternatively, GBL can be produced by hydrogenation of fossil fuel based maleic acid or maleic anhydride.[113] However, a suitable biobased method, if developed, can help in reduction in carbon footprint. In this regard, hydrogenation of succinic acid is promising because it structurally similar to maleic acid and a biobased feedstock.

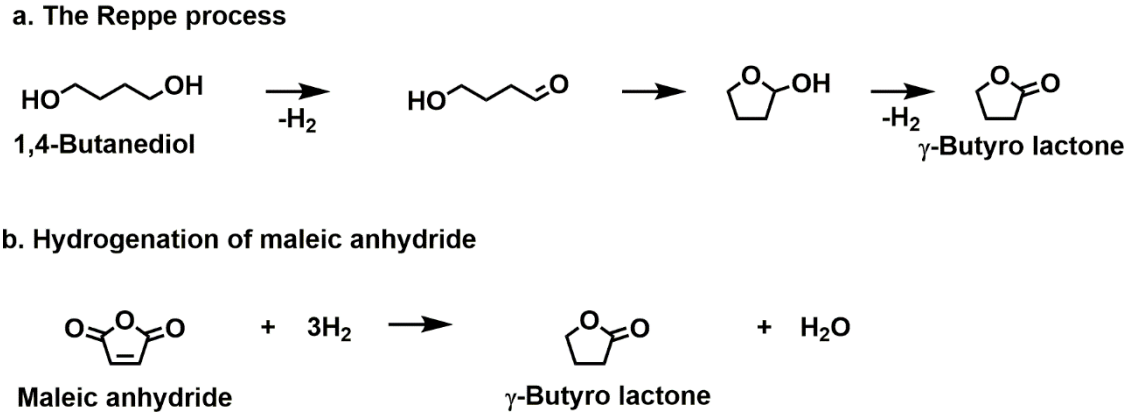

Scheme 1.4. Industrial production methods of GBL

1.6.1 Catalyt design approaches for succinic acid hydrogenation to GBL

The elementary reaction steps involved in this reaction are hydrogenation of a carboxylic acid group to an alcohol group and dehydration cyclization of the hydroxy alcohol to lactone (Scheme 1.5). While metal catalyst can catalyze hydrogenation of carboxylic acid with H_2, acid sites are needed for the dehydration reaction. However, due to factors like low stability of γ-hydroxy acids, the possibility of non-catalytic dehydration cyclization cannot be ignored. Catalyst design for the reaction is based on these basic facts.

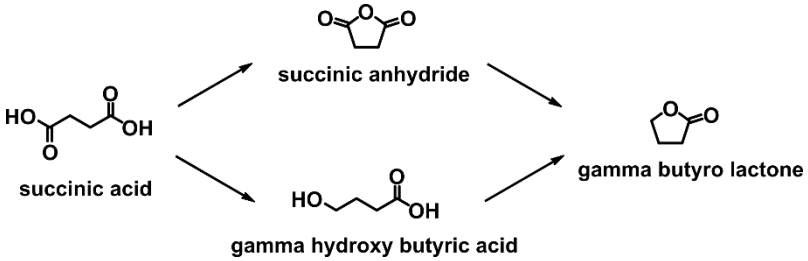

Scheme 1.5. Succinic acid hydrogenation to GBL through different pathways

Selective hydrogenation of SA to GBL competes with C-C bond breaking under hydrogenation reaction conditions to produce propionic acid and other smaller alkanes. In addition, further conversion of GBL to THF or BDO can also occur. Hence the number

of studies intending to selectively produce GBL are limited (Table 1.3). SA hydrogenation to GBL proceeds through a γ-hydroxybutyric acid intermediate after hydrogenation of one of the carboxylic acid group, which then cyclizes to GBL. In some of the studies, a succinic anhydride intermediate is hypothesized.[114,115] This reaction pathway is possible in presence of an acidic support in non-aqueous condition, which promotes dehydration of succinic acid. The authors showed that, combination of alumina xerogels, hydrothermally engineered to have higher acidity, with supported palladium metal results in succinic acid hydrogenation to GBL. In the same study, corresponding ruthenium catalyst led to complete hydrogenation of succinic anhydride to form THF and other side products. In another study, Pd on a alumina support prepared via coprecipitation was used to hydrogenate succinic acid to GBL with 89% selectivity with 70% conversion at 170 °C.[116] Selective reduction of one of the carbonyl groups of succinic acid is hypothesized to be the key factor to produce GBL from succinic acid over palladium. Atomically dispersed Pd/AlOOH exhibited 1100 times higher activity (turn over frequency) compared to that of supported palladium clusters catalyst on alumina.[117] The increase in activity was attributed to the higher adsorption energy of Pd on Al(100) planes. Apart from alumina supported palladium catalysts, titanium supported palladium catalyst also produces GBL as the main product in succinic acid hydrogenation.[118] Pd on amine functionalized silica support, shows better activity compared to Pd supported on normal silica support.[119] The catalyst was highly selective to produce 94% GBL with 100% conversion. Apart from palladium catalysts, gold over titania was also reported to produce GBL directly from succinic acid.[120] Addition of slight amount of platinum to gold provided better hydrogen dissociation activity to gold catalyst increasing its catalytic activity.

Table 1.3. Comparision of reports on succinic acid hydrogenation to GBL

Catalyst	Reaction conditions	$S_{GBL}(C)^b$
5 wt % Pd/AX [a]	0.2 g of SA in dioxane, 240 °C, 6 MPa, 4h	71(76)[114,115]
5 wt % Pd/Al_2O_3	15 mL of 0.2 M SA in 1,4-dioxane, 2 mol. % metal with respect to SA, 170 °C, 3 MPa H_2	89[116]
0.2 wt %Pd/Al_2O_3	0.4 g of SA and 0.2 g of catalyst in 40 ml of 1,4-dioxane at 513 K, 6 MPa, 7h	98.0(75.5)[121]
1 wt % Au/TiO_2	12 mmol of succinic anhydride, 50 mL of dioxane, 0.2 g of catalyst, 240 °C,5MPa, 800 mg of molecular sieve	97 (97)[122]
2 wt.% Pd/TiO_2	5 wt. % SA in water, 1g of catalyst, 160°C, 15MPa, 48h	95(100)[123]
Pd/SiO_2-NH_2	0.2 g catalyst, 0.4 g SA, 30 ml 1,4-dioxane, 4 h 240°C and 60 bar for 4 h.	94(100)[119]

[a]Alumina xerogel, [b]C stands for conversion

All of the above-mentioned reports use harsh reaction conditions. Additionally, most of them use 1,4-dioxane as solvent because the catalysis is dependent on use of acidity or basicity of support. Hence, future research should focus on development of catalysts with mild operating conditions and water as green solvent. Additionally, metals cheaper than palladium and gold should be employed.

1.7 Arrangement of the thesis

This thesis starts with a focus on synthesis of a catalyst for isomerization of glucose to fructose in Chapter 2. In this chapter, tetrahedrally coordinated Sn sites with Lewis acidic character were incorporated on the surface of silica containing materials and used for glucose isomerization reaction. Characterizations showed that different support properties affect the properties of surface Sn sites. Silica with abundant hydroxyl groups promoted the stabilization Sn sites which increased the activity and stability of catalyst.

Chapter 3 deals with oxidation of furfural, which is obtained from xylose or fructose, to succinic acid a biobased C4 platform chemical. This chapter discusses the difference

between Lewis acidic character of Sn and Ti incorporated zeolites and compares the role of other active sites on product selectivity. A detailed mechanism for this reaction is proposed, which is supported by identification of key intermediates, pseudo-first-order kinetic modeling, and study on catalyst substrate interaction.

Chapter 4 deals with influence of V_2O_3 support on catalytic hydrogenation of succinic acid to γ-butyrolactone. Ruthenium on V_2O_3 support showed higher activity compared to V_2O_5, SiO_2 and Al_2O_3 supports. Characterization showed presence of catalyst in strong metal-support interaction. Favorable adsorption mode of succinic acid on interface between ruthenium and V_2O_3 and possibly role of the later in C-O bond cleavage led to higher reaction rate. A mechanism has been proposed for the reaction to explain higher activity of ruthenium on V_2O_3 for succinic acid hydrogenation.

1.8 References

(1) Joselin Herbert, G. M.; Iniyan, S.; Sreevalsan, E.; Rajapandian, S. *Renewable Sustainable Energy Rev.* **2007**, *11* (6), 1117–1145.

(2) Rabaia, M. K. H.; Abdelkareem, M. A.; Sayed, E. T.; Elsaid, K.; Chae, K. J.; Wilberforce, T.; Olabi, A. G. *Sci. Total Environ.* **2021**, *754*, 141989.

(3) Chidambaram, P. K.; Thamilarasan, K.; Barath Kumar, J.; Auxcilia Mary, L. *Mater. Today Proc.* **2021**, https://doi.org/10.1016/j.matpr.2020.12.1242

(4) Crabtree, R. H. *Chem. Rev.* **2002**, *95* (4), 987–1007.

(5) Saha, D.; Grappe, H. A.; Chakraborty, A.; Orkoulas, G. *Chem. Rev.* **2016**, *116* (19), 11436–11499.

(6) Schwach, P.; Pan, X.; Bao, X. *Chem. Rev.* **2017**, *117* (13), 8497–8520.

(7) Ye, R. P.; Ding, J.; Gong, W.; Argyle, M. D.; Zhong, Q.; Wang, Y.; Russell, C. K.; Xu, Z.; Russell, A. G.; Li, Q.; Fan, M.; Yao, Y. G. *Nat. Commun.*, **2019**, 10, 1-15

(8) Gao, P.; Zhang, L.; Li, S.; Zhou, Z.; Sun, Y. *ACS Cent. Sci.* **2020**, *6* (10), 1657–1670.

(9) Huber, G. W.; Iborra, S.; Corma, A. *Chem. Rev.* **2006**, 106 (9), 4044–4098.

(10) Mika, L. T.; Cséfalvay, E.; Németh, Á. *Chem. Rev.* **2018**, 118 (2), 505–613.

(11) Besson, M.; Gallezot, P.; Pinel, C. *Chem. Rev.* **2014**, *114* (3), 1827–1870.

(12) Lesueur, D. *Adv. Colloid Interface Sci.* **2009**, *145* (1–2), 42–82.

(13) Shrotri, A.; Kobayashi, H.; Kaiki, H.; Yabushita, M.; Fukuoka, A. *Ind. Eng. Chem. Res.* **2017**, *56* (49), 14471–14478.

(14) Shrotri, A.; Kobayashi, H.; Fukuoka, A. *Acc. Chem. Res.* **2018**, *51* (3), 761–768.

(15) Kobayashi, H.; Komanoya, T.; Hara, K.; Fukuoka, A. *ChemSusChem* **2010**, *3* (4), 440–443.

(16) Shrotri, A.; Kobayashi, H.; Fukuoka, A. *ChemCatChem* **2016**, *8* (6), 1059–1064.

(17) Komanoya, T.; Kobayashi, H.; Hara, K.; Chun, W. J.; Fukuoka, A. *Appl. Catal. A Gen* **2011**, *407*, 188–194.

(18) Moliner, M.; Roman-Leshkov, Y.; Davis, M. E. *Proc. Natl. Acad. Sci.* **2010**, *107* (14), 6164–6168.

(19) Palai, Y. N.; Shrotri, A.; Asakawa, M.; Fukuoka, A. *Catal. Today* **2020**, *365*, 241-248.

(20) Yabushita, M.; Shibayama, N.; Nakajima, K.; Fukuoka, A. *ACS Catal.* **2019**, *9* (3), 2101–2109.

(21) Noma, R.; Nakajima, K.; Kamata, K.; Kitano, M.; Hayashi, S.; Hara, M. *J. Phys. Chem. C* **2015**, *119* (30), 17117–17125.

(22) Asakawa, M.; Shrotri, A.; Kobayashi, H.; Fukuoka, A. *Green Chem.* **2019**, *21* (22), 6146–6153.

(23) Kruger, J. S.; Choudhary, V.; Nikolakis, V.; Vlachos, D. G. *ACS Catal.* **2013**, *3* (6), 1279–1291.

(24) Zhang, X.; Durndell, L. J.; Isaacs, M. A.; Parlett, C. M. A.; Lee, A. F.; Wilson, K. *ACS Catal.* **2016**, *6* (11), 7409–7417.

(25) Yin, W.; Tang, Z.; Venderbosch, R. H.; Zhang, Z.; Cannilla, C.; Bonura, G.; Frusteri, F.; Heeres, H. J. *ACS Catal.* **2016**, *6* (7), 4411–4422.

(26) Sun, P.; Yu, D. H.; Hu, Y.; Tang, Z. C.; Xia, J. J.; Li, H.; Huang, H. *Korean J. Chem. Eng.* **2011**, *28* (1), 99–105.

(27) Yokoyama, H.; Kobayashi, H.; Hasegawa, J. Y.; Fukuoka, A. *ACS Catal.* **2017**, *7* (7), 4828–4834.

(28) Liu, L.; Cao, J.; Nakagawa, Y.; Betchaku, M.; Tamura, M.; Yabushita, M.; Tomishige, K. *Green Chem.* **2021**, *23* (15), 5665–5679.

(29) Stalpaert, M.; Janssens, K.; Marquez, C.; Henrion, M.; Bugaev, A. L.; Soldatov,

A. V; De Vos, D. *ACS Catal.* **2020**, *10* (16), 9401–9409.

(30) Onda, A.; Ochi, T.; Kajiyoshi, K.; Yanagisawa, K. *Appl. Catal. A Gen* **2008**, *343*, 49–54.

(31) Liu, W. J.; Xu, Z.; Zhao, D.; Pan, X. Q.; Li, H. C.; Hu, X.; Fan, Z. Y.; Wang, W. K.; Zhao, G. H.; Jin, S.; Huber, G. W.; Yu, H. Q. *Nat. Commun.*, **2020**, *11*, 1–11.

(32) Gupta, N. K.; Fukuoka, A.; Nakajima, K. *ACS Catal.* **2017**, *7* (4), 2430–2436.

(33) Wisniak, J.; Hershkowitz, M.; Leibowitz, R.; Stein, S. *Ind. Eng. Chem. Prod. Res. Dev.* **1974**, *13* (1), 75–79.

(34) Li, Z.; Huang, Y.; Chi, X.; Li, D.; Zhong, L.; Li, X.; Liu, C.; Peng, X. *Green Energy Environ.* **2021,** https://doi.org/10.1016/j.gee.2021.01.004.

(35) Hronec, M.; Fulajtarová, K. *Catal. Commun.* **2012**, *24*, 100–104.

(36) Sitthisa, S.; An, W.; Resasco, D. E. *J. Catal.* **2011**, *284* (1), 90–101.

(37) Kijeński, J.; Winiarek, P.; Paryjczak, T.; Lewicki, A.; Mikolajska, A. *Appl. Catal. A Gen* **2002**, *233*, 171–182.

(38) Nakagawa, Y.; Tamura, M.; Tomishige, K. *Catal. Surv. Asia.*, **2015**, *19*, 249–256.

(39) Dong, F.; Zhu, Y.; Ding, G.; Cui, J.; Li, X.; Li, Y. *ChemSusChem* **2015**, *8* (9), 1534–1537.

(40) Yazdani, P.; Wang, B.; Rimaz, S.; Kawi, S.; Borgna, A. *Mol. Catal.* **2019**, *466*, 138–145.

(41) Zheng, M.; Pang, J.; Sun, R.; Wang, A.; Zhang, T. *ACS Catal.* **2017**, *7* (3), 1939–1954.

(42) Choudhary, H.; Nishimura, S.; Ebitani, K. *Appl. Catal. A Gen* **2013**, *458*, 55–62.

(43) Biradar, N. S.; Hengne, A. A.; Birajdar, S. N.; Swami, R.; Rode, C. V. *Org. Process Res. Dev.* **2014**, *18* (11), 1434–1442.

(44) Wang, X.; Song, Y.; Huang, C.; Liang, F.; Chen, B. *Green Chem.* **2014**, *16* (9), 4234–4240.

(45) De Jong, E.; Stichnothe, H.; Bell, G.; Jorgensen, H. *Bio-Based Chemicals: A 2020 Update*; IEA Bioenergy, February 2020.

(46) Mitsusashi, S.; Lampen, J. O. *J. Biol. Chem.* **1953**, *204* (2), 1011–1018.

(47) Jokela, J.; Pastinen, O.; Leisola, M. *Enzyme Microb. Technol.* **2002**, *31* (1–2), 67–76.

(48) Gottfried, J. B.; Benjamin, D. G. *Ind. Eng. Chem.* **1952**, *44* (1), 141–145.

(49) Mendicino, J. F. *J. Am. Chem. Soc.* **2002**, *82* (18), 4975–4979.

(50) Despax, S.; Estrine, B.; Hoffmann, N.; Le Bras, J.; Marinkovic, S.; Muzart, J.

Catal. Commun. **2013**, *39*, 35–38.

(51) Liu, C.; Carraher, J. M.; Swedberg, J. L.; Herndon, C. R.; Fleitman, C. N.; Tessonnier, J.-P. *ACS Catal.* **2014**, *4* (12), 4295–4298.

(52) Ekeberg, D.; Morgenlie, S.; Stenstrøm, Y. *Carbohydr. Res.* **2005**, *340* (3), 373–377.

(53) Rendleman, J. A.; Hodge, J. E. *Carbohydr. Res.* **1979**, *75*, 83–99.

(54) Watanabe, M.; Aizawa, Y.; Iida, T.; Nishimura, R.; Inomata, H. *Appl. Catal. A Gen* **2005**, *295* (2), 150–156.

(55) Kitajima, H.; Higashino, Y.; Matsuda, S.; Zhong, H.; Watanabe, M.; Aida, T. M.; Smith, R. L. *Catal. Today* **2016**, *274*, 67–72.

(56) Lima, S.; Dias, A. S.; Lin, Z.; Brandao, P.; Ferreira, P.; Pillinger, M.; Rocha, J.; Calvino-Casilda, V.; Valente, A. A. *Appl. Catal. A Gen* **2008**, *339* (1), 21–27.

(57) Yu, S.; Kim, E.; Park, S.; Song, I. K.; Jung, J. C. *Catal. Commun.* **2012**, *29*, 63–67.

(58) Delidovich, I.; Palkovits, R. *Catal. Sci. Technol.* **2014**, *4* (12), 4322–4329.

(59) Lee, G.; Jeong, Y.; Takagaki, A.; Jung, J. C. *J. Mol. Catal. A: Chem.* **2014**, *393*, 289–295.

(60) Delidovich, I.; Palkovits, R. *J. Catal.* **2015**, *327*, 1–9.

(61) Moreau, C.; Durand, R.; Roux, A.; Tichit, D. *Appl. Catal. A Gen* **2000**, *193*, 257–264.

(62) Souza, R. O. L.; Fabiano, D. P.; Feche, C.; Rataboul, F.; Cardoso, D.; Essayem, N. *Catal. Today* **2012**, *195* (1), 114–119.

(63) Yang, Q.; Lan, W.; Runge, T. *ACS Sustain. Chem. Eng.* **2016**, *4* (9), 4850–4858.

(64) Yang, Q.; Zhou, S. F.; Runge, T. *J. Catal.* **2015**, *330*, 474–484.

(65) Son, P. A.; Nishimura, S.; Ebitani, K. *React. Kinet. Mech. Catal.* **2014**, *111* (1), 183–197.

(66) Yang, Q.; Runge, T. *ACS Sustain. Chem. Eng.* **2016**, *4* (12), 6951–6961.

(67) Yang, Y.; Hu, C.; Abu-Omar, M. M. *J. Mol. Catal. A Chem.* **2013**, *376*, 98–102.

(68) Weingarten, R.; Kim, Y. T.; Tompsett, G. A.; Fernandez, A.; Han, K. S.; Hagaman, E. W.; Conner, W. C.; Dumesic, J. A.; Huber, G. W. *J. Catal.* **2013**, *304*, 123–134.

(69) Ren, L.; Guo, Q.; Kumar, P.; Orazov, M.; Xu, D.; Alhassan, S. M.; Mkhoyan, K. A.; Davis, M. E.; Tsapatsis, M. *Angew. Chem., Int. Ed.* **2015**, *54* (37), 10848–10851.

(70) Gounder, R.; Davis, M. E. *ACS Catal.* **2013**, *3* (7), 1469–1476.

(71) Lew, C. M.; Rajabbeigi, N.; Tsapatsis, M. *Micropor. Mesopor. Mater.* **2012**, *153*, 55–58.

(72) Dijkmans, J.; Gabriels, D.; Dusselier, M.; de Clippel, F.; Vanelderen, P.; Houthoofd, K.; Malfliet, A.; Pontikes, Y.; Sels, B. F. *Green Chem.* **2013**, *15* (10), 2777–2785.

(73) Witvrouwen, T.; Dijkmans, J.; Paulussen, S.; Sels, B. *J. Energy Chem.* **2013**, *22* (3), 451–458.

(74) Saravanamurugan, S.; Paniagua, M.; Melero, J. A.; Riisager, A. *J. Am. Chem. Soc.* **2013**, *135* (14), 5246–5249.

(75) Zhang, L. X.; Xi, G. Y.; Chen, Z.; Jiang, D.; Yu, H. B.; Wang, X. C. *Chem. Eng. J.* **2017**, *307*, 868–876.

(76) Li, L.; Ding, J.; Jiang, J. G.; Zhu, Z.; Wu, P. *Chinese J. Catal.* **2015**, *36* (6), 820–828.

(77) Corma, A.; Nemeth, L. T.; Renz, M.; Valencia, S. *Nature* **2001**, *412*, 423–425.

(78) Liu, M.; Jia, S. Y.; Li, C. Z.; Zhang, A. F.; Song, C. S.; Guo, X. W. *Chin. J. Catal.* **2014**, *35* (5), 723–732.

(79) Wang, Y.; Yang, X.; Zheng, H.; Li, X.; Zhu, Y.; Li, Y. *Mol. Catal.* **2019**, *463*, 130–139.

(80) Wang, L.; Guo, H.; Xie, Q.; Wang, J.; Hou, B.; Jia, L.; Cui, J.; Li, D. *Appl. Catal. A Gen* **2019**, *572*, 51–60.

(81) Wang, Y.; Ding, G.; Yang, X.; Zheng, H.; Zhu, Y.; Li, Y. *Appl. Catal. B Environ.* **2018**, *235*, 150–157.

(82) Gupta, N. K.; Fukuoka, A.; Nakajima, K. *ACS Sustain. Chem. Eng.* **2018**, *6* (3), 3434–3442.

(83) Lam, E.; Chong, J. H.; Majid, E.; Liu, Y.; Hrapovic, S.; Leung, A. C. W.; Luong, J. H. T. *Carbon* **2012**, *50* (3), 1033–1043.

(84) Dias, A. S.; Pillinger, M.; Valente, A. A. *J. Catal.* **2005**, *229* (2), 414–423.

(85) Harmsen, P. F. H.; Hackmann, M. M.; Bos, H. L. *Biofuels, Bioprod. Biorefin.* **2014**, *8* (3), 306–324.

(86) Coggio, W.; Hevus, I.; Schrock, A.; Thompson, B.; Ulrich, K.; Dzadek, N. *Adv. Adhes.* **2015**, *3*, 36–42.

(87) Luman, N. R.; Kim, T.; Grinstaff, M. W. *Pure Appl. Chem.* **2004**, *76* (7–8), 1375–1385.

(88) Sacan, L.; Cirpan, A.; Camurlu, P.; Toppare, L. *Synth. Met.* **2006**, *156* (2–4), 190–195.

(89) Sonnenschein, M. F.; Guillaudeu, S. J.; Landes, B. G.; Wendt, B. L. *Polymer* **2010**, *51* (16), 3685–3692.

(90) Tashihiro, M.; Nagare, Y.; Matsui, T. US 2020/0155440 A1, May 21, 2020.

(91) Sarosi, C.; Moldovan, M.; Miuta, F.; Prodan, D.; Antoniac, A.; Prejmerean, C.; Silaghi Dumitrescu, L.; Popescu, V.; Raiciu, A. D.; Saceleanu, V. *Materials* **2019**, *12* (13), 2106.

(92) Pfister, B.; Jonsson, J.; Gustafsson, M. *BMC Pharmacol. Toxicol.* **2017**, *18* (1), 52.

(93) Zhang, F.; Zhou, F.; Wei, W. *Chinese J. Biochem. Pharm.* **2017**, *37* (2), 68–71.

(94) Plumb, D. C. *Plumb's Veterinary Drug Handbook: Desk*, 9th ed., John Wiley & Sons, 2018.

(95) Cao, G.-Y.; Li, K.-X.; Jin, P.-F.; Yue, X.-Y.; Yang, C.; Hu, X. *Clin. Ther.* **2011**, *33* (12), 2054–2059.

(96) Ly, B. K.; Minh, D. P.; Pinel, C.; Besson, M.; Tapin, B.; Epron, F.; Especel, C. *Top. Catal.* **2012**, *55* (7–10), 466–473.

(97) Minh, D. P.; Besson, M.; Pinel, C.; Fuertes, P.; Petitjean, C. *Top. Catal.* **2010**, *53* (15–18), 1270–1273.

(98) Haus, M. O.; Louven, Y.; Palkovits, R. *Green Chem.* **2019**, *21* (23), 6268–6276.

(99) Liu, Y.; Fu, J.; Ren, D.; Song, Z.; Jin, F.; Huo, Z. *ChemistrySelect* **2018**, *3* (2), 724–728.

(100) Song, H.; Lee, S. Y. *Enzyme Microb. Technol.* **2006**, *39* (3), 352–361.

(101) Li, X.; Mupondwa, E. *Renew. Sustain. Energy Rev.* **2021**, *137*, 110587.

(102) Choudhary, H.; Nishimura, S.; Ebitani, K. *Chem. Lett.* **2012**, *41* (4), 409–411.

(103) Zhu, W.; Tao, F.; Chen, S.; Li, M.; Yang, Y.; Lv, G. *ACS Sustain. Chem. Eng.* **2019**, *7* (1), 296–305.

(104) Gu, Y.; Fang, S.; Yang, L.; Hirano, S. *Electrochim. Acta* **2021**, *394*, 139120.

(105) Kim, H.; Yang, S.; Kim, D. H. *Environ. Res.* **2020**, *187*, 109667.

(106) Wang, L.; Guo, H.; Xie, Q.; Wang, J.; Hou, B.; Jia, L.; Cui, J.; Li, D. *Appl. Catal. A Gen* **2019**, *572*, 51–60.

(107) Ter Horst, J. H.; Geertman, R. M.; Van Rosmalen, G. M. In *J. Cryst. Growth*, **2001**, 230, 277–284.

(108) Tani, M.; Sugiura, T. *SID seminar notes*, 1995; F5.1–F5.23.

(109) Hirai, Y.; Katoh, H. *Proc. IDW* 1995, 49.

(110) Schwarz, W.; Schossig, J.; Rossbacher, R.; Pinkos, R.; Höke, H. *Ullmann's Encycl. Ind. Chem.* **2019**, 1–7.

(111) Hong, M.; Chen, E. Y.-X. *Nat. Chem.* **2016**, *8* (1), 42–49.

(112) Moore, T.; Adhikari, R.; Gunatillake, P. *Biomaterials*. **2005**, 26(18), 3771–3782.

(113) Oka, S. *Bull. Chem. Soc. Jpn.* **1962**, *35* (6), 986–989.

(114) Hong, U. G.; Hwang, S.; Seo, J. G.; Lee, J.; Song, I. K. *J. Ind. Eng. Chem.* **2011**, *17* (2), 316–320.

(115) Hong, U. G.; Hwang, S.; Seo, J. G.; Yi, J.; Song, I. K. *Catal. Letters* **2010**, *138* (1–2), 28–33.

(116) Yakabi, K.; Jones, A.; Buchard, A.; Roldan, A.; Hammond, C. *ACS Sustain. Chem. Eng.* **2018**, *6* (12), 16341–16351.

(117) Zhang, C.; Chen, L.; Cheng, H.; Zhu, X.; Qi, Z. *Catal. Today* **2016**, *276*, 55–61.

(118) Tapin, B.; Epron, F.; Especel, C.; Ly, B. K.; Pinel, C.; Besson, M. *ACS Catal.* **2013**, *3* (10), 2327–2335.

(119) You, C.; Zhang, C.; Chen, L.; Qi, Z. *Appl. Organomet. Chem.* **2015**, *29* (10), 653–660.

(120) Budroni, G.; Corma, A. *J. Catal.* **2008**, *257* (2), 403–408.

(121) Zhang, C.; Chen, L.; Cheng, H.; Zhu, X.; Qi, Z. *Catal. Today* **2016**, *276*, 55–61.

(122) Budroni, G.; Corma, A. *J. Catal.* **2008**, *257* (2), 403–408.

(123) Tapin, B.; Epron, F.; Especel, C.; Ly, B. K.; Pinel, C.; Besson, M. *ACS Catal.* **2013**, *3* (10), 2327–2335.

Chapter 2

Silica supported Sn catalysts with tetrahedral Sn sites for selective isomerization of glucose to fructose

Abstract

Lewis acid catalyzed isomerization of glucose to fructose is an important reaction for production of renewable chemicals. Detailed investigation of Lewis acid catalysts in this reaction, like Sn-Beta, reveals tetrahedral Sn sites as active sites. However, in such catalysts Sn sites are in the framework, which means all the sites are not accessible. In contrast, if synthesis of such species is achieved on the surface of catalyst, it can improve the catalytic activity. In this study, we show the synthesis of tetrahedral Sn sites on the surface of SBA15 by controlling Sn dispersion via a simple impregnation method. Catalyst characterization showed a high surface area with high concentration of hydrogen bonded silanol nests were controlling factors. Roughly, one Sn-O-Si is formed for each five Si-OH bond, hence Sn loading of 1 wt. % over SBA15 (Sn/SBA15) maximized the formation of tetrahedral Sn species on the catalyst surface. Increasing the loading or changing support caused formation of SnO_2 clusters which reduced fructose selectivity. A mechanism based on condensation of Sn with silanol group of SBA15 is proposed. The catalyst showed high selectivity of 93 % after 2 h with 57 % fructose yield. The Lewis acid catalyzed isomerization of glucose was proven by isotopic labeling study using D-glucose-2-d. The catalyst deactivated in the third cycle owing to byproduct deposition,

but the activity was restored by recalcining the catalyst.

2.1 Introduction

Cellulose depolymerization to glucose and its subsequent isomerization to fructose is the gateway to many industrially important chemicals.[1–3] Isomerization of glucose to fructose converts the aldohexose sugar to its ketohexose form. The ketohexose fructose conforms to furanose ring structure in a solution, which enables the synthesis of 5-hydroxymethyl furfural (5-HMF),[4] a precursor for bio-based plastics.[5,6] Fructose is also the major component of high fructose corn syrup, an industrial sweetener, derived from corn starch.[7] Therefore, the isomerization of glucose to the less abundant fructose is an important reaction in food and chemical industries.

Industrial process for glucose isomerization utilizes immobilized xylose isomerase as a catalyst.[8] This enzyme can selectively catalyze glucose isomerization to fructose. However, low lifetime of enzyme and requirement of a buffer to maintain the pH of reaction medium increase the process cost.

Basic histidine groups present in the enzyme structure were initially thought to be the active sites for glucose isomerization.[9] Later it was found that the metal center has an essential role as Lewis acid, in stabilizing the acyclic glucose molecule and the subsequent isomerization reaction.[10–12] Since then, several reports on base or Lewis acid catalyzed reactions have appeared for glucose isomerization. [13,14,23–26,15–22]

Base catalyzed isomerization of glucose proceeds via the Lorry de Bruyn-Alberda van Ekenstein transformation of glucose initiated by proton abstraction at the C2 position.[13] Recently our group reported a hydrotalcite catalyst containing basic sites that achieved 56 % yield of fructose with 80 % selectivity.[14] Other examples include SBA15 grafted with tertiary amine groups acting as base catalysts that achieved 41 % fructose

yield with 85 % selectivity.[15] Zhang et al. reported a series of imidazolium and tertiary amine based ionic liquids that serve as base catalysts for this reaction.[16] Several other base catalysts have been reported for glucose to fructose reactions.[17–20] However, the inadequate stability of these basic catalysts is still a hinderance for industrial application. Additionally, most of the further downstream processing of fructose takes place in presence of acid catalysts.

Corma et al. first showed that Sn-Beta zeolites with Lewis acid sites can do the Meerwein–Ponndorf–Verley (MPV) reduction of carbonyl compounds via hydride shift from a hydroxyl group to the carbonyl group.[21] Glucose to fructose isomerization over Lewis acid catalysts can be explained by a similar mechanism where the C2 carbon donates a hydride ion to the C1 aldehyde group which leads to the formation of a ketone group at the C2 position. Sn and Ti incorporated porous materials have been reported to facilitate this reaction with high yield.[13,22–25] Spectroscopic analysis has revealed that tetrahedral Sn open sites within the pores, containing three Si-O-Sn bonds and one Sn-OH bond, are most active for isomerization reaction.[25] Sn-Beta catalyst has received much attention over the years for this reaction. The reaction mechanism has been confirmed with experimental data,[13] and theoretical modelling has shown that 1,2-hydride shift is the rate determining step.[27] In zeolite catalysts, apart from nature of active site, pore size and surface area also plays a huge role, which is evident from the fact that , Sn-Beta catalyzes isomerization of glucose, xylose, and dihydroxyacetone, whereas Sn-MFI only catalyzes the isomerization of xylose and dihydroxyacetone. The larger pore size of Sn-Beta in comparison to Sn-MFI facilitates diffusion of the relatively bulkier glucose molecule within its pores.[26] However, in Sn-Beta, tetrahedral Sn sites are present in the zeolites framework and hence not all the active sites are accessible to the substrate.

Mesoporous materials based on SBA15, MCM-41 can provide larger surface area and pore volume as well bigger pore size compared to the microporous zeolites. Sn containing mesoporous materials such as Sn/SBA15 and Sn/MCM41 are alternative to zeolite-based catalysts. Lorenti et al. reported a series of Sn-SBA15 materials, where Sn is incorporated to the framework of SBA15, and reported glucose to fructose isomerization with 11.8 % glucose conversion and 84.5 % selectivity.[28]

In order to improve accessibility of active sites, we explored the synthesis of tetrahedral sites on mesoporous silica surface (not in the bulk framework) and compare the synthesis and catalytic property with other oxide supports. Key factors for formation of active sites are discussed via characterization.

2.2 Experimental

2.2.1 Materials

All materials and reagents used in this study are commercially available. Glucose and fructose were purchased from Wako Chemicals. D-Glucose-2-d and $SnCl_4 \cdot 5H_2O$ were purchased from Sigma Aldrich. Tetraethyl orthosilicate was bought from TCI Chemicals. H-Beta150 (Beta zeolite with SiO_2/Al_2O_3 ratio of 150) and zirconia were obtained from Japan Reference Catalysts (JRC). Titania (MC-150) was obtained from Ishihara Sangyo, Japan. γ-Alumina was bought from Sigma Aldrich.

2.2.2 Catalyst preparation

SBA15 was prepared according to a method reported by Stucky et al.[29] During synthesis, 450 mL of 1.6 M hydrochloric acid was added to 12 g of poly(ethylene glycol)-block-poly(propylene glycol)-block-poly(ethylene glycol) (P123) and stirred at room temperature until the P123 was hydrolyzed. The solution was stirred rapidly at 35 °C and

25.5 g of tetraethyl orthosilicate was added dropwise over a span of 30 minutes. The solution was kept standing at 35 °C for 24 h and further at 100 °C for another 24 h. The obtained solid was filtered and washed with water and ethanol until the presence of chloride ions was not detected in the filtrate. The solid was dried at 110 °C overnight and then calcined at 560 °C for 16 h to obtain SBA15.

Sn containing catalysts were prepared by impregnation method. Desired amount of $SnCl_4.5H_2O$, was dissolved in 5 mL of distilled water and then 500 mg of support was added to the solution. The mixture was sonicated for 5 minutes and then stirred continuously with a glass rod over a hot plate maintained at 110 °C until a powder was obtained. After further drying at 110 °C for 2 h, the powder was calcined at 500 °C for 2 h.

2.2.3 Catalyst characterization

X-ray diffraction (XRD) was measured with Rigaku MiniFlex using CuKα X-ray (λ = 1.54 Å) operating at 40 kV and 20 mA. UV visible diffuse reflectance spectroscopy (UV-vis) measurement was obtained using Jasco V-650 spectrophotometer, line width of light ray was kept at 1 nm and $BaSO_4$ was used as reference. N_2 adsorption isotherms were measured at −196 °C using a Belsorp mini analyzer. Surface area was calculated by using BET theory between the relative pressure range 0.05 to 0.35 in the N_2 adsorption isotherm.[30] STEM image was obtained in a JEOL JEM-ARM200F atomic resolution electron microscope at an acceleration voltage of 200 kV equipped with an EDS detector EX-24221M1G5T. X-ray photoelectron spectroscopy (XPS) was performed with JEOL JPS-9010MC instrument. Charge correction was made by adjusting the adventitious carbon peak to 286.4 eV. Pyridine IR spectrum was recorded in a Shimadzu IRSpirit instrument. The samples were pressed into self-supported disks and placed in a quartz

cell inside a high vacuum chamber with NaCl windows. The sample was pretreated under high vacuum at 150 °C for 1 h, before recording any spectrum in order to remove physisorbed moisture. Energy dispersive X-ray spectroscopy (EDX) analysis of reaction solution was done with Shimadzu EDX – 720 instrument.

2.2.4 Catalytic experiments

Catalytic glucose isomerization was performed in a 15 mL high pressure glass tube. In a typical reaction 90 mg glucose, 90 mg catalyst, 7 mL ethanol was taken in the high-pressure tube, which was then heated at 90 °C in an oil bath, with magnetic stirring. After the reaction was complete the mixture was centrifuged to separate the catalyst and the solution. Additionally, the catalyst was washed with deionized water (2 ml × 3 times) to extract physically adsorbed reactant and product species. The wash off water was mixed with the reaction mixture and analyzed with a HPLC system equipped with Shodex SH1011 sugar column. Conversion and yield were calculated with an absolute calibration using the formulae:

$$\text{Conversion} = \frac{moles\ of\ glucose\ remaining}{moles\ of\ glucose\ taken} \times 100$$

$$\text{Fructose yield} = \frac{moles\ of\ fructose\ formed}{moles\ of\ glucose\ taken} \times 100$$

$$\text{Selectivity} = \frac{fructose\ yield}{conversion} \times 100$$

$$\text{TOF} = \frac{number\ of\ moles\ of\ fructose\ formed}{number\ moles\ of\ metal\ \times\ reaction\ time}$$

The isotope tracer study was done using D-glucose-2-d as the reactant and adding sodium acetate-d_3 as an internal standard after the isomerization reaction. The final

reaction mixture was analyzed by ^{2}H nuclear magnetic resonance spectroscopy (NMR; JEOL, JNM- ECX600, 2H 92.1 MHz).

2.3 Results and discussion

2.3.1 Catalytic activity

Sn containing catalyst were prepared by impregnating Sn (1 wt. %) on supports such as SBA15, H-Beta150 zeolite, A380 silica, alumina, zirconia and titania. All catalysts were tested for isomerization of glucose to fructose at 90 °C in the presence of ethanol as the solvent with a glucose concentration of 1.6 wt. % (glucose to Sn ratio = 66). Ethanol was chosen as the solvent because it can be easily obtained from renewable biomass and it shows high fructose selectivity among polar organic solvents.[14,31] Sn/SBA15 showed the highest fructose selectivity of 98 % along with 38 % conversion after 45 min of reaction (Figure 2.1a). Sn/H-Beta150 showed slightly higher conversion (44 %) than Sn/SBA15 with a lower selectivity of 89 %. Beta zeolites are known to exhibit Brønsted acid sites originating from the presence of Al atoms in the framework resulting in unwanted side reactions. A small amount (less than 1 %) of 5-HMF was detected in this reaction which is formed by dehydration of fructose over Brønsted acid sites.[32–36] Formation of 5-HMF also results in humin production, a polymer of 5-HMF and other products, which is likely to reduce the selectivity towards fructose in the presence of Sn/HBeta150. Sn/A380 showed comparable selectivity towards fructose (90 %), although the conversion was markedly lower (24 %). Sn/Zirconia showed no activity for fructose formation. Titania and alumina based catalysts showed some activity ca. 64 % selectivity at 10 % conversion and 77 % selectivity at 16 % conversion, respectively. Overall, silica-based supports showed better activity and selectivity than other oxide supports. In

particular, SBA15 showed the highest selectivity with comparatively high conversion.

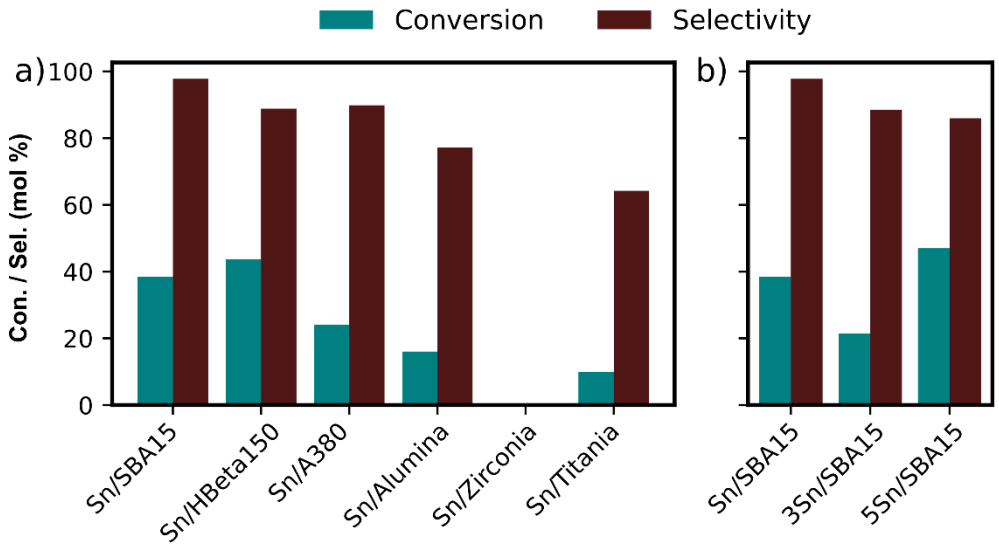

Figure 2.1. Fructose selectivity and glucose conversion in the presence of (a)1 wt. % Sn catalyst using different supports and (b) catalyst with different Sn loading over SBA15. Reaction conditions: 90 mg glucose, 90 mg catalyst, 7 mL ethanol, 90 °C, 45 minutes.

Next, we investigated the role of Sn loading over SBA15. Increasing the Sn content to 3 wt. % (3Sn/SBA15) reduced the selectivity to 89 % and also decreased the glucose conversion to 21 % (Figure 2.1b). Further increase in Sn loading to 5 wt. % (5Sn/SBA15) did not enhance the fructose selectivity (86 %). However, the glucose conversion increased to 47%. In this reaction, less than 1 % 5-HMF was observed, however the reaction mixture turned slightly yellow indicating the formation of soluble humins.

Based on the above results Sn/SBA15 with 1 wt. % Sn loading was chosen for optimization of reaction condition. Fructose selectivity of 99 % was obtained in the initial stage of reaction (30 min), which reduced slightly to 93 % after 2h. (Figure 2.2) Glucose conversion increased steadily to 62 % until 2 h resulting in 57 % fructose yield. At this time the reaction reached equilibrium and further prolonging the time to 3 h increased the

fructose yield to 60 % along with a reduction in selectivity to 85 % owing to byproduct formation. Increasing the glucose concentration to 10 % w/w (glucose to Sn ratio = 462) under the same reaction condition resulted in 34 % yield with 79 % selectivity for fructose after 2 h of reaction. The turnover frequency in this reaction at 45 min was 53.6×10^{-3} s^{-1}, (based on molar content of Sn), which is higher than the previously reported value of 27.8×10^{-3} s^{-1} for Sn-Beta catalyst in water. [25]

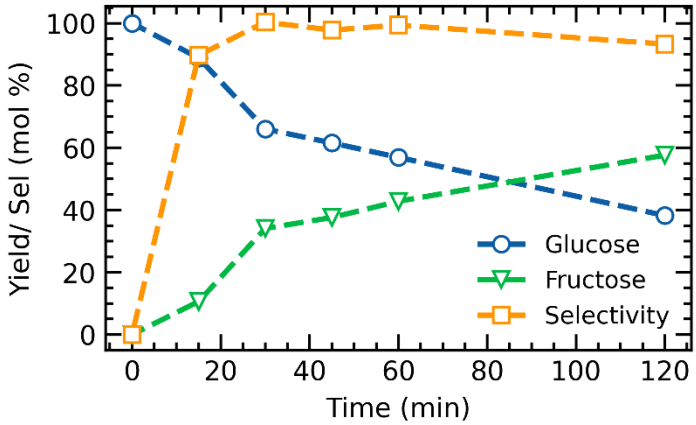

Figure 2.1. Reaction time course using Sn/SBA15 catalyst (1 wt. % Sn). Reaction conditions: 90 mg glucose, 90 mg catalyst, 7 mL ethanol, 90 °C.

2.3.2 Catalyst characterization

All catalysts were characterized to investigate the underlying factors responsible for change in fructose selectivity and yield with the change in catalyst support and Sn loading. The XRD pattern for 5Sn/SBA15 (Figure 2.3a), having the highest Sn loading, showed characteristic peaks for cassiterite SnO_2 (PDF card number 01-077-0449). The crystallite size for SnO_2 was calculated as 13.7 nm suggesting formation of large SnO_2 particles, which might contribute towards the poor selectivity for this catalyst. In case of 3Sn/SBA15 only the prominent peaks at 2θ value of 26.6, 33.8, 37.9 and 51.7 degrees were observed. The crystallite size was determined as 3.7 nm, which suggested formation

of smaller SnO_2 particles at lower loading. The XRD pattern for Sn/SBA15 was exactly similar to unsupported SBA15 and no peaks for SnO_2 were observed. This indicates that reducing the amount of Sn species on the surface increased the Sn dispersion and reduced the formation of SnO_2 clusters. SnO_2 peaks were not observed on other supports as well when the Sn loading was 1% (Figure 2.3b) suggesting high dispersion of Sn species at low loading irrespective of the type of support used, however, presence of SnO_2 of short range order can not be discarded.

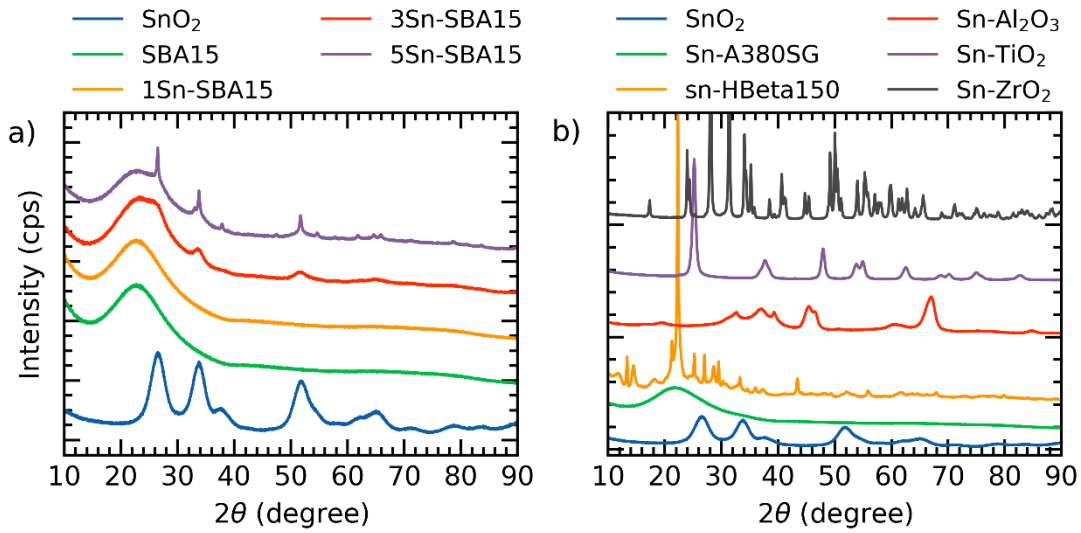

Figure 2.3. a. XRD pattern of Sn/SBA15 catalysts with different Sn loading, b. with 1 wt. % Sn on different supports

Diffuse reflectance UV-Visible spectroscopy is a much more sensitive technique to probe SnO_2 structure. Only Sn catalysts on silica-based supports are studied, as in case of other metal oxides, absorption band due to support materials interfere with the absorption band of SnO_2 (Figure 2.4). The region below 210 nm in the spectrum is a result of reflectance from the tetrahedrally coordinated Sn species responsible for high activity.[25] All of 1Sn/SBA15, 3Sn/SBA15 and 5Sn/SBA15 showed peak in this region, indicating all the catalysts, have tetrahedral Sn species. The region close to 280 nm can

be assigned to hexacoordinated Sn species present within the SnO_2 crystal.[25] Furthermore, the band close to 250 nm is a result of LMCT charge transfer due to interaction of tetrahedrally coordinated Sn species with other basic oxygen and nitrogen containing compounds.[25] Intensity around 280 nm for Sn/SBA15 was close to baseline. Increasing Sn loading to 3 and 5 wt. % , increased intensity in this region, indicating formation of inactive hexacoordinated Sn species with an increase in Sn loading. The band around 250 nm, with significantly low intensity for Sn/SBA15 was attributed to interaction of tetrahedrally coordinated Sn species with physisorbed water within the pores of SBA15. Similarly, for 3Sn/SBA15 and 5Sn/SBA15, which showed high intensity in this region, was assigned to interaction of tetrahedrally coordinated Sn species with physisorbed water and nearby basic SnO_2 species. However, in this case some contribution from blue shifting of ~280 nm band to ~250 nm due to small particle size of the SnO_2 is also likely .[37–40]

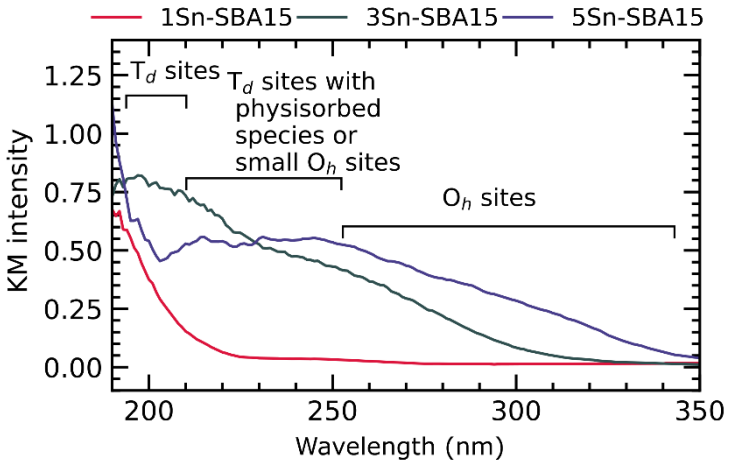

Figure 2.2. DRUV-VIS spectra of Sn/SBA15 with different metal content

The effect of different silica support with the same Sn loading on Sn species are compared in Figure 2.5. Sn/A380 catalyst shows the band due to tetrahedrally coordinated structure, with lower intensity compared to that of Sn/SBA15. However, Sn/A380 showed

higher intensity in the 280 nm and 250 nm region, which was attributed to the lower surface area of A380 silica gel (300 m^2 g^{-1}) in comparison to SBA15 (850 m^2 g^{-1}) (Table 2.1), resulting in poorer dispersion of Sn species at similar metal loading. The Sn/HBeta150 catalyst showed high intensity in the 210 nm region as well as 280 nm and 250 nm regions, which were attributed to formation of small SnO_2 clusters within the micropores of zeolite.

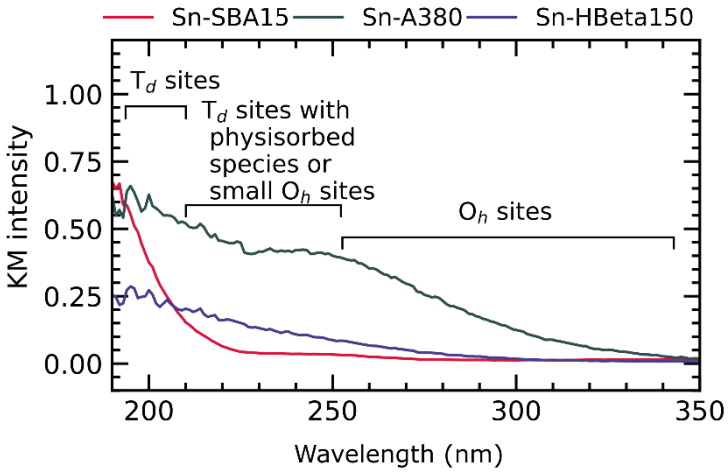

Figure 2.5. comparison of DRUV-VIS spectra of silica supports containing 1 wt. % Sn

Table 2.4. BET surface area of catalysts

Sample	Surface Area (m^2 g^{-1})
Sn/Alumina	166
Sn/HBETA150	459
Sn/SBA15	851
Sn/Titania	119
Sn/Zirconia	5.2
Sn/A380	300

These results indicated that the high selectivity towards fructose formation over Sn/SBA15 catalyst is a direct consequence of selective formation of tetrahedral Sn species on Sn/SBA15. We propose that the formation of tetrahedral Sn sites is a function of the abundance of hydroxyl groups on the catalyst surface. The hydroxyl groups on silica

surface can undergo condensation to form Si-O-Sn bonds under the acidic condition during catalyst preparation as shown in scheme 2.1.[41] SBA15 has higher abundance of surface hydroxyl groups in comparison to HBeta150 and A380 (Figure 2.6). The large number of -OH present in SBA15 would facilitate high dispersion of Sn. Large pores of SBA15 would also prevent formation of tetrahedral closed Sn sites that are not active for this reaction.

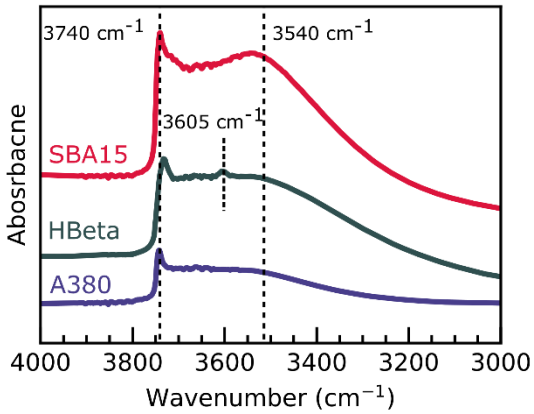

Figure 2.6. FTIR spectra of SBA15, HBeta and A380 supports. The peak at 3740 cm^{-1} corresponds the surface individual silanol (Si-OH) groups and the broad band around 3540 cm^{-1} corresponds to hydrogen bonded silanol groups along with some contribution from adsorbed water molecules. The small peak around 3605 cm^{-1} in HBeta sample represents bridged hydroxyl groups between silicon and aluminum in the framework. SBA15 shows highest peak intensity for silanol groups and hence it contains the greatest surface OH density.

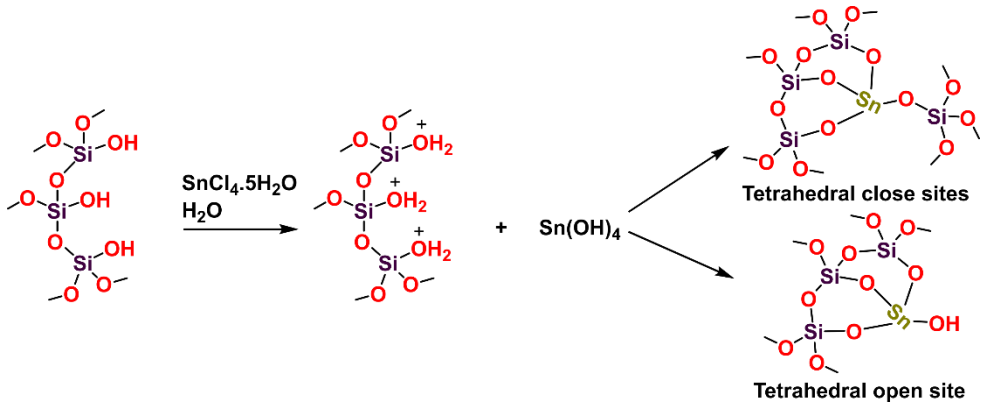

Scheme 2.1. Pathway for the formation of tetrahedral Sn sites the surface of SBA15. The -OH groups in red color are the surface hydroxyl groups (silanol) of SBA15.

Figure 2.7 shows the XPS spectra of the O1s region for silica supported Sn catalysts samples. The prominent peak for oxygen atoms at 533.2 eV was assigned to the oxygen in Si-O-Si framework.[42] Another peak at 534.5 eV was observed that was assigned to oxygen in the surface hydroxyl groups. A small peak was observed near 531 eV for all silica containing supports. This peak was attributed to the formation of Si-O-M (M = metal) bond.[43–46] For Sn/HBeta150 this peak was prominent owing to the presence of Si-O-Al bonds in the zeolite framework. For Sn catalysts with SBA15 as support this peak appeared at 531.4 eV. In case of Sn/SBA15, the ratio of peak area for oxygen from Si-OH and Si-O-Sn bonds was 4.8: 1. Whereas for 3 wt. % Sn/SBA15 the same ratio was 4.7: 1 suggesting similar density of Si-O-Sn bonds despite higher loading. Therefore, we concluded that the formation of tetrahedral Sn species on the surface of catalyst is limited by the extent of surface hydroxyl groups present.

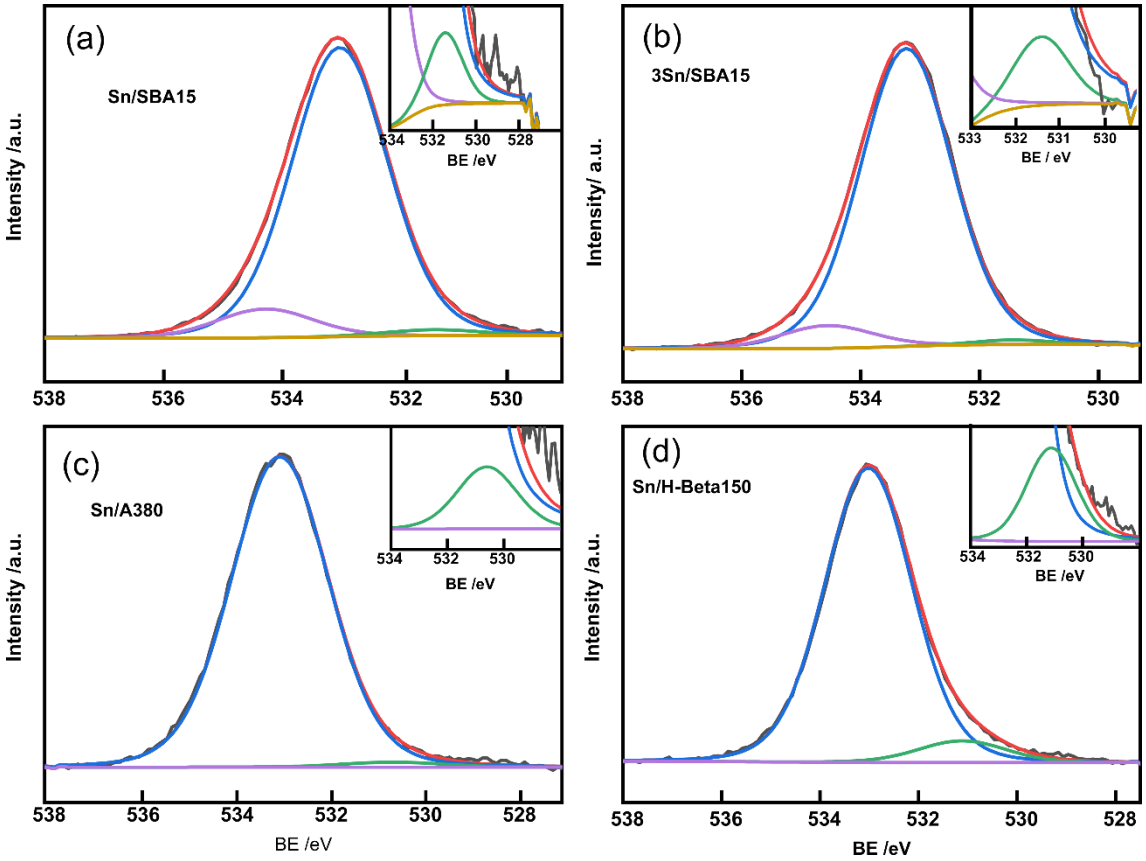

Figure 2.7. O1s XPS spectrum of a) Sn/SBA15, b) Sn/A380, c) 3Sn/SBA15, d) Sn/HBeta150

Finally, we performed high resolution microscopy of Sn/SBA15 to observe presence of Sn species. STEM image of Sn/SBA15 (Figure 2.8) revealed small contrasting dots of size less than 0.3 nm presumed to be small Sn clusters or atomically dispersed Sn species. Elemental mapping of Si and Sn showed uniform distribution of Sn over the SBA15 surface which further concluded that highly dispersed Sn species present in tetrahedral geometry were the active sites.

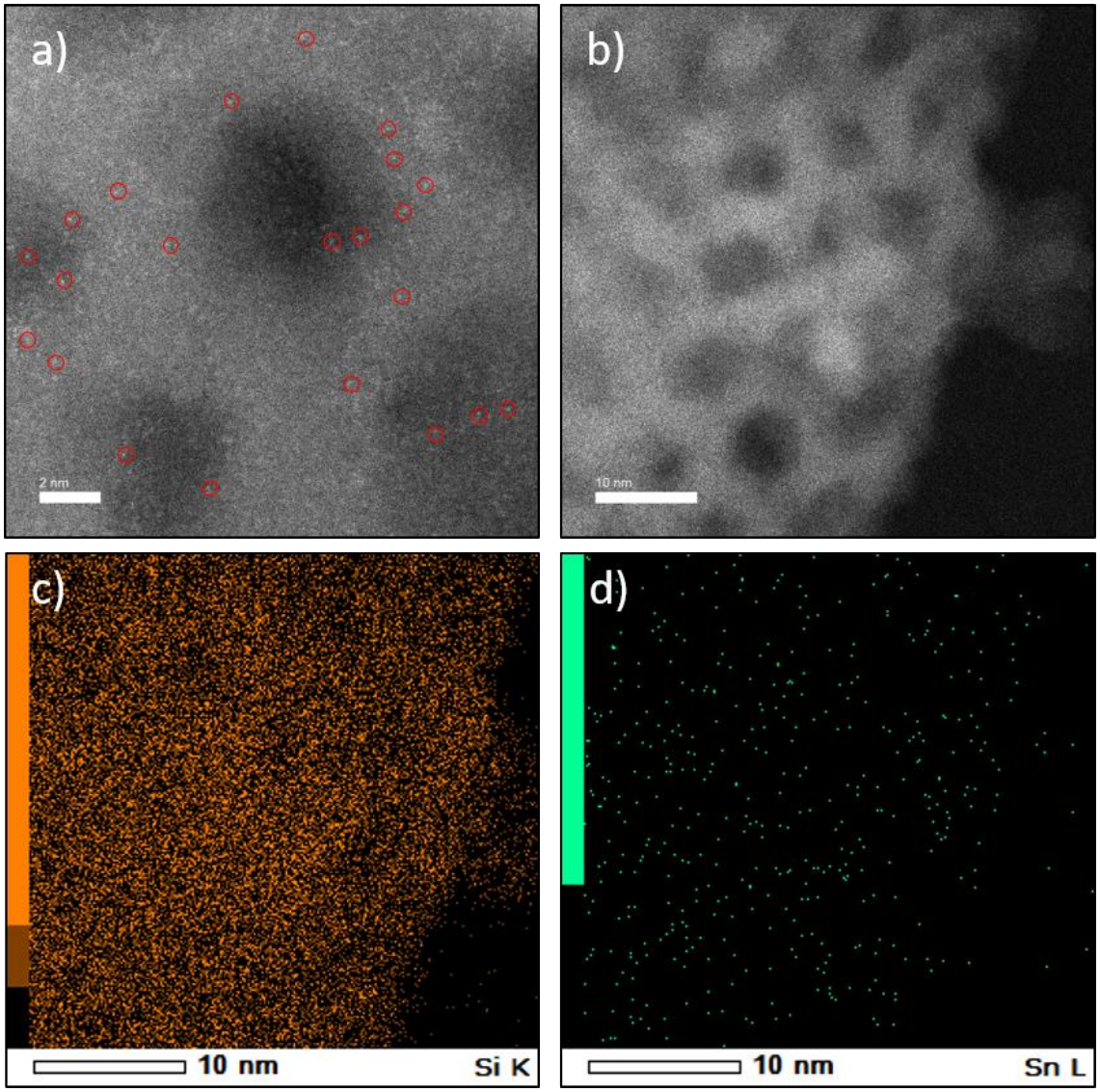

Figure 2.8. a) STEM image of Sn/SBA15, circles highlight the particles presumed to the Sn species. b) STEM image of area of Sn/SBA15 used for elemental mapping. c) and d) elemental mapping of Si and Sn, respectively.

Pyridine was used as basic probe molecule, monitored by FTIR spectroscopy, to study the nature and strength of acid sites present in the catalysts. Sn/SBA15 showed a strong band at 1452 cm^{-1} (Figure 2.9), which corresponds to interaction of basic pyridine molecule with Lewis acidic Sn centres [47–49]**.** The band at 1491 cm^{-1} can be ascribed to presence of both Lewis and Brønsted acidic centres. The silanol groups of SBA15

supports can act as weak Brønsted sites and contribute towards this peak. 3Sn/SBA15 and 5Sn/SBA15 catalysts also showed similar bands. However, the relative intensity for band at 1452 cm^{-1} for these catalysts was lower than that for Sn/SBA15 catalyst after desorption at 150 °C. Therefore, the strength of Lewis acid sites decreased with increasing Sn loading, which correlates with their catalytic performance. The spectra for Sn/HBeta150 catalyst exhibited both strong Brønsted acidity and Lewis acidity (the intense bands at 1491 cm^{-1} and 1546 cm^{-1}) as expected. Strength of Lewis acid sites in Sn/HBeta150 was similar to Sn/SBA15 as evidenced from similar peak intensity after 25 min evacuation under 0.03 torr pressure and desorption at 150 °C.

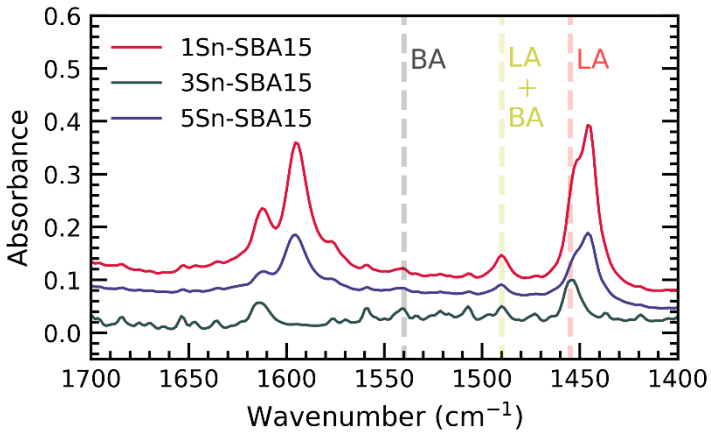

Figure 2.9. IR spectra of catalysts after treatment with pyridine and evacuation at 150 °C

2.3.3 Isotopic labelling study

The presence of highly dispersed Lewis acidic tetrahedral Sn sites would promote the glucose isomerization to proceed through the intramolecular hydride transfer mechanism, in which the proton attached to the C2 carbon is transferred to the C1 atom (Scheme 2.2). In order to ascertain whether the glucose isomerization over Sn/SBA15 catalyst occurs *via* this mechanism, we performed an isotopic tracer study. D-glucose-2-d was used as the reactant instead of normal D-glucose and ^{2}H NMR spectroscopy of the

product mixture was performed to detect the presence of deuterium (Figure 2.10). The ^{2}H NMR spectrum of D-glucose-2-d standard showed two peaks centered at 3.49 and 3.27 ppm corresponding to ^{2}H at C2 position of the α and β anomers of glucose. After reaction, a new peak at 3.65 ppm corresponding to ^{2}H at C1 position of fructose appeared.[14] The presence of this peak confirmed the hydride transfer from C2 to C1 position, leading to the conclusion that glucose isomerization progressed through the Lewis acid catalyzed pathway over tetrahedral Sn sites.

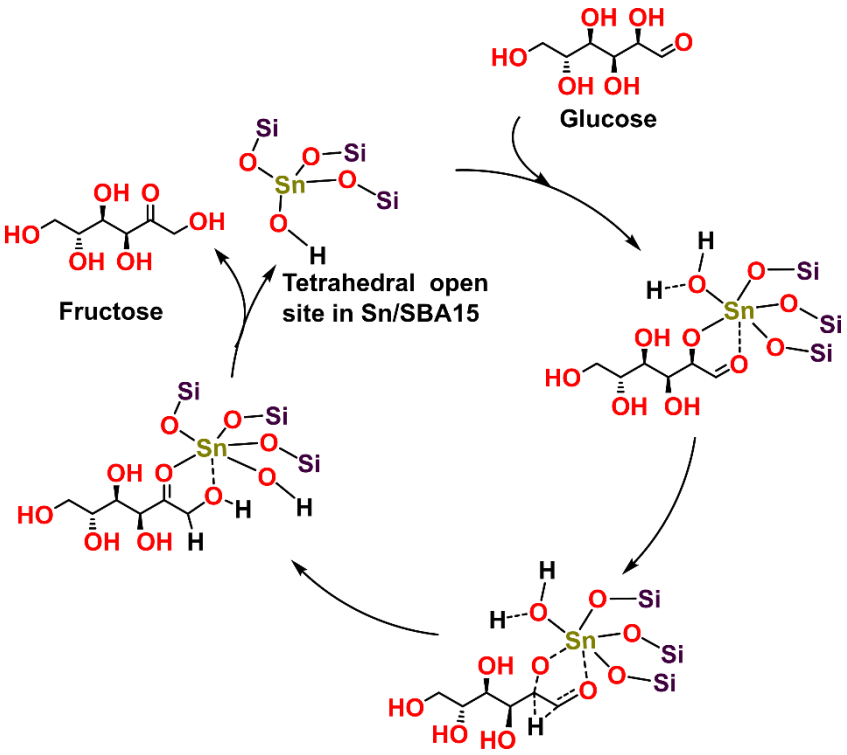

Scheme 2.2. Mechanism showing hydride transfer from C2 carbon of glucose to C1 carbon in fructose during isomerization over Lewis acidic Sn sites.

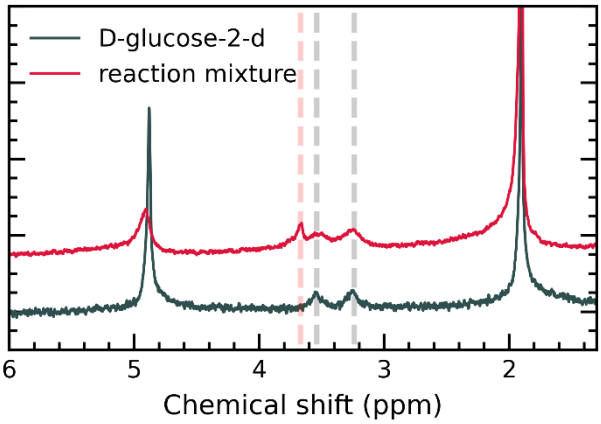

Figure 2.10**.** ^{2}H NMR spectrum of reaction mixture, where D-glucose-2-d is taken as reactant. The reaction mixture is diluted with water and sodium acetate-d_3 was used as internal standard. The spectrum for D-glucose-2-d is also shown for reference. Reaction conditions: D-glucose-2-d 10 mg, Sn/SBA15 10 mg, 2mL ethanol 90 °C temperature, 2 h reaction time.

2.3.4 Recyclability study

Finally, we tested the reusability of Sn/SBA15 catalyst for glucose isomerization (Figure 2.11). The recyclability test was done at 30 min of reaction time to keep the conversion below equilibrium. After each run the catalyst was washed with fresh ethanol and reused. The selectivity of fructose in the second cycle was the same as that for the fresh catalyst (99 %), although the glucose conversion dropped from 32% to 29%. In the third cycle the selectivity dropped to 78 % indicating deactivation of the catalyst. Deposition of small amount of humin might be attributed to the poor activity of catalyst. The catalyst was calcined again at 500 °C for 2 h after the third cycle, which regenerated the catalyst and the selectivity increased to 91 % with 32 % glucose conversion. To investigate weather Sn species leached into the reaction mixture, we carried out a reaction with Sn/SBA15 catalyst for 15 minutes, which produced 11 % fructose with 12 % glucose

conversion. Then the catalyst was filtered and the filtrate was allowed to react further. No change was observed in either the glucose conversion or the fructose yield under this condition. Furthermore, Sn species were not detected in the EDX analysis of the reaction mixture. These results confirmed that leaching of Sn did not occur and the isomerization reaction was heterogeneously catalyzed.

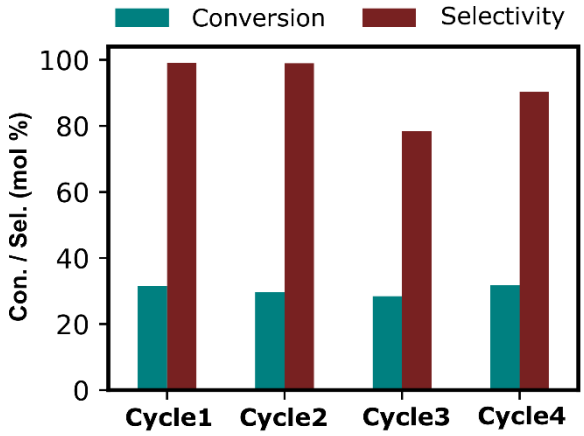

Figure 2.11. Recyclability test of 1 wt. % Sn/SBA15. Reaction conditions: 90 mg glucose, 90 mg catalyst, 7 mL ethanol, 90 °C, 30 minutes.

2.4 Conclusion

We explored the formation of Lewis acidic tetrahedral Sn sites on the surface of oxides for isomerization of glucose to fructose. Silica based supports performed better than other oxides in catalytic isomerization when loaded with 1 wt. % Sn. Diffused reflectance UV-vis analysis showed a preference for formation of tetrahedral Sn sites instead of hexacoordinated SnO_2 over SBA15 support, which showed the best selectivity for fructose. The activity of SBA15 was attributed to the formation of Si-O-Sn bonds owing to high -OH density over SBA15. Increasing Sn loading beyond 1 wt. % over SBA15 also caused SnO_2 formation, which reduced selectivity. O1s XPS spectra for catalysts confirmed that increasing loading of Sn does not cause formation of new Si-O-

Sn bonds, which is required for increasing number of tetrahedral Sn sites. Sn/SBA15 (1 wt. % Sn) showed high selectivity of 93 % with 57 % fructose yield after 2 h of reaction in the presence of ethanol. The reaction mechanism was confirmed to proceed through a 1,2-hydride shift by tracing the ^{2}H isotope in D-glucose-2-d, which indicated the Lewis acidic tetrahedral Sn sites as active sites in the reaction. The catalyst showed a decrease in activity after three cycles but removal of deposited organic compounds by calcination restored the activity.

2.5 References

(1) Yang, Y.; Hu, C.; Abu-Omar, M. M. *Green Chem.* **2012**, *14* (2), 509–513.

(2) Ding, D.; Wang, J.; Xi, J.; Liu, X.; Lu, G.; Wang, Y. *Green Chem.* **2014**, *16* (8), 3846–3853.

(3) Kobayashi, H.; Fukuoka, A. *Green Chemistry*. July 2013, pp 1740–1763.

(4) Yang, G.; Pidko, E. A.; Hensen, E. J. M. *ChemSusChem* **2013**, *6* (9), 1688–1696.

(5) Pacheco, J. J.; Davis, M. E. *Proc. Natl. Acad. Sci.* **2014**, *111* (23), 8363–8367.

(6) Kim, M.; Su, Y.; Aoshima, T.; Fukuoka, A.; Hensen, E. J. M.; Nakajima, K. *ACS Catal.* **2019**, *9* (5), 4277–4285.

(7) Casey, J. P.; Elkhart, I. *Starch - Stärke* **1977**, *29* (6), 196–204.

(8) Jokela, J.; Pastinen, O.; Leisola, M. *Enzyme Microb. Technol.* **2002**, *31* (1–2), 67–76.

(9) Rose, I. A.; O'Connell, E. L.; Mortlock, R. P. *BBA - Enzymol.* **1969**, *178* (2), 376–379.

(10) Allen, K. N.; Lavie, A.; Farber, G. K.; Glasfeld, A.; Petsko, G. A.; Ringe, D. *Biochemistry* **1994**, *33* (6), 1481–1487.

(11) Allen, K. N.; Lavie, A.; Glasfeld, A.; Tanada, T. N.; Gerrity, D. P.; Carlson, S. C.; Farber, G. K.; Petsko, G. A.; Ringe, D. *Biochemistry* **1994**, *33* (6), 1488–1494.

(12) Kovalevsky, A. Y.; Hanson, L.; Fisher, S. Z.; Mustyakimov, M.; Mason, S. A.; Forsyth, V. T.; Blakeley, M. P.; Keen, D. A.; Wagner, T.; Carrell, H. L.; Katz, A. K.; Glusker, J. P.; Langan, P. *STRUCTURE* **2010**, *18* (6), 688–699.

(13) Román-Leshkov, Y.; Moliner, M.; Labinger, J. A.; Davis, M. E. *Angew. Chem., Int. Ed.* **2010**, *49* (47), 8954–8957.

(14) Yabushita, M.; Shibayama, N.; Nakajima, K.; Fukuoka, A. *ACS Catal.* **2019**, *9* (3), 2101–2109.

(15) Xu, J.; Li, K.; Zhang, L.; Li, H.; Biobased, T. W.-J. of; 2019, undefined. *ingentaconnect.com*.

(16) Zhang, X.; Li, H.; Li, X. X.; Liu, Y.; Li, X. X.; Guan, J.; Long, J. *ACS Sustain. Chem. Eng.* **2019**, *7* (15), 13247–13256.

(17) Souza, R. O. L.; Fabiano, D. P.; Feche, C.; Rataboul, F.; Cardoso, D.; Essayem, N. *Catal. TODAY* **2012**, *195* (1), 114–119.

(18) Deshpande, N.; Cho, E. H.; Spanos, A. P.; Lin, L. C.; Brunelli, N. A. *J. Catal.* **2019**, 119–127.

(19) Zhang, N.; Meng, X. G.; Wu, Y. Y.; Song, H. J.; Huang, H.; Wang, F.; Lv, J. *ChemCatChem* **2019**, *11* (9), 2355–2361.

(20) Zhang, L.; Deng, B.; Li, N.; Zhong, H. *Bioresour. Bioprocess.* **2019**, *6* (1).

(21) Corma, A.; Domine, M. E.; Nemeth, L.; Valencia, S. *J. Am. Chem. Soc.* **2002**, *124* (13), 3194–3195.

(22) Moliner, M.; Roman-Leshkov, Y.; Davis, M. E. *Proc. Natl. Acad. Sci.* **2010**, *107* (14), 6164–6168.

(23) Bermejo-Deval, R.; Assary, R. S.; Nikolla, E.; Moliner, M.; Roman-Leshkov, Y.; Hwang, S. J.; Palsdottir, A.; Silverman, D.; Lobo, R. F.; Curtiss, L. A.; Davis, M. E. *Proc. Natl. Acad. Sci.* **2012**, *109* (25), 9727–9732.

(24) Nikolla, E.; Román-Leshkov, Y.; Moliner, M.; Davis, M. E. *ACS Catal.* **2011**, *1* (4), 408–410.

(25) Bermejo-Deval, R.; Gounder, R.; Davis, M. E. *ACS Catal.* **2012**, *2* (12), 2705–2713.

(26) Chang, C. C.; Wang, Z. P.; Dornath, P.; Cho, H. J.; Fan, W. *RSC Adv.* **2012**, *2* (28), 10475–10477.

(27) Li, Y. P.; Head-Gordon, M.; Bell, A. T. *ACS Catal.* **2014**, *4* (5), 1537–1545.

(28) Lorenti, J. P.; Scolari, E.; Albuquerque, E. M.; Fraga, M. A.; Gallo, J. M. R. *Appl. Catal. A Gen.* **2019**, *581*, 37–42.

(29) Zhao, D.; Feng, J.; Huo, Q.; Melosh, N.; Fredrickson, G. H.; Chmelka, B. F.; Stucky, G. D. *Science* **1998**, *279* (5350), 548–552.

(30) Brunauer, S.; Emmett, P. H.; Teller, E. *J. Am. Chem. Soc.* **1938**, *60* (2), 309–319.

(31) Upare, P. P.; Chamas, A.; Lee, J. H.; Kim, J. C.; Kwak, S. K.; Hwang, Y. K.; Hwang, D. W. *ACS Catal.* **2020**, *10* (2), 1388–1396.

(32) Osatiashtiani, A.; Lee, A. F.; Granollers, M.; Brown, D. R.; Olivi, L.; Morales, G.; Melero, J. A.; Wilson, K. *ACS Catal.* **2015**, *5* (7), 4345–4352.

(33) Qi, L.; Mui, Y. F.; Lo, S. W.; Lui, M. Y.; Akien, G. R.; Horváth, I. T. *ACS Catal.* **2014**, *4* (5), 1470–1477.

(34) Kruger, J. S.; Choudhary, V.; Nikolakis, V.; Vlachos, D. G. *ACS Catal.* **2013**, *3* (6), 1279–1291.

(35) Huang, H.; Denard, C. A.; Alamillo, R.; Crisci, A. J.; Miao, Y. R.; Dumesic, J. A.; Scott, S. L.; Zhao, H. M. *ACS Catal.* **2014**, *4* (7), 2165–2168.

(36) Tang, J.; Zhu, L.; Fu, X.; Dai, J.; Guo, X.; Hu, C. *ACS Catal.* **2017**, *7* (1), 256–266.

(37) Chiodini, N.; Paleari, A.; Dimartino, D.; Spinolo, G. *Appl. Phys. Lett.* **2002**, *81* (9), 1702–1704.

(38) Gu, F.; Wang, S. F.; Song, C. F.; Lü, M. K.; Qi, Y. X.; Zhou, G. J.; Xu, D.; Yuan, D. R. *Chem. Phys. Lett.* **2003**, *372* (3–4), 451–454.

(39) Pang, G.; Chen, S.; Koltypin, Y.; Zaban, A.; Feng, S.; Gedanken, A. *Nano Lett.* **2001**, *1* (12), 723–726.

(40) Bhagwat, M.; Shah, P.; Ramaswamy, V. *Mater. Lett.* **2003**, *57* (9–10), 1604–1611.

(41) Shah, P.; Ramaswamy, A. V.; Lazar, K.; Ramaswamy, V. *Microporous Mesoporous Mater.* **2007**, *100* (1–3), 210–226.

(42) Post, P.; Wurlitzer, L.; Maus-Friedrichs, W.; Weber, A. P. *Nanomaterials* **2018**, *8* (7), 1–19.

(43) Elizondo-Villarreal, N.; Obregón-Guerra, R.; García-Méndez, M.; Sánchez-Espinoza, A. P.; Alcorta-García, M. A.; Torres-Barrera, R. O.; Coello, V.; Castaño, V. M. *Rev. Adv. Mater. Sci.* **2016**, *47* (1–2), 74–78.

(44) Cui, X.; Chen, C.; Sun, S.; Zhou, D.; Ndayisenga, F.; Huo, M.; Zhu, S.; Zhang, L.; Crittenden, J. C. *Water Res.* **2018**, *143* (June), 136–145.

(45) Fu, H.; Ding, X.; Ren, C.; Li, W.; Wu, H.; Yang, H. *RSC Adv.* **2017**, *7* (27), 16513–16523.

(46) Zhang, J.; Liang, L.; Tian, Z.; Chen, L.; Subirade, M. *Food Chem.* **2012**, *133* (2), 390–399.

(47) Parry, E. P. *J. Catal.* **1963**, *2* (5), 371–379.

(48) Maronna, M. M.; Kruissink, E. C.; Parton, R. F.; Soulimani, F.; Weckhuysen, B. M.; Hoelderich, W. F. *Phys. Chem. Chem. Phys.* **2016**, *18* (32), 22636–22646.

(49) Van Der Graaff, W. N. P.; Tempelman, C. H. L.; Pidko, E. A.; Hensen, E. J. M. *Catal. Sci. Technol.* **2017**, *7* (14), 3151–3162.

(50) Capelli, S.; Cattaneo, S.; Stucchi, M.; Vandegehuchte, B. D.; Chieregato, A.; Villa, A.; Prati, L. *Catalysts* . 2022.

Chapter 3

Selective oxidation of furfural to succinic acid over Lewis acidic Sn-Beta

Abstract

Selective production of succinic acid from furfural with H_2O_2 over a pure Lewis acid catalyst Sn-Beta is reported. Under optimized reaction conditions 53 % yield of succinic acid was obtained and the catalyst was recyclable. 2(3H)-Furanone was detected as an intermediate in the reaction in 1H NMR, HH COSY NMR, LC-MS and GC-MS. Kinetic modeling reveals that Bayer-Villiger oxidation of furfural to 2(3H)-furanone is accelerated compared to other competing reactions in the presence of purely Lewis acidic Sn-Beta. The Lewis acid density of Sn-Beta catalyst was directly correlated to formation rate of products, confirming a Lewis acid catalyzed mechanism. Detailed characterization showed that Sn-Beta only activates furfural by coordinating to the carboxyl group and does not activate H_2O_2. On the other hand, parent HBeta-38 zeolite produced activated H_2O_2 in solution, which caused side reactions to produce maleic acid. Selectivity of Sn-Beta was also compared with TS-1, another Lewis acid zeolite, which produced maleic acid because of ability of TS-1 to activate H_2O_2 as hydroperoxy species. Therefore, Sn-Beta is a selective and reusable catalyst for succinic acid synthesis from biomass derived furfural.

3.1 Introduction

Succinic acid is a four-carbon dicarboxylic acid with versatile industrial application. The global market for succinic acid is expected to grow from US$132 to US$ 183 million during a period of 2018 to 2023 at a cumulative annual growth rate of 6.8 %.[1] Succinic acid is used as a C4 building block for synthesis of polyesters,[2–4] polyurethane,[5] cosmetics[6,7] and pharmaceuticals.[8–11] In addition, it is also a precursor for 1,4-butanediol,[12,13] vinyl pyrrolidone,[14] and succinimide.[15] Currently, oil-derived succinic acid is produced by oxidation of butane through maleic anhydride[16–18] or maleic acid[19] intermediates. Other methods involve oxidation of 1,4-butanediol and carbonylation of ethylene glycol.[20] These processes are no longer attractive from the perspective of a sustainable and carbon neutral future. Therefore, alternative means of producing succinic acid from biomass is attractive.

Being a four-carbon chemical the synthesis of succinic acid from biomass is difficult because of low abundance of tetrose sugars such as erythrose. Until now bacterial fermentation of C6 sugars with the help of bovine rumen bacteria is the most successful method for synthesis of bio-succinic acid.[21] Although, bacterial fermentation provides succinic acid in good selectivity, its industrial application has not been successful due to high operation cost.[22]

Catalytic synthesis of succinic acid from biomass is possible by oxidation of furfural, produced by dehydration of pentoses (xylose and arabinose)[23–26] and hexoses (glucose and fructose).[27–30] Eliminating one carbon atom from furfural through oxidative cleavage of the formyl group can produce succinic acid (Scheme 3.1). Until now Brønsted acid catalysts having an aromatic framework have been reported as catalysts for this reaction. Amberlyst 15, a catalyst with -SO_3H groups on polymeric resin, produces 72 %

succinic acid in the presence of aq. H_2O_2.[31,32] A π-π interaction between the benzene rings of polymeric resin and furfural stabilized the furfural during the reaction. Sulphonated graphene oxide, which has a polyaromatic extended 2D π-electron network, showed improved result of 88 % succinic acid yield owing to better interaction with furfural.[33] However, catalyst deactivation due to formation of humins is a major issue in furfural chemistry and catalyst with organic framework cannot be reactivated by calcination to remove organic deposits. Therefore, alternative catalysts should be designed for this reaction.

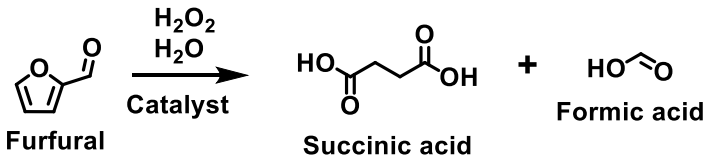

Scheme 3.1. Catalytic oxidation of furfural to bio-based succinic acid.

Here, we report a different approach to produce succinic acid through Bayer-Villiger oxidation (BVO) of furfural in the presence of Lewis acid catalysts. Water tolerant zeolites having tetravalent cations like Sn^{4+}, and Ti^{4+} in the framework instead of aluminum are known to exhibit pure Lewis acidity.[34] The catalytic property of such zeolites is well studied and they are known to be active for BVO[35,36] and Meerwein–Ponndorf–Verley reduction.[37,38] Among these catalysts, titanosilicalite-1 zeolite (TS1), has been reported for furfural oxidation to maleic acid in 53% yield.[39–42] In contrast, we show that Sn containing Sn-Beta zeolite catalyzes furfural oxidation to succinic acid. In our study, we identify the key intermediate for succinic acid formation and investigate the reasons for high selectivity of Sn-Beta towards succinic acid and propose a detailed reaction mechanism.

3.2 Experimental

3.2.1 Catalyst preparation

Sn/Beta catalyst was prepared according to a procedure mentioned elsewhere.[43] In a typical synthesis procedure, 4 g of zeolite (Zeolyst CP814C*, SiO_2/Al_2O_3 = 38, hereafter HBeta-38) was added to 100 mL of 13 N HNO_3 and the solution was refluxed at 100 °C for 20 h. Then the mixture was cooled to room temperature, followed by filtration, and washed with 2 liter of deionized water and then dried at 100 °C for 18 h. The resultant dealuminated zeolite was named as DeAl-Beta and 1.5 g of this material was mixed with 0.0562 g of Sn(II) acetate in a mortar. The mixture was ground for 10 min along with scratching with a teflon spatula at regular intervals and then heated under N_2 flow at 500 °C for 3 h ,with a ramp rate of 10 °C / min, followed by additional 3 h under air flow. The resulting catalyst was named as 2Sn-Beta with 2 wt% Sn loading. Catalysts with higher Sn loadings were prepared by increasing the amount of Sn(II) acetate used . TS-1 was purchased from ACS Material and used without modification. SnO_2 powder was bought from FUJIFILM Wako Pure Chemical Corporation and used as it is.

3.2.2 Catalyst Characterization

X-ray diffraction (XRD) was measured with Rigaku MiniFlex using CuKα X-ray (λ = 1.54 Å) operating at 40 kV and 20 mA. UV-visible diffuse reflectance spectroscopy (UV-vis) measurement was obtained using Jasco V-650 spectrophotometer, line width of light source was kept at 1 nm and polytetrafluoroethylene (PTFE) was used as reference. UV-Vis of liquids samples of TMB oxidation reaction was carried out in the same instrument, using water as reference. N_2 adsorption isotherms were measured at −196 °C using a

Belsorp mini analyzer. Surface area was calculated by using the BET theory in the relative pressure range 0.05 to 0.35 in the N_2 adsorption isotherm.[44]

Pyridine IR was done in a Shimadzu IR spirit instrument. For the pyridine adsorption IR experiment, the catalysts were pressed into self-supported wafers of 1 cm diameter of approximately 40 mg cm^{-2} wafer density. A pretreatment procedure of heating to 150 °C at 10 °C min^{-1} with vacuum was followed to make sure there is no physisorbed moisture or other possible contaminants. Pyridine was dosed at room temperature until the spectrum showed shoulder peaks to the major peaks (which is a sign of saturation). Initial desorption was done with vacuum until no desorption was observed. Finally, desorption was done via heating up to 150 °C.

Quantitative calculation of number of acid sites were done using the following equation:

$$N = \frac{A}{\epsilon \times \rho}$$

Where N is density of acid sites in μmol g^{-1}, A is the integrated peak area in cm^{-1}, ϵ is the integrated molar extinction coefficient (cm μmol^{-1}) and ρ is the wafer density (mg cm^{-2}). Peak deconvolution was performed using Fityk curve fitting program. The value of integrated molar extinction coefficient was taken from Datka et al.[45]

Furfural adsorption DRIFTS was performed with Perkin Elmer Spectrum 100 instrument. Prior to DRIFTS experiment the catalyst was dehydrated at 150 °C for 1 hour. Furfural was introduced by dropping 10 mg of furfural to the sample using a Gilson Pipetman micropipette. After making sure of adsorption, from the spectrum, desorption process was carried out by evacuation along with heating.

3,3',5,5'-tetramethylbenzidine(TMB) oxidation reactions were carried out at room

temperature in a glass tube. In a typical reaction 1 mL TMB solution (10 mg per mL in DMSO) was added to 4 mL pH 4 buffer solution, followed by 5 mL H_2O_2. 50 mg Catalyst was used (5 mg per mL dispersion). Once the catalyst was added the time was marked as 0 and sampling was done at 5-minute intervals, filtered with 0.22 μm syringe filter and the UV Vis measurement was done against that of deionized water.

3.2.3 Catalytic oxidation of Furfural

In a typical oxidation reaction, 1 mmol of furfural (distilled before use) was dissolved in 5 mL water in a two neck round bottom flask and 50 mg of catalyst was added. The flask was placed in a preheated oil bath and 44 mmol of H_2O_2 was added and the reaction time was set to zero. After the completion of reaction, the catalyst was separated by centrifugation and washed with acetonitrile to extract the compounds with poor water solubility. An additional wash was performed with water and all the collected liquids were mixed together and diluted to a fixed volume. This solution was analyzed using a Shimadzu HPLC system equipped with a Biorad Aminex HPX-87H column and an RID detector. Furfural conversion (X_F) and product yields (Y_P) were calculated using the following equations.

$$X_F = \frac{N_F\ initial - N_F\ remaining}{N_F\ initial} \times 100\ \%$$

$$Y_P = \frac{N_P\ obtained}{N_F\ initial} \times 100\ \%$$

Where N_F is the number of moles of furfural and N_P is the number of moles of product.

3.3 Results and discussion

3.3.1 Sn-Beta characterization

Sn-Beta catalysts were prepared by dealumination of HBeta-38 to remove Brønsted acid sites followed by inclusion of Sn atoms in the empty T-sites in order to have pure Lewis acid sites. Nature of acid sites in the prepared catalysts was analyzed by pyridine adsorption IR experiment to study the change in Brønsted and Lewis acid density (Figure 3.1a). After pyridine adsorption, the peak at 1455 cm^{-1} was assigned to ring vibration of coordinatively bound surface pyridine species to Lewis acid sites and the peak at 1540 cm^{-1} was assigned to that of surface pyridinium ions interacting with Brønsted acid sites.[45] Lewis acid density of 2Sn-Beta (containing 2 wt% Sn loading) was significantly higher than the parent HBeta-38 zeolite, whereas the Brønsted acid density was negligible. The Brønsted acid sites were lost during dealumination of HBeta-38 because the charge imbalance between tetra valent Si and trivalent Al was no longer present. Sn itself being tetravalent leads to an electrically neutral framework, hence there is no proton as counter balancing ion to generate Brønsted acidity in the 2Sn-Beta catalyst. DeAl-Beta showed no acidity at all and the peaks at 1445 and 1435 cm^{-1} were assigned to hydrogen bonding interaction with pyridine, probably because of high number of silanol groups. Hence, it can be concluded that Lewis acidity in the 2Sn-Beta catalyst was due to Sn incorporation.

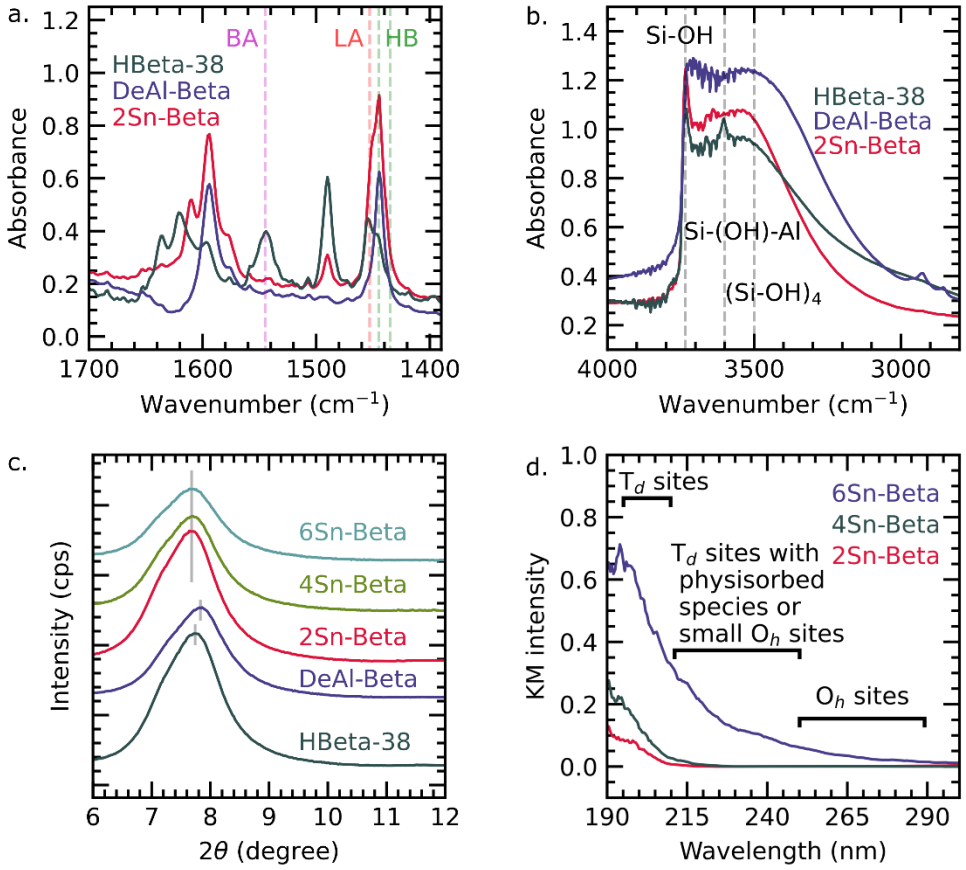

Figure 3.1. a) Pyridine adsorption IR spectrum for HBeta-38, DeAl-Beta and 2Sn-Beta. BA, LA and HB indicate peaks due to Brønsted acidity, Lewis acidity and hydrogen bonded pyridine, respectively. b) IR spectrum of silanol region showing dealumination and Sn incorporation into zeolite Beta. c) XRD of catalysts. d) UV-Visible spectrum of Sn-Beta with different Sn loading.

The dealumination and Sn incorporation process was also monitored by FTIR analysis of the silanol region (Figure 3.1b). Spectrum for HBeta-38 consisted of two sharp peaks at 3710 cm^{-1} and 3600 cm^{-1} that were assigned to -OH stretching of individual surface terminated silanol groups (Si-OH)[46] and -OH stretching of bridged -OH groups between neighboring Si and Al, respectively. A broad peak with relatively less intensity ranging from 3200 to 3600 cm^{-1} was assigned to hydrogen bonded silanol nests.[46] After

dealumination the -OH stretching of bridged -OH groups at 3600 cm^{-1} disappeared as Si-O-Al bridges were no longer present. Simultaneously, the relative intensity of the broad peak increased due to creation of new hydrogen bonded silanol nests. These silanol nests serve as anchoring site for the incoming Sn cations. After incorporation of Sn, the relative intensity of the broad peak decreased in comparison to terminated -OH stretching peak at 3710 cm^{-1} because some of the nests were now occupied with Sn atoms.

The dealumination and Sn incorporation also caused a change in the lattice structure of zeolite, which was observed by powder XRD of the catalysts. The diffraction peak of zeolite crystal at $2\theta = 7.8^{\circ}$ shifted towards higher 2θ value after dealumination (Figure 3.1c), which was attributed to lattice shrinkage due to removal of Al atoms from the HBeta-38 unit cell.[47] The peak position shifted back to lower 2θ value after incorporation of Sn. Moreover, diffraction peaks for SnO_2 were not observed in XRD even when Sn loading was increased to 6 wt. % (Figure 3.2). SnO_2 can form due to oligomerization of Sn species that are unable to form a tetrahedrally coordinated Sn site in the empty silanol nests. The absence of diffraction for SnO_2 could either mean that there are no SnO_2 particles or that the SnO_2 particles are small and lack long range order.

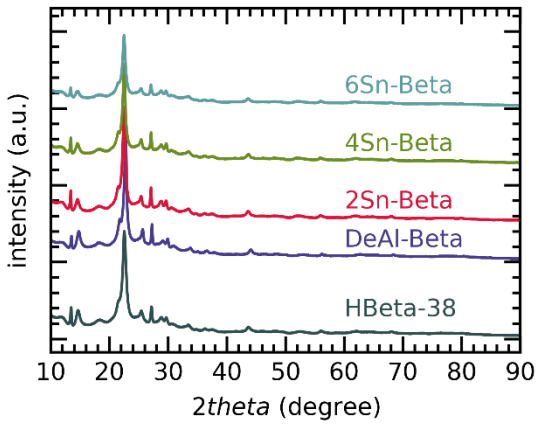

Figure 3.2. Powder XRD of zeolite (HBeta-38) (SiO_2/Al_2O_3 = 38), Dealuminated Beta (DeAl-Beta) and different amount of Sn incorporated Sn-Beta

Further insight into SnO_2 formation was obtained by observing the shift in UV-visible absorption maxima with respect of Sn loading in Sn-Beta catalyst. The shift in absorption maxima can be correlated with Sn coordination number and particle size domain.[48–50] 2Sn-Beta and 4Sn-Beta catalysts, having 2 and 4 wt% Sn content, only showed absorption below 210 nm assigned to isolated tetrahedral Sn atoms (T_d) of Sn-Beta zeolite (Figure 3.1d).[51] For 6Sn-Beta, having 6 wt% Sn loading, absorption at higher wavelength was also present, which suggests formation of small SnO_2 particles with octahedral Sn species (O_h).[48–50] Therefore, 2Sn-Beta and 4Sn-Beta catalysts had Sn exclusively present as Lewis acidic tetrahedral Sn sites and catalyst with higher Sn loading contained some SnO_2 species although the presence of tetrahedral Sn species was still dominant.

3.3.2 Furfural Oxidation over different catalysts

Furfural oxidation in water and H_2O_2 in the absence of any catalyst showed 5 % succinic acid yield along with slight amount of 2(5H)-furanone (Figure 3.3). In the presence of 2Sn-Beta, under optimized condition the yield of succinic acid was 53 %.

Maleic acid, malic acid and 2(5H)-furanone were the major by-products. HBeta-38 catalyst was not selective and produced comparable amounts of succinic acid, 2(5H)-furanone and maleic acid. Activity of pure SnO_2 was not much different from HBeta-38, which shows that pure Lewis acidic nature of Sn is important for succinic acid selectivity. In contrast, another Lewis acid zeolite TS-1 produced maleic acid selectively with low amount of succinic acid. This behavior of TS-1 is consistent with previous reports describing selective synthesis of maleic acid.[39–42] From these results it is evident that while Brønsted acid zeolite was not selective towards any product, Lewis acid catalysts (Sn-Beta and TS-1) were able to selectively produce succinic acid or maleic acid.

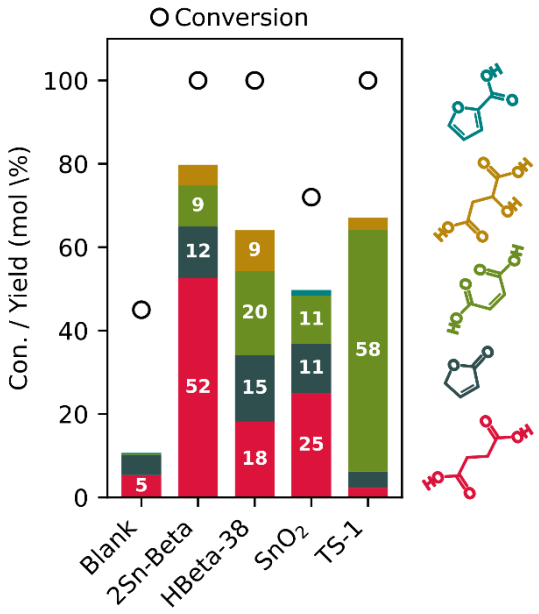

Figure 3.3. Catalytic activity of different catalysts for furfural oxidation reaction. Reaction conditions: furfural 1 mmol (96 mg), catalyst 50 mg, 15 % H_2O_2 solution 10 mL, 50 °C

Recyclability of 2Sn-Beta was investigated and the catalyst activity did not drop for 4 runs (Figure 3.4a). However, the color of the catalyst changed to pale yellow, which suggested deposition of organic matter on the catalyst (Figure 3.4b). After the 4th catalytic

cycle we calcined the catalyst in the same conditions as in its preparation, which recovered back the catalyst color back to white. The recalcined catalyst when tested in the reaction showed no loss of activity. This shows that after several runs if the catalyst is deactivated it can be calcined to reactivate, which is a big advantage over the carbon based catalysts.

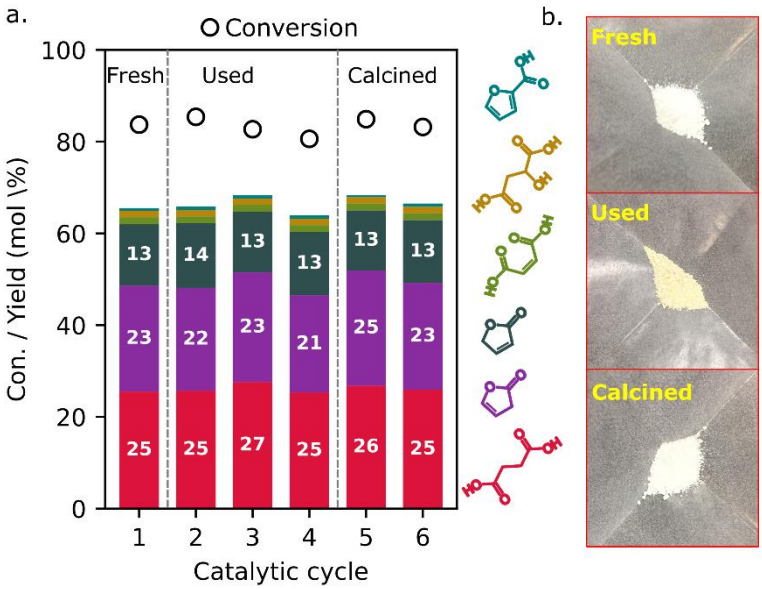

Figure 3.4. a. Catalyst recyclability test reactions. Reaction conditions: furfural 1 mmol, catalyst 50 mg, 15 % H_2O_2 solution 10 mL, 50 °C, 1 h., b. picture of fresh catalyst (Fresh), used catalyst (Used catalyst) after 4 runs and after calcining the used catalyst (Calcined)

The time course of reaction in the presence of 2Sn-Beta showed that the formation of succinic acid was preceded by formation of 2(3H)-furanone (Figure 3.5a). This compound has been suggested as an intermediate in earlier studies.[31,32] We were able to positively identify 2(3H)-furanone by using NMR (Figure 3.6) and GC-MS (Figure 3.7) and quantify it using LC. In contrast to 2Sn-Beta, the formation of 2(3H)-furanone over HBeta-38 was not prominent. In the presence of TS-1, 5-hydroxy-2(3H)-furanone was formed as the major intermediate for maleic acid.

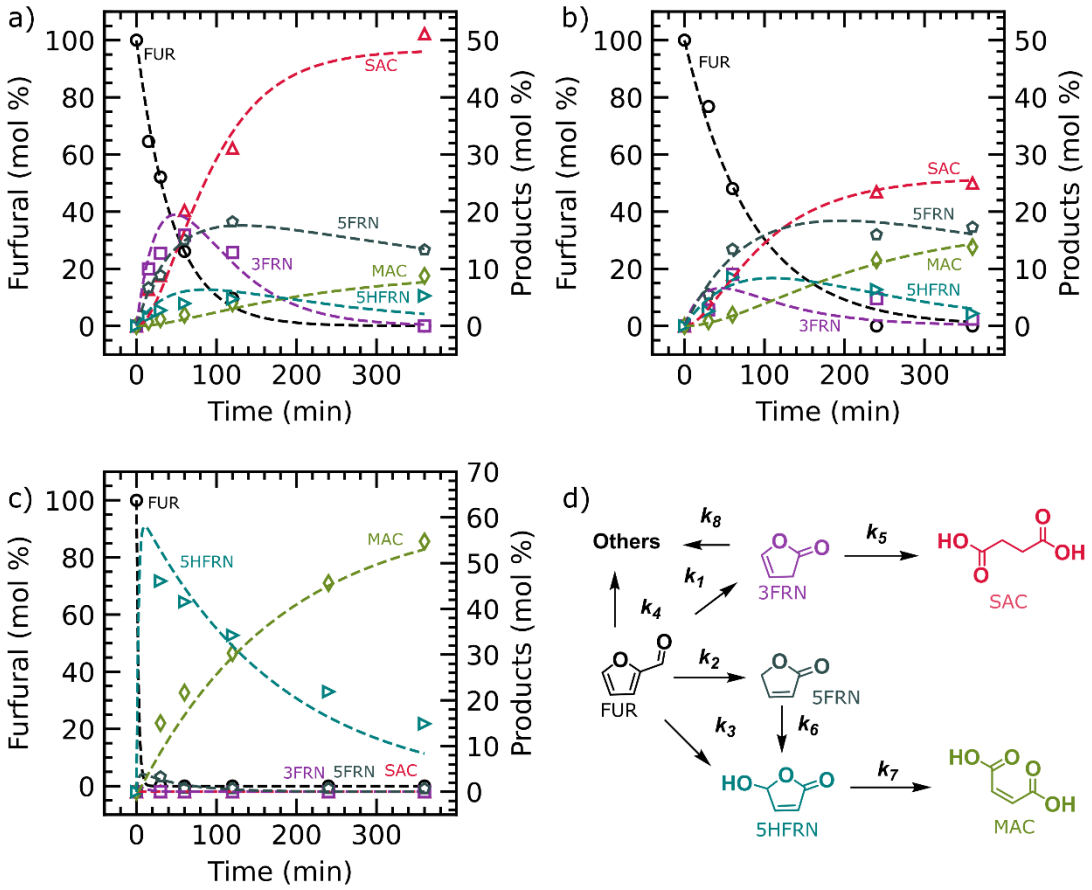

Figure 3.5. Time course of furfural oxidation in the presence of (a) 2Sn-Beta, (b) HBeta-38 and (c) TS-1. The symbols represent experimental data and the lines show fitting of experimental data with reaction model shown in d. Reaction conditions: furfural 1 mmol (96 mg), catalyst 50 mg, 15 % H_2O_2 solution 10 mL, 50 °C

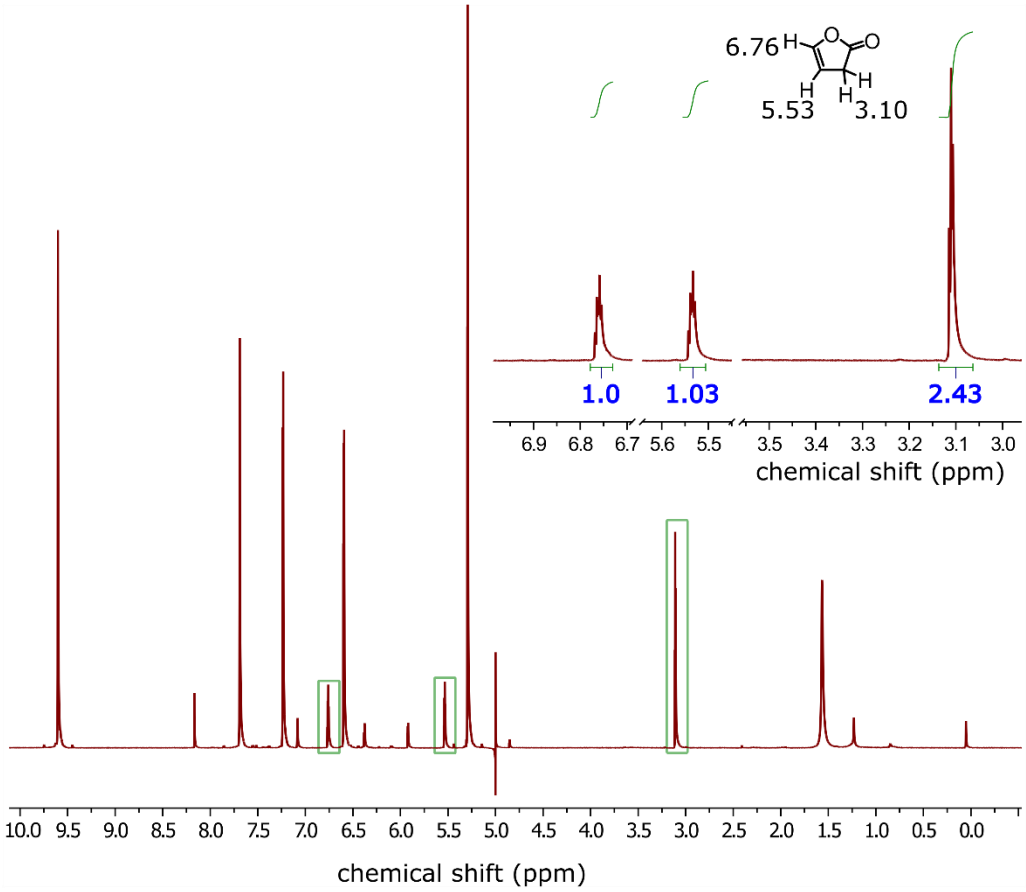

Figure 3.6. Ex-situ 1D NMR detection of 2(3H)-furanone

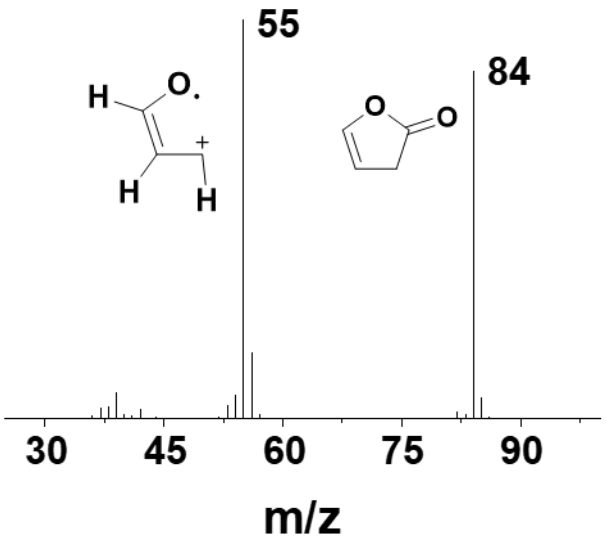

Figure 3.7. EI-MS of 2(3H)-furanone in GC-MS extracted from reaction mixture with dichloromethane

We performed kinetic analysis of the reaction by using reaction scheme shown in

Figure 3.3d and modelling the experimental data using equations 1-6.

$$\frac{d[FUR]}{dt} = -(k_1 + k_2 + k_3 + k_4) \times [FUR] \quad (1)$$

$$\frac{d[3FRN]}{dt} = k_1[FUR] - (k_5 + k_8) \times [3FRN] \quad (2)$$

$$\frac{d[5FRN]}{dt} = k_2 \times [FUR] - k_6 \times [5FRN] \quad (3)$$

$$\frac{d[5HFRN]}{dt} = k_3 \times [FUR] + k_6 \times [5FRN] - k_7 \times [5\text{HFRN}] \quad (4)$$

$$\frac{d[SAC]}{dt} = k_5 \times [3FRN] \quad (5)$$

$$\frac{d[MAC]}{dt} = k_7 \times [5HFRN] \quad (6)$$

where k_1-k_7 represent rate constants for reactions shown in Figure 3.5d, FUR stands for furfural, 3FRN 2(3H)-furanone, 5FRN 2(5H)-furanone, 5HFRN 5-hydroxy-2(5H)-furanone, SAC succinic acid and MAC maleic acid. Products like furoic acid and malic acid were not modeled in the reaction as their concentration was too low.

Rate constants were estimated by fitting the model to experimental data by assuming pseudo-first order-reactions (Table 3.1). The formation rate of 2(3H)-furanone (k_1 = 0.64 h^{-1}) and 2(5H)-furanone (k_2 = 0.28 h^{-1}) was higher in the presence of 2Sn-Beta catalyst in comparison to other reaction pathways. Whereas, in the case of Brønsted acid containing H-Beta38, both 2(3H)-furanone and 2(5H)-furanone has similar formation rate. Moreover, the rate of formation for 5-hydroxy-2(3H)-furanone and furfural degradation was also comparable to the hydrofuranone formation rates, which was the reason for nonselective reaction. The kinetic analysis of reaction in the presence of TS-1 catalyst showed that formation of 5-hydroxy-2(5H)-furanone was highly favored. This is why TS-1 selectively produces maleic acid. Therefore, it is evident that higher rate of formation

of 2(3H)-furanone over Lewis acidic 2Sn-Beta is the primary reason for selective succinic acid formation. Moreover, the subsequent conversion of 2(3H)-furanone to succinic acid was faster than its formation from furfural ($k_5 > k_1$). The formation of 2(3H)-furanone is possible via BVO of furfural as shown in scheme 3.2. BVO of furfural would produce a formate ester which would undergo hydrolysis in the presence of water to yield a furan alcohol. The isomerization of furan alcohol would produce 2(3H)-furanone and 2(5H)-furanone.

Table 3.5. Estimated rate constants from the kinetic fitting. The rate constants are in the unit of h^{-1}.

Catalyst	k_1	k_2	k_3	k_4	k_5	k_6	k_7	k_8
2Sn-Beta	0.64	0.28	0.13	0.28	1.12	0.09	0.30	0
HBeta-38	0.24	0.18	0.13	0.17	1.63	0.09	0.41	0.48
TS-1	-	-	12.5	6.67	-	-	0.33	-

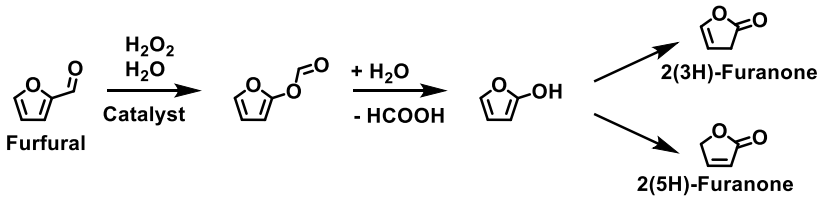

Scheme 3.2. Formation pathway of hydrofuranones from furfural.

The BVO reaction of aldehydes is catalyzed by Lewis acid sites.[52,53] Therefore, we investigated the influence of Lewis acid density of Sn-Beta catalysts for furfural oxidation. The Lewis acid density was calculated by quantitative analysis after pyridine adsorption IR spectra of catalysts with different Sn loading. The peak intensity of adsorbed pyridine at 1455 cm^{-1} increased steadily with increase in Sn loading (Figure 3.8a). The initial

catalytic activity (here expressed as sum of moles of succinic acid and 2(3H)-furanone per hour) increased with the Lewis acid density (Figure 3.8b). This indicates that activation of furfural over Lewis acidic Sn sites followed by BVO was important for higher selectivity.

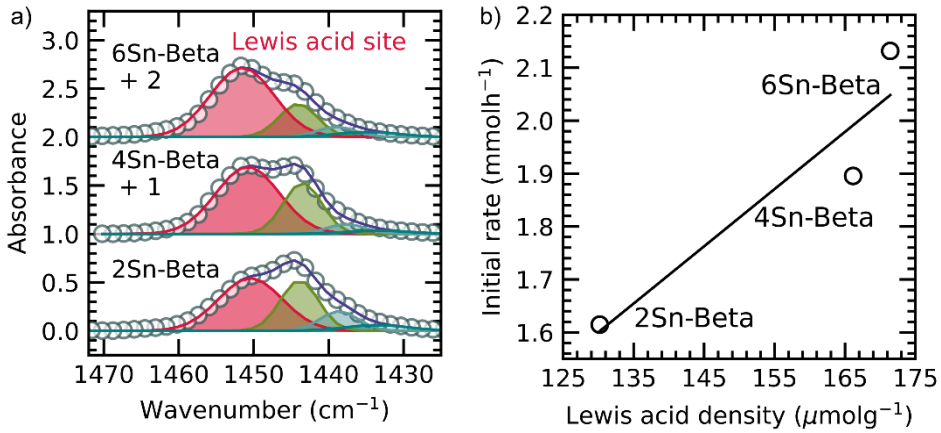

Figure 3.8. (a) Deconvoluted pyridine adsorption IR spectrum of Sn-Beta catalysts in the Lewis acid region, the crimson color peak at 1455 cm^{-1} represents ring vibration of pyridine interacting with Lewis acid sites, other peaks corresponds to ring vibration of hydrogen bonded pyridine to silanol groups, line with blue markers represents experimental data. (b) Plot of Lewis acid site (LAS) density vs initial activity. Reaction conditions: furfural 5 mmol (480 mg), catalyst 50 mg, 15 % H_2O_2 solution 10 mL, 50 °C, 1 h.

In order to investigate the role of Sn-Beta in promoting BVO reaction we investigated the interaction of catalyst with furfural and H_2O_2. DRIFTS experiment was performed to observe the activation of furfural over 2Sn-Beta. Prior to DRIFTS analysis, the catalyst surface was saturated with furfural and then excess furfural was desorbed by heating under vacuum. DRIFTS analysis of adsorbed furfural on 2Sn-Beta catalyst showed two major peaks at 1724 cm^{-1} and 1671 cm^{-1} in the carbonyl region (Figure 3.9).

The first peak was assigned to carbonyl stretching frequency of uncoordinated furfural and second one to coordinated furfural to a strong Lewis acid site. A shoulder peak to the 1671 cm^{-1} appeared at 1690 cm^{-1}, which can assigned to furfural coordinated to a possible weak lewis acidic site on the catalyst. From this observation it can be inferred that Sn sites of Sn-Beta strongly interacted with the carbonyl group of furfural. Similar interaction was not observed for the parent zeolite HBeta-38 in which Brønsted acid sites are dominant species compared to Lewis acid sites. On the other hand, TS-1 showed a weaker adsorption of furfural carbonyl group in comparison to 2Sn-Beta. The redshift in carbonyl peak position was less severe at 1690 cm^{-1} for TS-1. Therefore, we can conclude that 2Sn-Beta strongly adsorbed the carbonyl group of furfural and adsorption on TS-1 was weaker. In contrast, the interaction of carbonyl group with HBeta-38 was negligible. When coordinated to the Lewis acid sites, electrophilicity of the carbonyl carbon atom increases and from the above observations 2Sn-Beta was most effective in this regard.

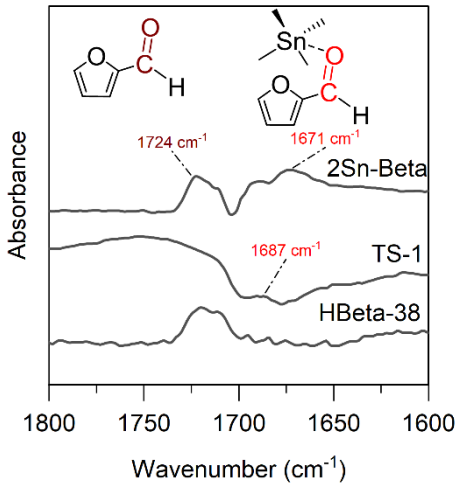

Figure 3.9. DRIFTS spectra of furfural adsorbed on various catalysts.

The interaction of catalysts with H_2O_2 is also a major factor that influences selectivity. Activation of H_2O_2 may produce species that are even stronger nucleophiles in comparison to H_2O_2. We treated the catalysts with aqueous H_2O_2 solution and observed

the diffuse reflectance UV-visible spectra. H_2O_2 is activated on the surface of the catalyst to form metal-hydroperoxy (M-OOH) species, which gives rise to a yellow color, and it appears as a peak around 390 nm in UV-vis (Figure 3.10). Only TS-1 showed activity for formation of Ti-OOH species and both 2Sn-Beta and HBeta-38 zeolite were inactive. Formation of Ti-OOH species with TS-1 in the presence of H_2O_2 is consistent with literature.[54,55]

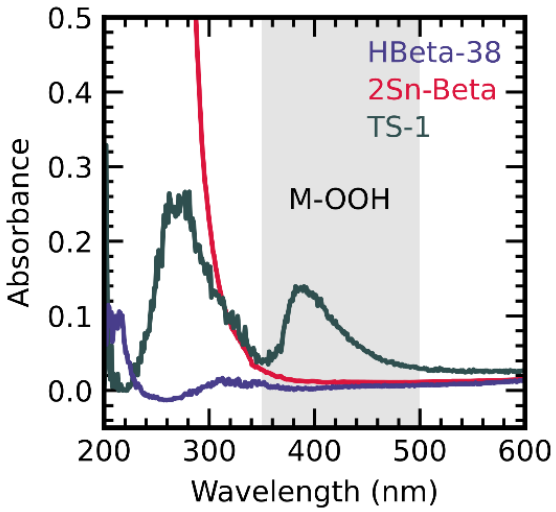

Figure 3.10. UV-vis spectroscopy to determine formation of M-OOH species in the presence of H_2O_2 on various catalysts.

At this point it is worth mentioning that metal hydroperoxy species are known to catalyze epoxidation reaction; hence the formation of 5-hydroxy-2(5H)-furanone over TS-1 could be a direct result of epoxidation of the double bond between C4-C5 carbon atoms of furfural in the presence of Ti-OOH species (Scheme 3.3).

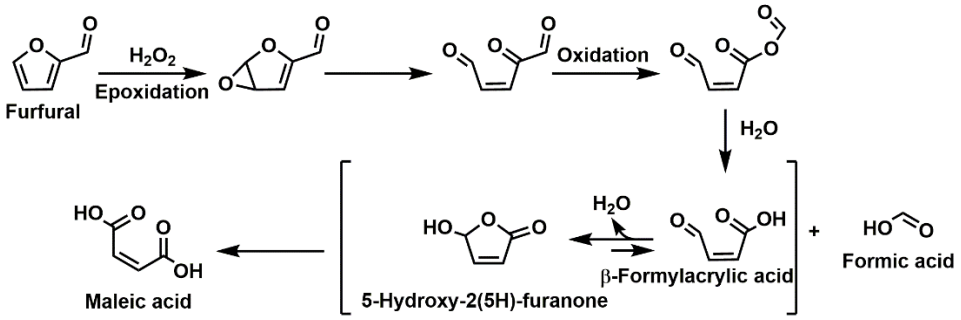

Scheme 3.3. Reaction pathway for formation of maleic acid, via furfural epoxidation.

In addition to surface activation, H_2O_2 can also be activated in solution. The activation of H_2O_2 with HBeta-38 was tested by two-electron oxidation of 3,3',5,5'-tetramethylbenzidine (TMB), shown in Figure 3.11a.[56–58] The oxidation product is a blue color compound, which can be monitored with UV-visible spectrum. The activity of 2Sn-Beta for oxidation of TMB was quite low and almost no reaction occurred after 30 min (Figure 3.11b), which shows 2Sn-Beta has limited ability to activate H_2O_2 in solution. On the other hand, in the presence of HBeta-38, rapid oxidation of TMB proceeded, which implies that H_2O_2 was activated by HBeta-38, probably via protonation of H_2O_2. This leads to the conclusion that pure Lewis acid nature of Sn-Beta catalyst is important for formation of succinic acid.

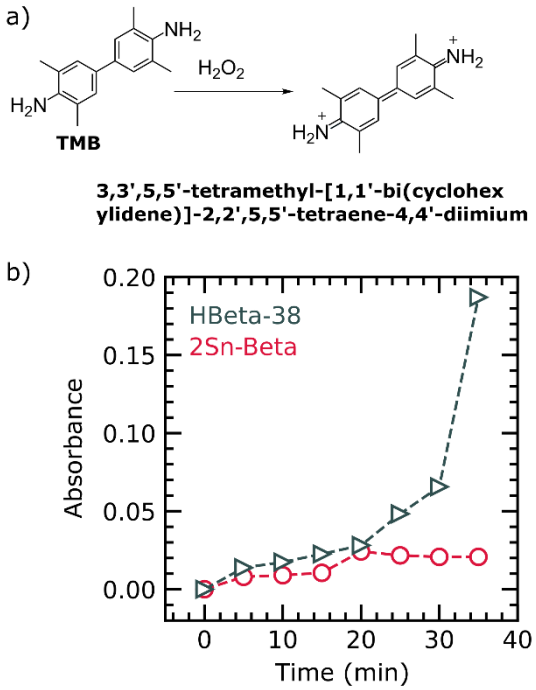

Figure 3.11. Evolution of TMB oxidation product with time monitored using UV-Vis spectroscopy. (a) TMB oxidation reaction scheme. (b) Time course of band centered around 660 nm in UV-Vis spectra of TMB oxidation reaction in the presence of HBeta-

38 and 2Sn-Beta.

From the above observations, it can be summarized that 2Sn-Beta does not interact with H_2O_2 either to form M-OOH or to activate H_2O_2 in solution. In contrast, TS-1 makes surface hydroperoxy species and HBeta-38 activates H_2O_2 via protonation.

Considering the strong adsorption of furfural on Lewis acid sites of 2Sn-Beta catalyst and the lack of interaction between H_2O_2 and catalyst, we propose the following reaction mechanism for succinic acid formation (Scheme 3.4). Furfural is first adsorbed on the tetrahedrally coordinated Sn site of Sn-Beta, which polarizes the C=O bond to make the carbon more electron deficient. A nucleophilic attack of non-activated H_2O_2 on the electron deficient carbonyl carbon forms formate easter via Bayer-Villiger oxidation, followed by hydrolysis to form a furan alcohol. Keto-enol tautomerization of the furan alcohol produces 2(3H)-furanone and 2(5H)-furanone. While 2(5H)-furanone was stable, 2(3H)-furanone underwent hydrolysis with oxidative ring opening to form a succinic semialdehyde. This compound is not stable in aqueous solution and underwent oxidation to form succinic acid.

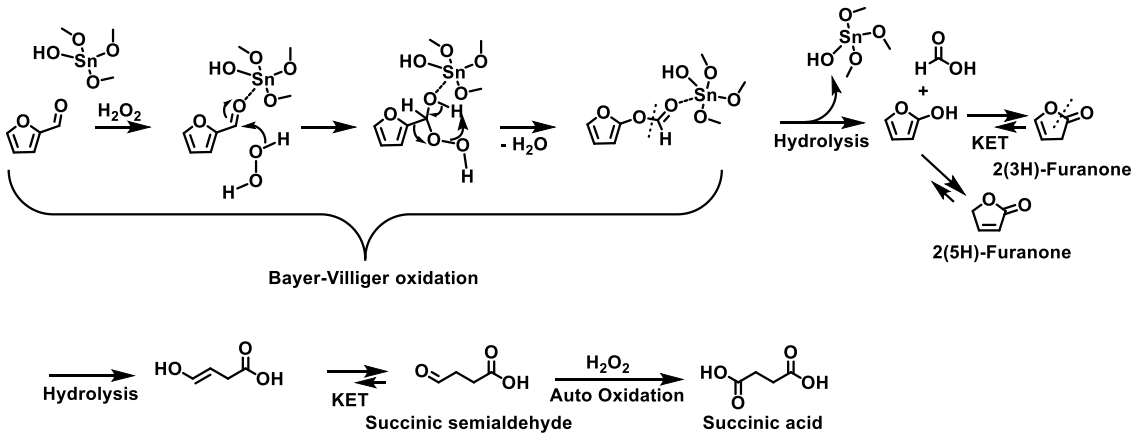

Scheme 3.4. Proposed reaction pathway for furfural oxidation to succinic acid over Sn-Beta Lewis acid catalyst.

3.4 Conclusion

In conclusion, we have shown that furfural oxidation with pure Lewis acidic Sn-Beta forms succinic acid with a yield of 53 %. 2(3H)-Furanone was identified as the intermediate for succinic acid formation and kinetic analysis showed that its formation by Bayer-Villiger oxidation was promoted over Sn-Beta catalyst. The rate of reaction was directly correlated with the density of Lewis acid sites, which activated the aldehyde group of furfural as observed in DRIFTS analysis. In addition, the inability of Sn-Beta to activate H_2O_2 suppressed the side reactions to achieve a high succinic acid selectivity. In contrast, furfural oxidation reaction over HBeta-38 and TS-1 was not selective because they activated H_2O_2 either in solution form or as metal hydroperoxyl species. Consequently, Sn-Beta was a unique and reusable Lewis acid catalyst for furfural oxidation to succinic acid.

3.5 References

(1) Markets and Markets. Succinic Acid Market by Type (Bio-Based Succinic Acid, Petro-Based Succinic Acid), End-Use Industry (Industrial, Food & Beverage, Coatings, Pharmaceutical), and Region (APAC, Europe, North America, South America, Middle East & Africa) - Forecast to 2023 https://www.marketsandmarkets.com/Market-Reports/succinic-acid-market-402.html (accessed 2021 -09 -06).

(2) Harmsen, P. F. H.; Hackmann, M. M.; Bos, H. L. *Biofuels, Bioprod. Biorefining* **2014**, *8* (3), 306–324.

(3) Luman, N. R.; Kim, T.; Grinstaff, M. W. *Pure Appl. Chem.* **2004**, *76* (7–8), 1375–1385.

(4) Sacan, L.; Cirpan, A.; Camurlu, P.; Toppare, L. *Synth. Met.* **2006**, *156* (2–4), 190–195.

(5) Sonnenschein, M. F.; Guillaudeu, S. J.; Landes, B. G.; Wendt, B. L. *Polymer (Guildf).* **2010**, *51* (16), 3685–3692.

(6) Tashihiro, M.; Nagare, Y.; Matsui, T. US 2020/0155440 A1, May 21, 2020.

(7) Sarosi, C.; Moldovan, M.; Miuta, F.; Prodan, D.; Antoniac, A.; Prejmerean, C.; Silaghi Dumitrescu, L.; Popescu, V.; Raiciu, A. D.; Saceleanu, V. *Materials*

(Basel). **2019**, *12* (13), 2106.

(8) Pfister, B.; Jonsson, J.; Gustafsson, M. *BMC Pharmacol. Toxicol.* **2017**, *18* (1), 52.

(9) Zhang, F.; Zhou, F.; Wei, W. *Chinese J. Biochem. Pharm.* **2017**, *37* (2), 68–71.

(10) Plumb, D. C. *Plumb's Veterinary Drug Handbook: Desk*; John Wiley & Sons, 2018.

(11) Cao, G.-Y.; Li, K.-X.; Jin, P.-F.; Yue, X.-Y.; Yang, C.; Hu, X. *Clin. Ther.* **2011**, *33* (12), 2054–2059.

(12) Ly, B. K.; Minh, D. P.; Pinel, C.; Besson, M.; Tapin, B.; Epron, F.; Especel, C. *Top. Catal.* **2012**, *55* (7), 466–473.

(13) Minh, D. P.; Besson, M.; Pinel, C.; Fuertes, P.; Petitjean, C. *Top. Catal.* **2010**, *53* (15–18), 1270–1273.

(14) Haus, M. O.; Louven, Y.; Palkovits, R. *Green Chem.* **2019**, *21* (23), 6268–6276.

(15) Liu, Y.; Fu, J.; Ren, D.; Song, Z.; Jin, F.; Huo, Z. *ChemistrySelect* **2018**, *3* (2), 724–728.

(16) Huang, Y.; Ma, Y.; Cheng, Y.; Wang, L.; Li, X. *Appl. Catal. A Gen.* **2015**, *495*, 124–130.

(17) Liao, X.; Zhang, Y.; Hill, M.; Xia, X.; Zhao, Y.; Jiang, Z. *Appl. Catal. A Gen.* **2014**, *488*, 256–264.

(18) Torres, C. C.; Alderete, J. B.; Mella, C.; Pawelec, B. *J. Mol. Catal. A Chem.* **2016**, *423*, 441–448.

(19) Granados, M. L.; Moreno, J.; Alba-Rubio, A. C.; Iglesias, J.; Alonso, D. M.; Mariscal, R. *Green Chem.* **2020**, *22* (6), 1859–1872.

(20) Cornils, B.; Lappe, P.; by Staff, U. *Ullmann's Encycl. Ind. Chem.* **2014**, 1–18.

(21) Song, H.; Lee, S. Y. *Enzyme Microb. Technol.* **2006**, *39* (3), 352–361.

(22) Li, X.; Mupondwa, E. *Renew. Sustain. Energy Rev.* **2021**, *137*, 110587.

(23) Wang, Y.; Yang, X.; Zheng, H.; Li, X.; Zhu, Y.; Li, Y. *Mol. Catal.* **2019**, *463*, 130–139.

(24) Wang, Y.; Ding, G.; Yang, X.; Zheng, H.; Zhu, Y.; Li, Y. *Appl. Catal. B Environ.* **2018**, *235*, 150–157.

(25) Asakawa, M.; Shrotri, A.; Kobayashi, H.; Fukuoka, A. *Green Chem.* **2019**, *21* (22), 6146–6153.

(26) Wang, L.; Guo, H.; Xie, Q.; Wang, J.; Hou, B.; Jia, L.; Cui, J.; Li, D. *Appl. Catal. A Gen.* **2019**, *572*, 51–60.

(27) Gupta, N. K.; Fukuoka, A.; Nakajima, K. *ACS Sustain. Chem. Eng.* **2018**, *6* (3), 3434–3442.

(28) Gupta, N. K.; Fukuoka, A.; Nakajima, K. *ACS Catal.* **2017**, *7* (4), 2430–2436.

(29) Lam, E.; Chong, J. H.; Majid, E.; Liu, Y.; Hrapovic, S.; Leung, A. C. W.; Luong, J. H. T. *Carbon N. Y.* **2012**, *50* (3), 1033–1043.

(30) Dias, A. S.; Pillinger, M.; Valente, A. A. *J. Catal.* **2005**, *229* (2), 414–423.

(31) Choudhary, H.; Nishimura, S.; Ebitani, K. *Appl. Catal. A Gen.* **2013**, *458*, 55–62.

(32) Choudhary, H.; Nishimura, S.; Ebitani, K. *Chem. Lett.* **2012**, *41* (4), 409–411.

(33) Zhu, W.; Tao, F.; Chen, S.; Li, M.; Yang, Y.; Lv, G. *ACS Sustain. Chem. Eng.* **2019**, *7* (1), 296–305.

(34) Wolf, P.; Hammond, C.; Conrad, S.; Hermans, I. *Dalt. Trans.* **2014**, *43* (11), 4514–4519.

(35) Renz, M.; Blasco, T.; Corma, A.; Fornes, V.; Jensen, R.; Nemeth, L. *Chem. Eur. J.* **2002**, *8* (20), 4708–4717.

(36) Corma, A.; Nemeth, L. T.; Renz, M.; Valencia, S. *Nature* **2001**, *412* (6845), 423–425.

(37) Corma, A.; Domine, M. E.; Nemeth, L.; Valencia, S. *J. Am. Chem. Soc.* **2002**, *124* (13), 3194–3195.

(38) Corma, A.; Domine, M. E.; Valencia, S. *J. Catal.* **2003**, *215* (2), 294–304.

(39) Alonso-Fagúndez, N.; Agirrezabal-Telleria, I.; Arias, P. L.; Fierro, J. L. G.; Mariscal, R.; Granados, M. L. *RSC Adv.* **2014**, *4* (98), 54960–54972.

(40) Lou, Y.; Marinkovic, S.; Estrine, B.; Qiang, W.; Enderlin, G. *ACS Omega* **2020**, *5* (6), 2561–2568.

(41) Rodenas, Y.; Mariscal, R.; Fierro, J. L. G.; Martín Alonso, D.; Dumesic, J. A.; López Granados, M. *Green Chem.* **2018**, *20* (12), 2845–2856.

(42) Rodenas, Y.; Fierro, J. L. G.; Mariscal, R.; Retuerto, M.; López Granados, M. *Top. Catal.* **2019**, *62* (5–6), 560–569.

(43) Hammond, C.; Conrad, S.; Hermans, I. *Angew. Chemie - Int. Ed.* **2012**, *51* (47), 11736–11739.

(44) Brunauer, S.; Emmett, P. H.; Teller, E. *J. Am. Chem. Soc.* **1938**, *60* (2), 309–319.

(45) Datka, J.; Turek, A. M.; Jehng, J. M.; Wachs, I. E. *J. Catal.* **1992**, *135* (1), 186–199.

(46) Tang, B.; Dai, W.; Wu, G.; Guan, N.; Li, L.; Hunger, M. *ACS Catal.* **2014**, *4* (8), 2801–2810.

(47) Hammond, C.; Padovan, D.; Al-Nayili, A.; Wells, P. P.; Gibson, E. K.; Dimitratos, N. *ChemCatChem* **2015**, *7* (20), 3322–3331.

(48) Bhagwat, M.; Shah, P.; Ramaswamy, V. *Mater. Lett.* **2003**, *57* (9–10), 1604–1611.

(49) Gu, F.; Wang, S. F.; Song, C. F.; Lü, M. K.; Qi, Y. X.; Zhou, G. J.; Xu, D.; Yuan, D. R. *Chem. Phys. Lett.* **2003**, *372* (3–4), 451–454.

(50) Pang, G.; Chen, S.; Koltypin, Y.; Zaban, A.; Feng, S.; Gedanken, A. *Nano Lett.* **2001**, *1* (12), 723–726.

(51) Moliner, M.; Roman-Leshkov, Y.; Davis, M. E. *Proc. Natl. Acad. Sci.* **2010**, *107* (14), 6164–6168.

(52) Renz, M.; Blasco, T.; Corma, A.; Fornés, V.; Jensen, R.; Nemeth, L. *Chem. - A Eur. J.* **2002**, *8* (20), 4708–4717.

(53) Corma, A.; Fornés, V.; Iborra, S.; Mifsud, M.; Renz, M. *J. Catal.* **2004**, *221* (1), 67–76.

(54) Waidmann, C. R.; Dipasquale, A. G.; Mayer, J. M. *Inorg. Chem.* **2010**, *49* (5), 2383–2391.

(55) Shetti, V. N.; Manikandan, P.; Srinivas, D.; Ratnasamy, P. *J. Catal.* **2003**, *216* (1), 461–467.

(56) Jianshuai Mu; Yan Wang; Min Zhao; Li Zhang. *Chem. Commun.* **2012**, *48* (19), 2540–2542.

(57) Chaiti Ray; Soumen Dutta; Sougata Sarkar; Ramkrishna Sahoo; Anindita Roy; Tarasankar Pal. *J. Mater. Chem. B* **2014**, *2* (36), 6097–6105.

(58) Huimin Jia; Dongfang Yang; Xiangna Han; Junhui Cai; Haiying Liu; Weiwei He. *Nanoscale* **2016**, *8* (11), 5938–5945.

Chapter 4

Succinic acid hydrogenation to γ-butyrolactone over Ru/V_2O_3

Abstract

In this chapter aqueous phase succinic acid hydrogenation reaction is demonstrated over Ru supported on V_2O_3. At optimized conditions, 77 % γ-butyrolactone (GBL) yield is obtained and the catalyst showed good recyclability. The reaction conditions are milder compared to those reported in literature. Compared to V_2O_5, the reduced phase V_2O_3 showed 5 times higher activity. TEM and CO chemisorption studies showed that Ru/V_2O_3 catalyst was under strong metal support interaction (SMSI) condition. In situ DRIFTS study showed that Ru/V_2O_3 catalyst adsorbs carboxylic acid as carboxylate species. A mechanism is proposed considering localization of the abstracted proton on V_2O_3 oxygen, which helps in keeping the dissociation equilibrium of succinic acid towards succinate anion making it more reactive.

4.1 Introduction

Bio-succinic acid can serve as an entry point for the synthesis of other C4 chemicals in a biomass centric process. γ-Butyrolactone (GBL) is a green solvent that can be obtained by hydrogenation of succinic acid. GBL is considered a safe electrolyte in Li-ion batteries and capacitors, because of its high flash point (98 °C) and particularly high

ability to solubilize Li^+ ions.[1] Owing to its polar nature, it can be used as polar aprotic solvent instead of chlorinated solvents that are hazardous.[2–4] Low melting point (-43.5 °C) and high boiling point (204 °C) makes it a green solvent in photosensitive resins synthesis.[5,6] In addition, GBL is used for production of 2-pyrrolidone (2P), N-methyl-2-pyrrolidone (NMP), N-vinyl-2-pyrrolidone (NVP) in a commercial scale.[7] It is recently reported that ring opening polymerization of GBL forms a polymer, which can be easily recycled by simple heat treatment in the range of 200 °C to 300 °C.[8,9] Therefore, GBL is a commercially important C4 chemical.

Industrially, GBL is produced by dehydrogenation of 1,4-butanediol over copper catalyst.[10] 1,4-Butanediol itself is produced either from oxidation of butane or base catalyzed condensation of acetylene and formaldehyde.[10] Mitsubishi Chemical Corporation produces GBL by hydrogenation of fossil based maleic anhydride. However, all the above processes utilize fossil feedstocks, which makes it important to develop biobased processes for GBL production from carbon neutrality point of view.

The existing literature shows that biobased succinic acid can be a good starting material for production of GBL.[11–16] Au or Pd based supported metal catalysts are used in literature to produce GBL from succinic acid. While Au or Pd catalysts have shown good activity, they require the use of carcinogenic organic solvent (namely dioxane) for better yields. Additionally, these reactions are carried out under harsh conditions (typically at 240 °C and long reaction time). Consequently, it is necessary to develop a catalyst that can work in milder conditions and support the use of water as a solvent.

Recently it has been proposed that Ru is a good metal for hydrogenation reaction in water because of its good wettability.[17] However, in the reported literature supported Ru catalysts were said to be less active and led to decarbonylation of succinic acid to form

propionic acid at higher temperatures. Active participation of support in the hydrogenation reaction can overcome the poor activity of Ru catalysts. In this study, we have shown how the activity of Ru can be increased in aqueous phase hydrogenation of succinic acid under milder conditions, by using a vanadium based support.

4.2 Experimental

4.2.1 Catalyst synthesis

All the catalysts were prepared via wet impregnation method. Ru/V_2O_3 was synthesized by dispersing 500 mg of V_2O_3 support in 20 mL water. Aqueous solution of $Ru(NO)NO_3$ was added to this dispersion to achieve 2 wt.% of ruthenium loading. Same amount of Ru was used for impregnation on other supports. After impregnation the catalysts were reduced at 400 °C for 1 h. Ru/V_2O_5 was prepared by chemical reduction method to avoid the reduction of V_2O_5 support. Same amount of V_2O_5 and $Ru(NO)NO_3$ were added to 20 mL of water followed by addition of 4 equivalent of $NaBH_4$. After stirring for 15 mins the suspension was centrifuged and washed with water.

4.2.2 Catalyst characterization

XRD was measured with Rigaku MiniFlex using CuKα X-ray (λ = 1.54 Å) operating at 40 kV and 20 mA. HR-TEM image was obtained in a JEOL JEM-ARM200F atomic resolution electron microscope at an acceleration voltage of 200 kV. X-ray photoelectron spectroscopy (XPS) was performed with JEOL JPS-9010MC instrument. Charge correction was made by adjusting the adventitious carbon peak to 284.6 eV. In situ DRIFTS was carried out in Perkin Elmer spectrum 100 IR instrument with a MCT detector.

4.2.3 Succinic acid hydrogenation reaction

Succinic acid hydrogenation reaction was performed in a 10 mL stainless steel autoclave reactor equipped with a teflon liner. In a typical reaction, 1 mmol of succinic acid and 50 mg of catalyst were added to 5 mL water. The reactor was closed and filled with 5 MPa of H_2 gas and placed in an oil bath preheated to 150 °C and was stirred through the entire course of reaction.

After the reaction, the reactor was cooled to room temperature and pressure was released. Recovered reaction mixture was centrifuged to separate catalyst from liquid product mixture. The product mixture was analyzed with a HPLC equipped with a Aminex HPX 87H column and a RID detector.

4.3 Results and discussion

4.3.1 Succinic acid hydrogenation

Scheme 4.1 shows the reaction network of succinic acid hydrogenation reaction. As a first elementary step, one of the carboxylic acid groups of succinic acid can undergo either hydrogenation reaction or decarbonylation reaction depending on the nature of the catalyst. Hydrogenation will lead to the formation of GBL. On the other hand, decarbonylation will lead to loss of one carbon to form propionic acid. GBL can further undergo a ring opening and hydrogenation to form 1,4-butanediol. Further hydrodeoxygenation of 1,4-butanediol may lead to formation of butanol. GBL can also undergo C=O hydrogenation followed by hydrodeoxygenation to form tetrahydrofuran (THF).

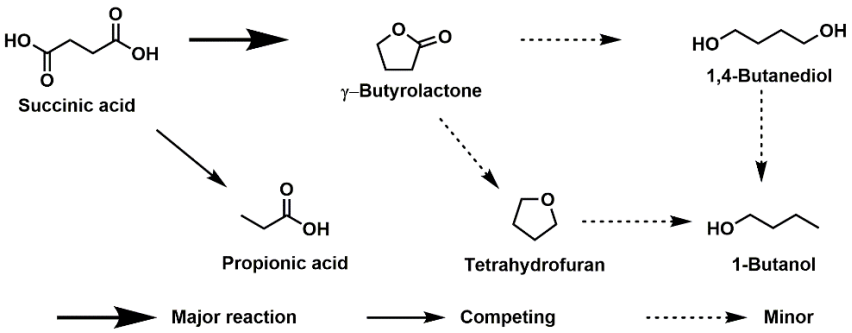

Scheme 4.1. Reaction scheme for succinic acid hydrogenation. Bold solid arrow represents major reaction pathway, regular solid arrow represents minor reaction pathways and dotted solid arrow represents unfavorable reaction pathways.

We conducted succinic acid hydrogenation over using 2 wt.% Ru supported over different supports. Ru/V_2O_3 showed 35 % GBL yield at 58 % conversion after 4 h at 150 °C and 5MPa H_2 pressure (Figure 4.1). Propionic acid (4 %) was the major side product. Yield of BDO, THF, BuOH was less than 3 % each. In contrast, Ru/V_2O_5 showed less than 5 % yield of GBL along with 48 % yield of unknown products. Ru/SiO_2 catalyst shows 13 % GBL yield at 20 % conversion, while Ru/Al_2O_3 showed only 17 % GBL yield at 38 % conversion.

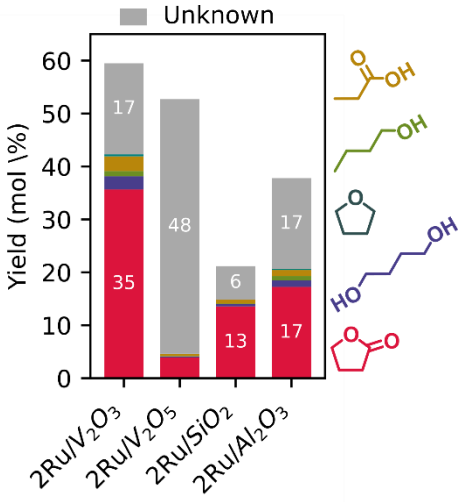

Figure 4.1. Comparison of activity of Ru succinic acid hydrogenation over different

supports.

Silica support is generally considered as inert support and does not participate in reaction. Hence, in the presence of $2Ru/SiO_2$, it can be assumed that the activity is derived mainly from Ru nanoparticles. Although the acidity of Al_2O_3 is reported to have a role in succinic acid hydrogenation,[13] the presence of water in our rection would deactivate the Lewis acid sites on Al_2O_3. Additionally, Al_2O_3 is prone to degradation to boehmite phase under hydrothermal conditions.[18] The low activity of $2Ru/V_2O_5$ and the high activity on $2Ru/V_2O_3$ shows that V_2O_3 support plays an important role in succinic acid hydrogenation reaction.

When only V_2O_3 support was used as a catalyst, there was no product formation (Figure 4.2a), but succinic acid conversion was 13 %. Considering V_2O_3 does not have H_2 dissociation ability the loss of succinic could be simply due to adsorption on V_2O_3 surface. Ru loading of 2 wt.% was optimal and after 6 hours of reaction succinic acid was completely converted with 77 % GBL yield. In comparison, only 51% yield of GBL was obtained in the presence of $5Ru/V_2O_3$ with 3.4 wt. % Ru Ru. It is worth nothing that the reaction conditions used are considerably mild in comparison to those reported in literature (150 °C, as opposed to 170 – 240 °C[11–16]) and water was used as solvent instead of 1,4-dioxane.

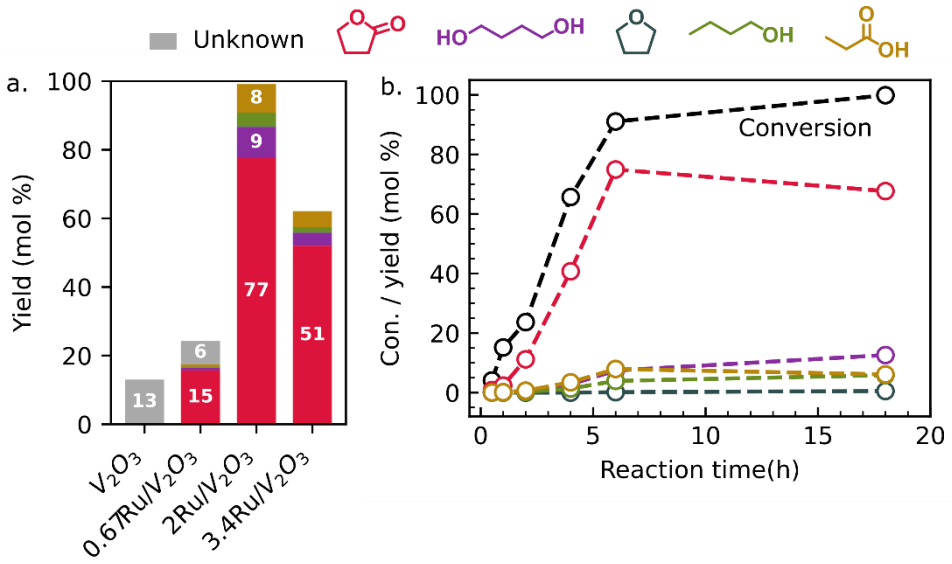

Figure 4.2. (a) Succinic acid hydrogenation reaction with Ru/V_2O_3 catalyst with different Ru loading. (b) Reaction time course with $2Ru/V_2O_3$. Reaction conditions : 1 mmol (118 mg) SA, 50 mg catalyst, 5 MPpa H_2, 150 °C, 6 h for (a) and various time for (b).

Evolution of products over time was studied to understand the reaction pathway and optimal reaction time (Figure 4.2b). After an initial induction period of about 0.5 h GBL is evolved as the main product. The initial delay might suggest change in catalyst structure, which then catalyzes the reaction. However, at this moment the reason of initial induction period is not clear. Succinic acid was completely converted in about 6 hours and maximum GBL yield was 77% at this time. At this point there were no unknown products, which means the initial difference succinic acid conversion and product yield was likely due to adsorption of succinic acid on the surface of catalyst. Further continuing the reaction to 12 hours caused only a slight degradation of GBL to 1,4-butanediol, which shows that GBL was stable under the reaction condition.

The $2Ru/V_2O_3$ catalyst was found to be recyclable at least up to 5 cycles and there was no loss of activity during the recycling experiments (Figure 4.3a). The XRD of fresh

catalyst showed only peaks for V_2O_3 species and peaks for Ru were not observed owing to small size of metal nanoparticles (Figure 4.3b). After first use the intensity of V_2O_3 peaks reduced and small peaks of VO_2 species were also present. The peak intensities remained constant after five cycles. This result indicates that VO_2 is either a spectator and does not take part in the reaction or it plays a role in the reaction and a reversible transition between V_2O_3 and VO_2 happens during the rection, which keeps the VO_2 amount constant.

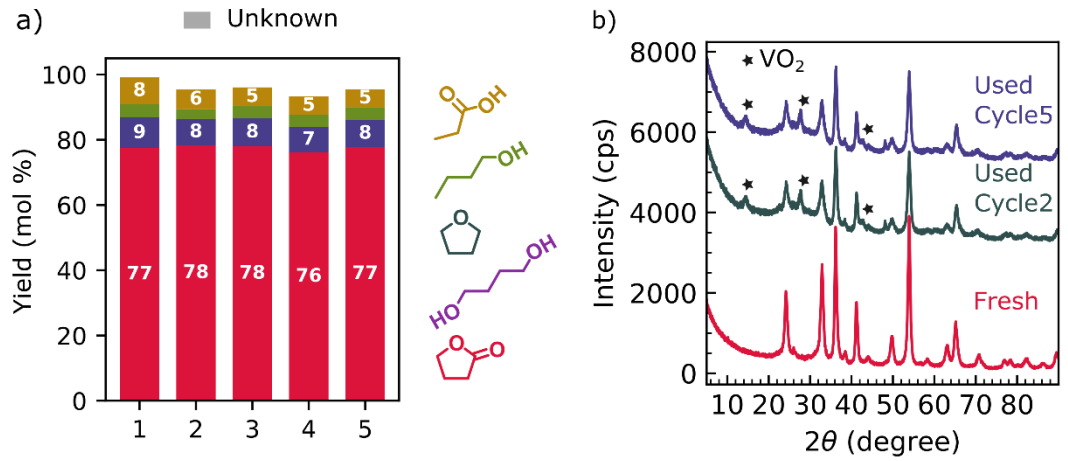

Figure 4.3. (a) Catalyst recyclability study. 1 mmol (118 mg) SA, 50 mg catalyst, 5 MPa H_2, 150 °C, 6 h. (b) XRD of catalysts at different stages.

4.3.2 Catalyst characterization

Figure 4.4a and b show the deconvoluted XPS spectrum of reduced $2Ru/V_2O_3$ catalyst. The catalyst contained mostly metallic Ru species with a small amount of RuO_2 species. V 2p XPS shows all the vanadium species are present in V^{3+} oxidation state. O 1s XPS shows presence of lattice oxygen at 530 eV as well as 37 % oxygen vacancy (532 eV). Presence of high amount of oxygen vacancy in V_2O_3 is an indication of presence of coordinatively unsaturated vanadium species, which can be helpful in coordination to carbonyl oxygen.

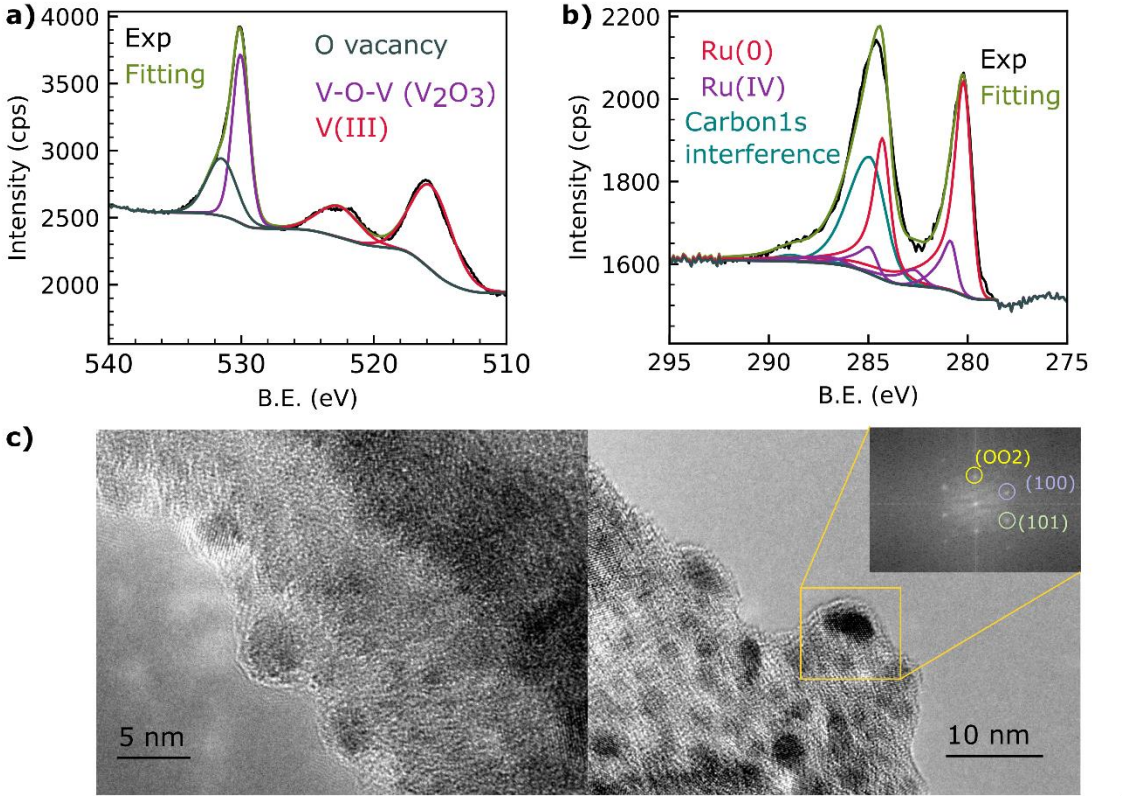

Figure 4.4. (a) Deconvoluted O 1s and V 2p XPS spectrum of $2Ru/V_2O_3$. (b) deconvoluted spectrum of Ru 1s XPS spectrum of $2Ru/V_2O_3$. (c) TEM images of $2Ru/V_2O_3$ with FFT of selected region (insert of right image).

Figure 4.4c and d show TEM image of $2Ru/V_2O_3$ catalyst. Dark color spots were characterized as ruthenium nanoparticles from fast Fourier transformation (FFT) of selected area highlighted by the yellow rectangle. The sports in FFT corresponded to (002), (100) and (101) planes of hexagonal ruthenium crystal lattice. It is important to note that ruthenium particles are covered by a thin layer of V_2O_3 which resembles the occurrence of strong metal support interaction (SMSI) between support and Ru metal.

SMSI would increase the metal support interaction but would also reduce the number of available Ru sites on the surface. In order to further quantify the availability of surface ruthenium sites, a temperature dependent CO chemisorption study was

conducted. Amount of CO adsorbed on catalyst reduced at different temperature is shown in Figure 4.5. As the reduction temperature increased the CO adsorption capacity decreased, indicating more and more Ru atoms are covered at higher temperature. However, significant amount CO adsorption was detected for catalyst reduced at 400 °C. Initial activity of the catalysts increased with increase in reduction temperature up to 400 °C and decreased significantly afterwards. Correlating the CO chemisorption trend and initial activity suggests that, the SMSI effect on the catalyst increased activity by increasing number of interfacial sites and after 400 °C, the active sites are severely blocked, hence the decrease in activity.

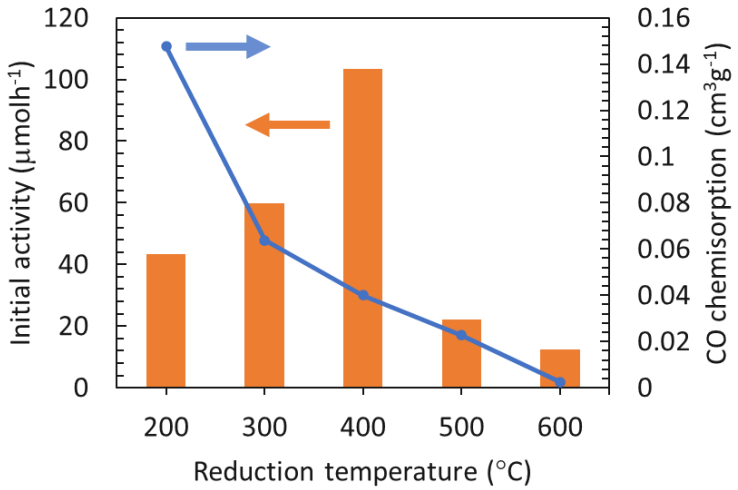

Figure 4.5. Corelation of CO chemisorption on $2Ru/V_2O_3$ at different reduction temperatures with initial acitivity in succinic acid hydrogenation reaction. Reaction conditions : - SA 1 mmol (118 mg), catalyst 50 mg, H_2 5 MPa, 150 °C, 4h.

4.3.3 Catalyst substrate interaction

To rationalize the influence of oxygen vacancy on V_2O_3 surface and the SMSI effect we investigated the interaction of succinic acid with $2Ru/V_2O_3$. For investigation of the mode of adsorption we used pivalic acid as a model compound to study carboxylic acid

adsorption over catalysts using DRIFTS analysis. Pivalic acid does not have any α-hydrogen and it cannot undergo lactonization, which reduces the possibility of interaction of other groups with the catalyst surface.

Figure 4.6a shows pivalic acid DRIFTS of $2Ru/V_2O_3$ catalyst. At room temperature pivalic acid was present as physisorbed species (black line). When temperature was increased to 50 °C under reduced pressure the intensity of peaks for physisorbed species reduced and new peaks emerged in the region of 1500–1650 cm^{-1}. These peaks are assigned to asymmetric stretching of adsorbed carboxylate species.[13,19] The peaks around 1200–1500 cm^{-1} shifted towards lower wavenumber. Their broadened shape indicates contribution from corresponding symmetric stretching frequency of carboxylate species.

Figure 4.6b shows spectra corresponding to pivalic acid adsorption over different catalysts at 50 °C. In case of pure V_2O_3, the peaks of physisorbed species disappeared after heating, however pivalate peaks did not appear. Spectra of $2Ru/SiO_2$ showed no features in the 1500–1650 cm^{-1} region, showing adsorption of pivalic acid over bare Ru nanoparticle or silica was not favorable. When similar experiments were performed with $2Ru/V_2O_5$ the carboxylate peaks were not visible. These observations suggest that the interface between V_2O_3 support and ruthenium was necessary to adsorb carboxylic acid as carboxylate species. Moreover, influence of V_2O_3 structure was also obvious, which contains coordinatively unsaturated V^{3+} species, instead of coordinatively saturated V^{5+} species found in V_2O_5. In summary, over $2Ru/V_2O_3$ catalyst carboxylic acid group is activated via a dissociative adsorption.

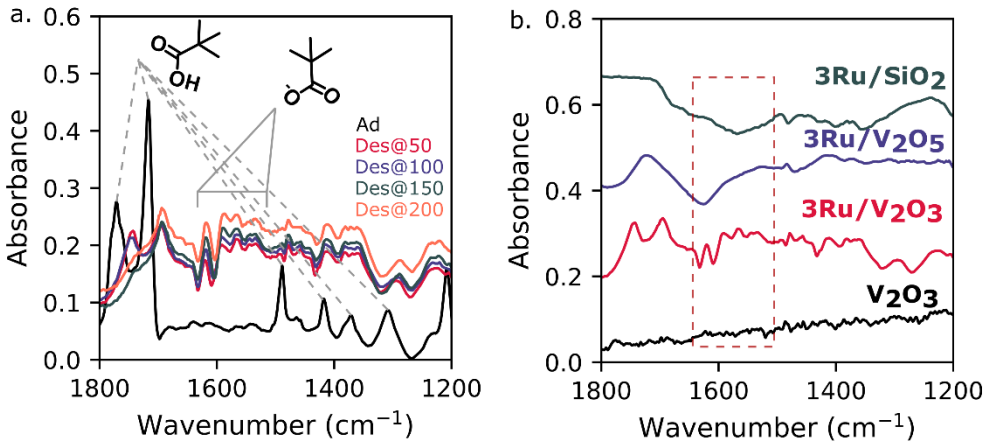

Figure 4.6. (a) In situ DRIFTS of pivalic adsorbed 2Ru/V_2O_3 showing spectra after adsorption at room temperature and after desorption at different temperatures. (b) Spectra at 50 °C for different samples. The region highlighted with dashed rectangle shows peaks for pivalate species.

Based on these observations we propose the following mechanism. The reaction starts with adsorption of succinic acid as succinate species at the interface of Ru and V_2O_3 and localization of the proton on a nearby V_2O_3 oxygen as shown in Scheme 4.2. After hydrogen dissociation over Ru nanoparticle, the first step of hydrogenation happens via a hydride transfer to the carbon of succinate group. This is followed by addition of another hydride to the carbon and breaking of one of the C–O bond to release one water molecule. In following reaction step cyclization dehydration takes place by abstraction of the proton localized on V_2O_3 oxygen. The localization of proton on the V_2O_3 oxygen might play a decisive role in the reaction as it shifts the dissociation equilibrium of succinic acid towards succinate anion. The presence of succinic acid as adsorbed succinate anion can make it more reactive by interfering with intermolecular hydrogen bonding between carboxyl groups.

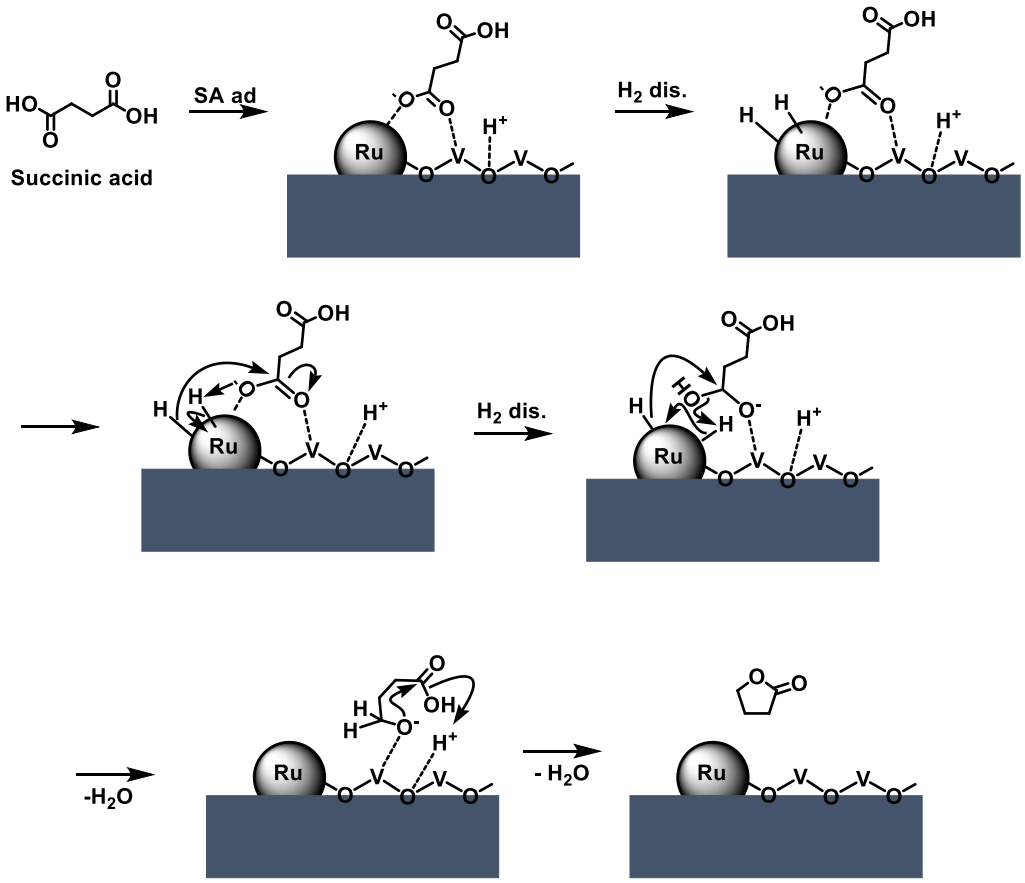

Scheme 4.2. Proposed mechanism of succinic acid hydrogenation over $2Ru/V_2O_3$ catalyst.

4.4 Conclusion

V_2O_3 support showed a positive effect on succinic acid hydrogenation reaction over ruthenium catalyst and produced 77 % yield of GBL after 6 h of reaction. The catalyst was highly recyclable and contrary to existing literature worked under milder conditions and in the presence of water as a solvent. Pivalic acid adsorption DRIFTS experiment as a model compound shows carboxylic acid group undergoes dissociative adsorption as carboxylate group over $2Ru/V_2O_3$ catalyst. VO_2 phase was also detected in XRD during catalytic cycles and its amount remained constant. We propose a mechanism where localization of the abstracted proton on V_2O_3 oxygen helping in keeping the dissociation equilibrium of succinic acid towards succinate anion making it more reactive.

4.5 References

(1) Gu, Y.; Fang, S.; Yang, L.; Hirano, S. *Electrochim. Acta* **2021**, *394*, 139120.

(2) Kim, H.; Yang, S.; Kim, D. H. *Environ. Res.* **2020**, *187*, 109667.

(3) Wang, L.; Guo, H.; Xie, Q.; Wang, J.; Hou, B.; Jia, L.; Cui, J.; Li, D. *Appl. Catal. A Gen.* **2019**, *572*, 51–60.

(4) Ter Horst, J. H.; Geertman, R. M.; Van Rosmalen, G. M. *J. Cryst. Growth*, **2001,** 230, 277–284.

(5) Tani, M.; Sugiura, T. *SID seminar notes*, **1995**; F5.1–F5.23.

(6) Hirai, Y.; Katoh, H. *Proc. IDW*, **1995**, 49.

(7) Schwarz, W.; Schossig, J.; Rossbacher, R.; Pinkos, R.; Höke, H. *Ullmann's Encycl. Ind. Chem.* **2019**, 1–7.

(8) Hong, M.; Chen, E. Y.-X. *Nat. Chem.* **2016**, *8* (1), 42–49.

(9) Moore, T.; Adhikari, R.; Gunatillake, P. *Biomaterials*. June 2005, pp 3771–3782.

(10) Oka, S. *Bull. Chem. Soc. Jpn.* **1962**, *35* (6), 986–989.

(11) Budroni, G.; Corma, A. *J. Catal.* **2008**, *257* (2), 403–408.

(12) Hong, U. G.; Hwang, S.; Seo, J. G.; Lee, J.; Song, I. K. *J. Ind. Eng. Chem.* **2011**, *17* (2), 316–320.

(13) Yakabi, K.; Jones, A.; Buchard, A.; Roldan, A.; Hammond, C. *ACS Sustain. Chem. Eng.* **2018**, *6* (12), 16341–16351.

(14) Zhang, C.; Chen, L.; Cheng, H.; Zhu, X.; Qi, Z. *Catal. Today* **2016**, *276*, 55–61.

(15) You, C.; Zhang, C.; Chen, L.; Qi, Z. *Appl. Organomet. Chem.* **2015**, *29* (10), 653–660.

(16) Tapin, B.; Epron, F.; Especel, C.; Ly, B. K.; Pinel, C.; Besson, M. *ACS Catal.* **2013**, *3* (10), 2327–2335.

(17) Michel, C.; Gallezot, P. *ACS Catal.* **2015**, *5* (7), 4130–4132.

(18) Van Cleve, T.; Underhill, D.; Veiga Rodrigues, M.; Sievers, C.; Medlin, J. W. *Langmuir* **2018**, *34* (12), 3619–3625.

(19) Chen, L.; Li, Y.; Zhang, X.; Zhang, Q.; Wang, T.; Ma, L. *Catal. Lett. 2016 1471* **2016**, *147* (1), 29–38.

Chapter 5

Conclusion

Use of non-edible lignocellulosic biomass as a feedstock for chemical production is attractive in terms of carbon neutrality. This goal requires the development of synthetic routes to value added chemicals that are currently being used in chemical industry. Two, three, five and six carbon compounds are easier to produce from biomass because of abundance of their platform chemicals and some of these chemicals are industrially produced. On the contrary, four carbon chemicals are still prepared from fossil sources because their formation requires oxidative or reductive C-C bond cleavage of larger platform chemicals obtained from biomass. In this thesis, we have explored the development of catalytic processes to produce four carbon chemicals from furfural that can be derived from abundantly available xylose and fructose.

In Chapter 2, a catalytic process for glucose to fructose isomerization is explored. Glucose is the most abundant biomass derived platform chemical and its conversion to fructose is the first step in several catalytic pathways, including the formation of furfural. For glucose isomerization, a Lewis acid catalyst was developed by anchoring highly dispersed Sn species on the surface of SBA-15. The dispersed Sn species with tetrahedral open sites were created on the surface of SBA-15 via simple impregnation by taking advantage of the abundance of hydroxyl groups and high surface area. Characterizations revealed that one active site could form with five silanol groups on catalyst surface. Isotopic labeling study proved that glucose was isomerized via the 1,2-hydride shift

mechanism, which validated the role of Lewis acid sites in our reaction. Turnover frequency over this Sn/SBA-15 catalyst was two times in comparison to conventional Sn-Beta catalyst.

Chapter 3 discusses oxidative C-C cleavage of carbonyl group in furfural to produce succinic acid. Succinic acid can be a gateway to biobased four carbon chemicals. For this reaction we have used a purely Lewis acidic Sn-Beta catalyst prepared by post-impregnation method. This catalyst was selective and reusable for furfural oxidation to succinic acid. NMR analysis of reaction mixture revealed that 2(3H)-furanone was the key intermediate. Sn-Beta accelerated the formation of 2(3H)-furanone via Baeyer-Villiger oxidation. Increase in Lewis acid density of the catalyst had a positive effect on initial rate of reaction. Sn-Beta polarized the carbonyl group of furfural making the carbon atom more electrophilic, which was then attacked by hydrogen peroxide to do Bayer-Villiger oxidation reaction. In contrast, when TS-1 was used as Lewis acid catalyst for comparison, maleic acid was produced, which was due to the formation of M-OOH species leading to epoxidation of furfural ring. Similarly, Brønsted acidic HBeta-38 zeolite produced a mixture of products as it reacted with hydrogen peroxide. The peculiar nature of Sn-Beta to activate furfural and not to react with hydrogen peroxide makes it a suitable catalyst for this reaction.

In Chapter 4, the use of succinic acid as precursor to synthesis of γ-butyrolactone (GBL) is discussed. GBL is a four-carbon lactone that serves a green aprotic solvent and chemical precursor. All the catalysts reported in literature for this reaction use 1,4-dioxane as solvent and expensive metals like Pd or Au as catalysts. In contrast, we found that Ru can also activate succinic acid in aqueous phase when supported on a suitable metal oxide. Ru/V_2O_3 catalyst showed improved activity compared to other supports such

as V_2O_5, SiO_2 and Al_2O_3. In situ DRIFTS study with pivalic acid as a model carboxylic acid suggested that succinic acid undergoes dissociative adsorption at the interface of Ru metal and V_2O_3 support. The catalytic activity was stable for at least five cycles. Some amount of VO_2 phase was observed after the reaction which remained constant through multiple cycles. We propose a mechanism involving dissociative adsorption of succinic acid on Ru/V_2O_3 followed by hydrogeneration in which the ability of V_2O_3 support to localize abstracted proton of succinic acid played a crucial role.

As a thesis this work is focused on creating chemical pathways for synthesis of four carbon chemicals from biomass. Future works in this direction requires development of economically viable catalytic routes for production of succinic acid or maleic acid as platform chemicals and their transformation to value added chemical such as 1,4-butanediol and butadiene. Majority of current four carbon chemicals are produced from butane as starting material, which is a fossil-based resource. Although succinic acid is being recognized in the literature as a platform chemical and its hydrogenative transformation to other chemicals are at developmental stage, there is not much research on catalytic production of succinic acid from biomass. More effort should be dedicated to Lewis acid catalysts for succinic acid synthesis from furfural. In addition, use of transition metals to replace H_2O_2 with molecular O_2 is highly desired. Similarly, future research for conversion of succinic acid to downstream chemicals should be done without use of organic solvents and precious metal catalysts.

Synopsis

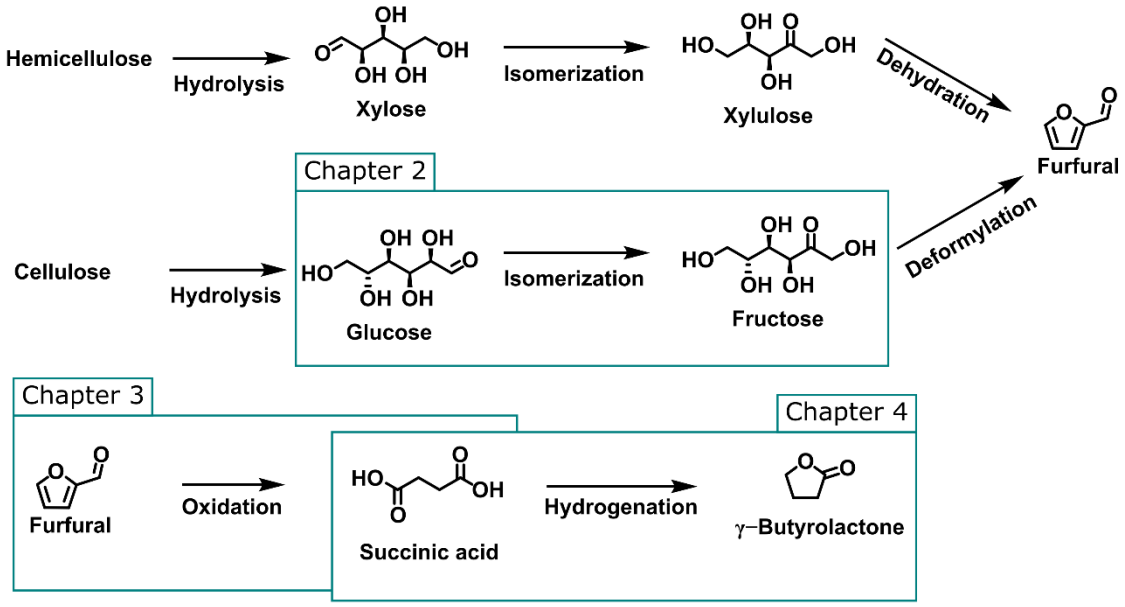
Hemicellulose
Hydrolysis
Xylose
Isomerization
Xylulose
Dehydration
Furfural
Chapter 2
Cellulose
Hydrolysis
Glucose
Isomerization
Fructose
Deformylation
Chapter 3
Furfural
Oxidation
Succinic acid
Chapter 4
Hydrogenation
γ–Butyrolactone

List of Publications

Journal publications

Yayati Naresh Palai, Abhijit Shrotri, Atsushi Fukuoka. Silica supported Sn catalysts with tetrahedral Sn sites for selective isomerization of glucose to fructose, *Catalysis Today*, **2021**, *365*, 241-248

Yayati Naresh Palai, Abhijit Shrotri, Atsushi Fukuoka. Selective oxidation of furfural to succinic acid over Lewis acidic Sn-Beta, *ACS Catalysis*, 2022, DOI:10.1021/acscatal.1c05348

Yayati Naresh Palai, Abhijit Shrotri, Atsushi Fukuoka. Succinic acid hydrogenation to γ-butyrolactone over Ru/V_2O_3. (Manuscript under preparation)

Journal publications (not related to this thesis)

Waqar Ahmed, Fan Liang Chan, Abhijit Shrotri, Yayati Naresh Palai, Huanting Wang, Akshat Tanksale. Dimethoxymethane production via CO_2 hydrogenation in methanol over novel Ru based hierarchical BEA, *Journal of Energy Chemistry*, **2022**, *66*, 181-189

Yayati Naresh Palai, Anjali K, Ayamperumal Shakthivel, Maqsood Ahmed, Dhananjay Sharma, Sushant K. Badamali. Cerium Ions Grafted on Functionalized Mesoporous SBA-15 Molecular Sieves: Preparation and Its Catalytic Activity on *p*-Cresol Oxidation,

Catalysis Letters, **2018**, *148*, 465-473

Conference contributions

Yayati Naresh Palai, Abhijit Shrotri, Atsushi Fukuoka, Silica supported Sn catalysts with tetrahedral Sn sites for selective isomerization of glucose to fructose, *18th Japan-Korea Symposium on Catalysis,* Online, November 23, **2021** (Oral)

Yayati Naresh Palai, Abhijit Shrotri, Atsushi Fukuoka, Silica supported Sn catalysts with tetrahedral Sn sites for selective isomerization of glucose to fructose, *The 128th annual meeting of Catalysis Society of Japan*, Online, September 15, **2021**, (Oral)

Yayati Naresh Palai, Abhijit Shrotri, Atsushi Fukuoka, Silica supported Sn catalysts with tetrahedral Sn sites for selective isomerization of glucose to fructose, *The 126th annual meeting of Catalysis Society of Japan*, Online, September 16, **2020** (Oral)

Acknoledgement

These are final few words of the thesis, and I would like to take this opportunity to remember the people I am grateful to, throughout my doctoral degree. I have had a wonderful time during my doctoral research. I have not only gained experience and skills in scientific research, but also in various different aspects of life.

At first, I would like to thank Professor Dr. Atsushi Fukuoka, my supervisor, for accepting me a as doctoral student in the group. You have been helpful to me since the day I arrived here. Your experience has been helpful for me during the entire doctoral degree. Thank you for making me prepared for the thesis presentation. Apart from this thank you for encouraging me to attend conferences, reviewing my papers.

Dr. Kiyotaka Nakajima, my co-supervisor, thank you for the valuable suggestions and questions you have asked me throughout the group meetings. They have helped a lot in shaping my research. Specially, your questions have led me to deeper investigations in my research. Thank you for helping me out during the preparation for doctoral defense. Apart from this, we have had some joyful conversations during the parties, which I will remember forever.

Dr. Abhijit Shrotri, thank you for mentoring me in everything rough out the doctoral degree. I have enjoyed working with you. Specially, the amount of freedom I had and you knowing when to step in made a perfect working environment. We always had fruitful discussions. Thank you for correcting a lot of typing mistakes in my papers and thesis. I have learnt a lot about scholarly writing from you. You have taught me how to use a lot

of instruments in the laboratory. Apart from this you helped me a lot in settling down in Sapporo and all other aspects of personal life during my doctoral studies. Most important of all, when I had tough time communicating my ideas during discussions in group meetings and other discussions, you have helped me a lot.

I would like to thank all the group members for being so helpful to me. Hiromi Matsushima, thank you for making all the administrative works easy for me. And thanks to Yumiko Yokoyama for helping me in administrative works as well. Dr. Minjune Kim, whatever little interactions we had I never understood your jokes, but thanks for being funny. Dr. Shazia Sharmin Satter, thank you for helping me a lot in many personal things and thank you for the parties at your home. Dr. Takuya Sagawa, thank you for being so kind. Many times, it was difficult to communicate with you, but you always helped whenever I needed any help in the lab. Dr. Eunhyeok Yang, I was always inspired to work by looking at you and thank you for helping me in lot of trouble shooting activities. Dr. Etty Nurlia Kusumawati, Dr. Li Lingcong and Dr. Pengru Chen, thank you for being a good senior in the lab. Dr. Shaikh Nazmul Hasan Mohammad Dostagir, we always had good discussions in the lab, thank you for being part parties at my home and with some other friends. Apart from this, thank you for guiding me during preparation of documents for thesis. Dr. Jan J. Wiesfeld, it was always easy for me to walk to you and speak anything. Thank you for being part of parties at my home and hosting parties at your home as well. Cheng Yang, we have graduated together, and along the way you have always helped me, when I needed any help in Japanese. I would like to thank Dr. Daniele Padovan, Tat Booniyakarn, Kazuya kato, Koichiro Endo, Yusuke Suzuki, Miyuki Asakawa. Natsumi Shibayama, you helped me in procedures in the ward office and setting up my bank account, thank you for that.

Finally, I would like to thank my parents for supporting me though out my life. You have gone through a lot of hardship but have never let me feel any of it.